A Study of Cellulose Nanocrystal Reinforcing Effect in Polyurethane and Vitrimer System

by

Mingrui Liang

A thesis
presented to the University of Waterloo
in fulfillment of the
thesis requirement for the degree of
Master of Applied Science
in
Chemical Engineering

Waterloo, Ontario, Canada, 2022

Author’s Declaration

I hereby declare that I am the sole author of this thesis. This is a true copy of the thesis, including any required final revisions, as accepted by my examiners. I understand that my thesis may be made electronically available to the public.

Abstract

Nanocellulose-based composites and materials have received remarkable attention due to their high mechanical performance, low weight, and environmental friendliness. However, the compatibility between CNCs and polymer may vary significantly according to the polarity and hydrophobicity of polymer. The dispersity of CNCs in the polymer matrix is also critical to the physical and chemical performance of final nanocomposites. These limitations challenge the reinforcing effect of nanocellulose in nanocomposite materials in practical applications. In this study, we used both solvent casting and *in situ* polymerization methods to add CNCs into polymer matrices to achieve an improved performance of CNC-reinforced nanocomposites.

In the first part, CNC suspension was directly mixed with waterborne polyurethane (WPU), and then a film was obtained after evaporation at room temperature. Further tensile tests confirmed the excellent reinforcing effect of CNCs, with improved values for stress of 27.8 MPa and Young's modulus of 100.46 MPa compared to 19.6 MPa and 16.73 MPa for neat WPU. The results of scratch and friction tests exhibited better scratch resistance and increased coefficient of friction, making it a potential material for coating and packing applications. The thermal stability of CNC-reinforced nanocomposites was not influenced by the addition of CNC particles, and the 5% weight loss and maximum weight loss temperatures also remained the same. The water contact angle did change with the addition of CNCs, due to their hydrophilic features, reducing from 89° to 31°.

In the second part, CNCs were incorporated into vitrimer by *in situ* polymerization method. CNCs were initially grafted with polycaprolactone (PCL) to allow CNCs to be directly incorporated into the synthesis of vitrimer material. The addition of PCL-grafted-CNCs (PCL) increased the tensile strength and storage modulus of the vitrimer both at room temperature and above the glass transition temperature (T_g). The CNC-vitrimer composites were all insoluble in toluene even at high temperatures, suggesting a three-dimensional network was formed. Furthermore, after several reprocessing cycles, the CNC-vitrimer still displayed good mechanical properties. The effect of PCL-CNCs on the vitrimer system was also evaluated by dynamic mechanical analysis, differential scanning calorimetry, thermogravimetric analysis, and swelling tests. It was found that the addition of polycaprolactone-grafted-CNCs (PCL-CNCs) increased the temperature values for the melting

point, crystallization, and glass transition. Also, the gradual decrease in activation energy with the increased amount of PCL-CNCs reflect that the stress relaxation behavior is less sensitive to the temperature. The thermo-dynamic properties are controlled by the concentration of PCL-CNCs. When PCL-CNCs were at lower amounts, the hydroxyl and ester groups dominate the covalent adaptable networks (CANs) dynamic, leading to a faster stress relaxation behavior. However, when the amount of PCL-CNC increased, the crystals and aggregation started to constrain the mobility of polymer chain, resulting a longer stress relaxation time.

Acknowledgements

I would like to sincerely thank my supervisor, Dr. Zhao, for his professional advice and support in this work. Without his guidance, I would not finish this project. His professional, honest, disciplined working style encourages me to study further in academia. I really appreciate the comments and questions from the examiners, Professor Bill Anderson and Professor Tizazu Mekonnen; their effort makes me look at my project in various aspects and gives me more inspirational ideas.

Also, I would like to thank Dr. Pengxiang Si and Dr. Jian Sun for their mentorship at the beginning of my project. Their suggestions and instruction help me construct and organize the outline and structure of my whole work. Special thanks to Dr. Aleksander Cholewinski, he helps me overcome the language difficulties and to be a professional researcher .I would like to express my gratitude to all my lab mates at the University of Waterloo.

Last but not least, I would like to express my deepest gratitude to my parents and family in China for their emotional support. Their support and companionship help me complete this challenging journey, especially during the pandemic. They help me go through all the challenges and difficulties I have met in my research and daily life.

Table of Contents

List of Figures

List of Tables

List of Abbreviations

CNC	Cellulose nanocrystal
CNF	Cellulose nanofiber
TEMPO	2,2,6,6-Tetramethylpiperidinyloxy
PU	Polyurethane
WPU	Water-based/waterborne polyurethane
VOC	Volatile organic compound
PCL	Polycaprolactone
PCL-CNC	Polycaprolactone grafted cellulose nanocrystal
BADGE	Bisphenol A diglycidyl ester
PETME	Pentaerythritol tetrakis(3-mercaptopropionate)
TBD	Triazabicyclodecene
PDMS	Polydimethylsiloxane
ROP	Ring-opening polymerization
CAN	Covalent adaptable network
TEM	Transmission electron microscopy
SEM	Scanning electron microscopy
XPS	X-Ray photoelectron spectrum
UMT	Universal macro-tribometer
DMA	Dynamic mechanical analysis
FT-IR	Fourier transform infrared spectroscopy
TGA	Thermogravimetric analysis
DSC	Differential scanning calorimetry
COF	Coefficient of friction
T_g	Glass transition temperature
T_v	Topology freezing temperature

Chapter 1. Introduction

The polymer materials currently in use are mainly synthesized based on petroleum products; however, petroleum resources will be depleted one day, and the massive use of petroleum-based polymers has begun to cause serious pollution to the environment on which human beings depend. Therefore, the world has begun to focus on the direct production of polymer materials from natural renewable biomass resources as an important strategy to meet the challenge of oil depletion and environmental pollution.

Cellulose is widely found in nature and is considered to be the most promising raw material for the future. It is widely used in the research and development of environment-friendly materials because of its advantages of a broad variety of sources, environmental protection, lack of pollution, ease of modification, good biocompatibility, and biodegradability. Cellulose nanocrystals (CNCs) extracted from cellulose not only have many advantages of cellulose, but also have properties such as high crystallinity, high modulus, high strength and nanoscale effects, which are expected to improve the comprehensive performance of waterborne polyurethane as modifiers and are in line with the concept of sustainable development. In addition, the abundant hydroxyl groups on the surface of cellulose nanocrystals facilitate their modification and can lead to additional functionalities. Therefore, the study of the modification of aqueous polyurethanes by cellulose nanocrystals has relatively important theoretical significance and application value for the preparation of high-performance environment-friendly materials.

Water-based polyurethane (WPU) is an environmentally friendly polymer material that uses water instead of organic solvents as the dispersing medium. It has no organic solvent evaporation in the process of use, avoiding waste of resources and harm to people and animals, and is widely used in the fields of coatings, adhesives, leather processing, textiles, wood processing, etc. Vitrimers have attracted much attention from academia due to their reprocessing, self-healing, and shape memory properties. Vitrimer materials have potential in fields of aerospace, military, transportation, and electrical devices. However, many of the vitrimers obtained from ester exchange, urethane

exchange, complex decomposition reaction, etc. are not very strong and are almost elastomeric at room temperature, which limits their application to load-bearing structural materials.

The objective of this study is to incorporate CNCs into polymer matrices by solvent casting methods and *in situ* polymerization to obtain CNC-reinforced nanocomposites with enhanced mechanical and chemical properties. The dispersion of CNCs directly into waterborne polyurethane and incorporation of PCL-grafted-CNCs into vitrimer resulted in improved tensile strength, thermal stability, water resistance, and scratch resistance, proving the excellent reinforcing effect of CNC particles. Chapter 1 briefly introduces the motivation and necessity of this project, Chapter 2 provides a literature review and background of CNC, waterborne polyurethane and vitrimer materials. Chapters 3 and 4 present the details of the experiments, results, and discussion. Finally, Chapter 5 gives the summary of the whole project and prospective work.

Chapter 2. Literature Review

2.1 Cellulose

2.1.1 Introduction of cellulose

Cellulose mostly exists in the cell wall of plants, sea animals, bacteria, and fungi[1]. Due to its biodegradability, non-toxicity, and excellent chemical and physical properties, cellulose is receiving extensive attention from both scientific and industrial research in recent decades[2], with an annual production estimated at 10^{12} tons[3]. Cellulose is a polysaccharide that consists of repeating units of D-glucose connected by beta-1,4-glycosidic bonds in chair conformation with the second rotated 180° around the molecular axis[4]. The repeating unit of the cellulose chain is shown in Fig. 1. The degree of polymerization (DP) of the cellulose chain can reach up to 20000, with shorter cellulose chains observed most in primary cell walls[5] (presented in Fig. 2).

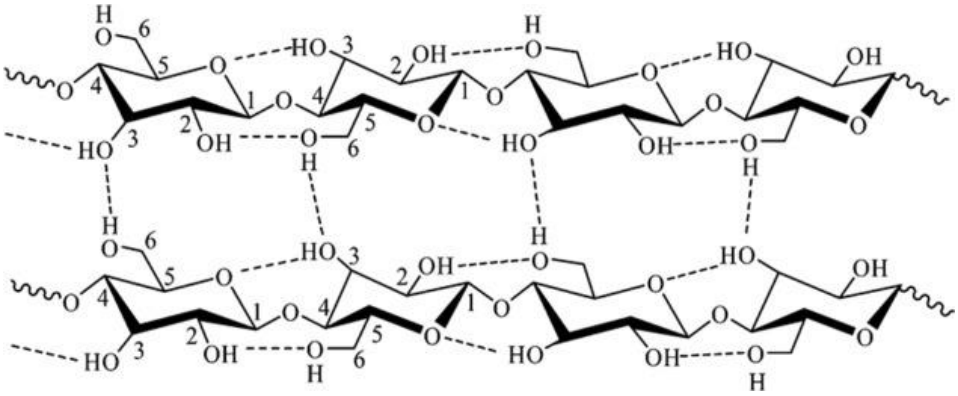

Figure 1. Chemical structure of cellulose[6].

Crystalline cellulose is made of four polymorphs, I, II, III, IV, which highly depends on the source of cellulose. Cellulose I (native cellulose), a mixture of cellulose Iα and Iβ, is mostly produced by wood, cotton, algae bacteria, and the shell of marine animals[7]. Cellulose II, the second most extensively studied form, was frequently prepared from cellulose I by two methods[8]: 1) regeneration, which involves dissolving cellulose I followed by reprecipitation by dilution in water to get cellulose II[9,10]; 2) mercerization, in which cellulose is intra-crystalline swelled in sodium hydroxide solution followed by rinsing and recrystallization[11]. Polymorph IV can be prepared from cellulose III through a thermal process in glycerol[12]. Since cellulose I (native cellulose) is the

easiest form to obtain from nature, commercial crystalline cellulose is primarily extracted by bleaching treatment of lignocellulosic fiber.

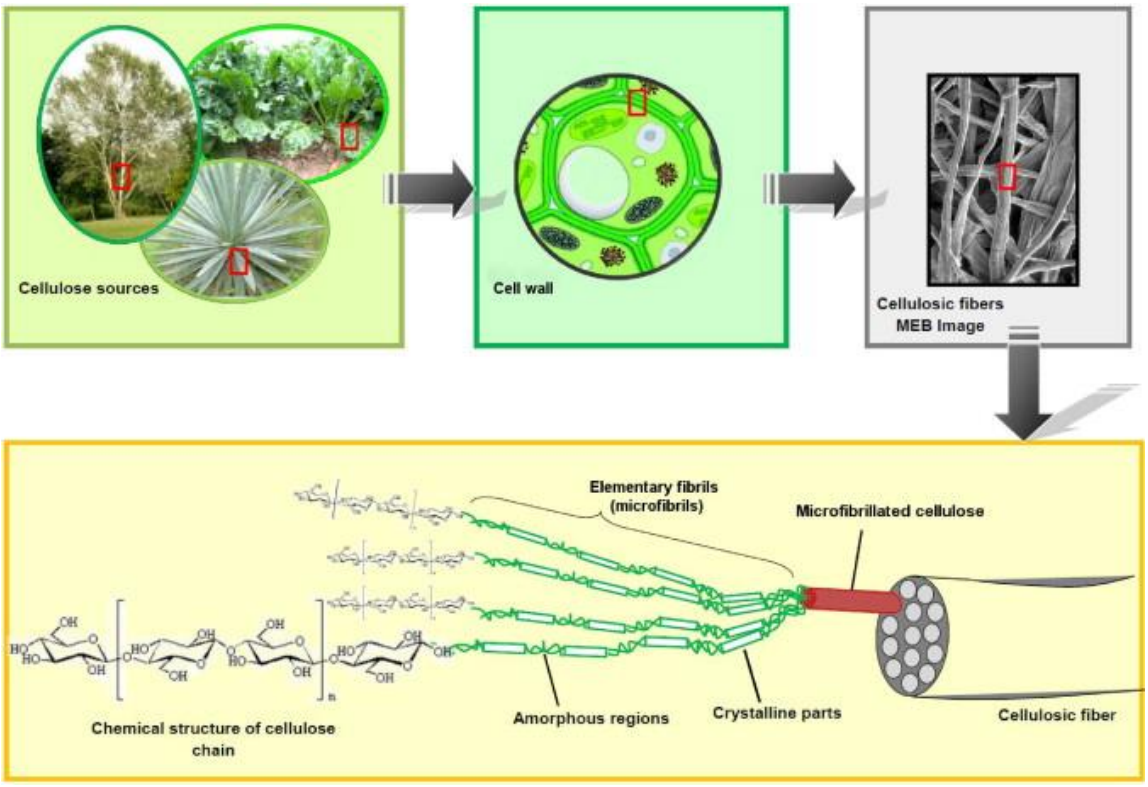

Figure 2. The source of cellulose and the process of obtaining cellulose[7].

The abundant hydroxyl groups on the cellulose chain cause strong intra- and intermolecular hydrogen bond interactions, leading to a high modulus and crystallinity, which impact the mechanical performance of CNCs[13]. The measured elastic modulus of CNCs themselves can reach 140-150 GPa, which can be equivalent to, or even better than, some high-performance reinforcing agents such as nanoclay, E-glass fiber, or Kevlar-49[14]. Also, the nanosized particles have been found to be promising fillers due to their extraordinary reinforcing effect. There are two categories of nanosized cellulose particles: the first type is cellulose nanocrystal (CNC) and the second kind is cellulose nanofiber or microfibrillated cellulose (MFC).

2.1.2 Cellulose nanofiber

Cellulose nanofiber, or microfibrillated cellulose, is usually obtained from a mechanical homogenization process followed by alkali and bleaching treatment. Cellulose nanofibers were first extracted from wood cells by Herrick *et al.*, and Tubark *et al.* in 1983[15,16]. The size of CNF is

hugely affected by the source of raw material and the manufacturing process; generally, the particle size is 2-100 nm in diameter with a length on the micrometer scale, though this is hard to determine due to the intertwining together of the fibers. The great mechanical properties of cellulose nanofibers have been previously reported; the elastic modulus of a single fiber can reach 145.2 GPa for TEMPO-oxidation treated microfiber and 150.7 GPa for acid hydrolyzed fiber[17].

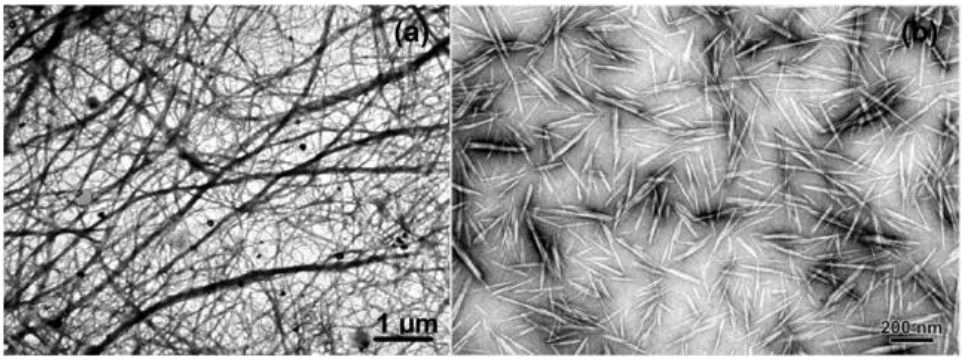

Figure 3. a) TEM image of dilute dispersion of cellulose nanofibers extracted from *Opuntia ficus-indica* fiber[18]. b) TEM image of cellulose nanocrystals obtained from ramie[19].

2.1.2.1 Production of CNF

The critical process to obtain cellulose fibers is mechanical homogenization; the Manton-Gaulin homogenizer and the microfluidizer are two kinds of equipment that are commonly used to achieve this process. In the 1980s, nanocellulose fibers were extracted from wood fibers by mechanical methods under high-pressure conditions of around 8000 psi – required to achieve a high enough shear force to grind the large wood pieces into nanofibers – and a temperature maintained at 70-80℃ by cooling water. However, this process requires large energy consumption of over 30 MWh/ton[16]. The microfluidizer is an alternative to the Gaulin homogenizer that can also allow the defibrillation of the wood pulp. The pulp suspension goes through a z-shape under 30000 psi high pressure to obtain a high-velocity product in the interaction chamber. There are two forces that affect this product. The first is the shear force between the wall and the feed stream, which is caused by the increase in velocity and leads to the deformation of the outlet product. Another force is the friction force, which results in raising the temperature, necessitating the heat exchanger to cool down the final product.

There are several pretreatments that have been applied to pulp to reduce energy consumption of CNF production. Zimmermann *et al.* reported that dried pulp was processed with sulfuric acid for

16 hours at 60℃[20]. After centrifugation and washing, the solution was neutralized with sodium hydroxide and homogenized with a microfluidizer. However, the strong acid hydrolysis would weaken the hydrogen bond interaction, which can lead to the reduction of mechanical properties. Enzymatic hydrolysis pretreatment is a more environmental-friendly method that can enhance the degree of fibrillation[21]. The CNFs treated by enzyme have favorable structures with a higher aspect ratio[22]. However, with the increase in the concentration of enzyme, there is decrease in the fiber length and an increase in the cost of the material. Compared with acid hydrolysis, the enzyme treatment is more stable and provides longer nanosized fibers. Enzymatic pretreatment also solves the blocking issues in homogenization[21]. The addition of charged groups onto the cellulose fibers is another way to obtain CNFs. Satio *et al*. reported that CNFs were prepared by the TEMPO-catalyzed oxidation method[23,24], which caused electrostatic repulsion and broadened the range of CNF applications introducing carboxyl groups to their surface.

2.1.3 Cellulose nanocrystal

The same as for CNF, cellulose nanocrystal can be isolated from various raw materials such as wood, cotton, tunicate, and bacteria. The source and the isolation method of CNCs control the chemical and physical properties. A comparison has been made between CNCs from wood and from sea animals by investigating SEM images; the size of CNC particles typically varies between 5-30 nm in diameter and 3-100nm in length[5,25].

As mentioned before, the cellulose chain contains two parts, the amorphous domains and ordered crystalline regions. Acid hydrolysis is employed to remove the amorphous regions, whereas the ordered domains remain behind due to their higher resistance to acid. The purification methods used are critical to the surface properties of the final products. For one method, sulfuric acid has been extensively used for CNC preparation; when CNCs are obtained from sulfuric hydrolysis, the hydroxyl groups react with the acid to yield a negatively charged surface ($-OSO_3^-$)[26,27]. The introduction of sulfate groups benefits the dispersion of CNCs in the water due to the electrostatic repulsion between the particles[25]. Research has also been undertaken on hydrolysis using hydrochloric acid. Since the final product is not negatively charged, this results in an unstable dispersion and aggregation of CNCs via hydrogen-bonding interactions. However, one benefit of

hydrochloric hydrolysis is that it enhances thermal stability. Additionally, thixotropic behavior has been observed for CNCs extracted by hydrochloric hydrolysis when the concentration was higher than 0.5 wt%, with anti-thixotropic properties at 3 wt%[28]. Phosphoric and hydrobromic acids have also been studied as hydrolyzing agents[29,30], and offer both good thermal stability and dispersibility. As another alternative, the combination of hydrochloric and sulfuric acids produced spherical CNC particles instead of whiskers of nanocellulose, contributing to a better thermal stability[31].

There are many other process methods that have been investigated to produce CNC, including TEMPO-oxidation[32], ionic liquid[33], ammonium persulfate oxidation[34], enzyme hydrolysis[35], etc. However, acid hydrolysis is currently still the most cost-efficient procedure to isolate CNCs on a large scale. Using this process, CelluForce Inc. in Canada is the largest CNC manufacturer in the world with a capacity of 1 ton/day.

2.1.4 Properties of cellulose nanomaterials

2.1.4.1 Specific surface area and aspect ratio

The specific surface area per unit mass increases with decreasing size of the material. The specific surface area can be calculated from the average geometric dimension of the nanoparticles, assuming the density of cellulose nanocrystal is around 1.5-1.6 g/cm^3. It's reported that the specific surface areas of CNCs and CNFs extracted from sisal are 533 and 51 $m^3 \cdot g^{-1}$, respectively[37]. There is a huge drop in the specific surface area with the increasing particle diameters, especially for diameters smaller than 20 nm (Fig.4). Differences in specific surface area are always accompanied with a change in the concentration of dispersion. Furthermore, the higher specific surface area of CNCs has enabled their use as a porous templet for the preparation of aerogels[38].

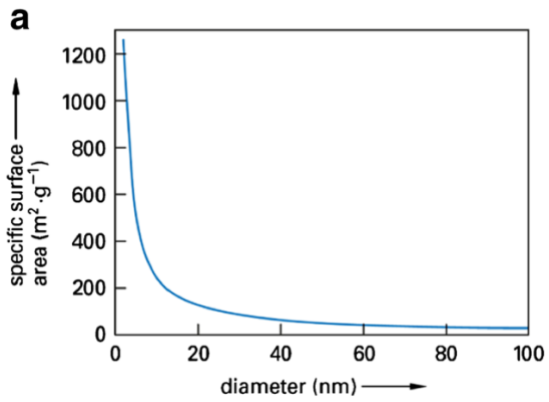

Figure 4. Evolution of the specific surface area of rod-like nanoparticles versus their diameter[39].

Another property that is also important to the application of cellulosic materials toward nanocomposites is the aspect ratio. This is mainly decided by the source of the cellulose fibers; some parameters of CNCs isolated from different biomass sources are listed in Table 1. The enhancement in mechanical properties of nanocomposites relies on the amorphous network connected by hydrogen bonds. The aspect ratio plays an important role in percolation theory, which is highly related to the reinforcing effect of the mechanical performance of nanomaterials. The percolation threshold is a critical volume fraction of the filler content at which the fillers form an infinite connected component, determining many of the characteristics of the film prepared by evaporation. Neto *et al.* reported the improved mechanical properties of natural rubber nanomaterial reinforced by high aspect ratio CNCs[40].

Table 1. Some common sources of CNCs extracted by acid hydrolysis and their characteristics

Sources	Length (nm)	Diameter (nm)	Aspect ratio (L/d)
Corncob[41]	198±51	5.5±1.9	37±14
Barley[42]	329±123	10±4	32
Southern pine[43]	77±12	9±2	8.5
Sugarcane bagasse[44]	96±39	7.5±2.3	13
Tunicates[45]	1720±514	25±6	69
Cotton[46]	171.6±48.2	14.6±3.9	11-12
Soy hull[40]	503±155	4.9±1.1	100

2.1.4.2 Mechanical properties

Mechanical properties of nanocomposites are their most important and well-studied asset. Compared to common-used fillers such as carbon black, silica oxide, clay, and metal oxide, CNCs possess a low density of around 1.5-1.6 g/cm, light weight, renewability, biodegradability, eco-compatibility, low cost, and reduced energy consumption and environmental pollution. Mariano *et al.* reported that the tensile modulus for native cellulose ranges between 56 and 220 GPa theoretically and experimentally[47], with an average modulus of 130 GPa and tensile strength of 10 GPa. Incorporation of CNCs dramatically increases the mechanical performance of resulting composites, resulting from the specific behavior of each phase, as well as the composition, morphology, and interfacial properties.

2.1.4.3 Thermal properties

Thermal properties such as thermal expansion coefficient (TEC), thermal conductivity, thermal stability, and glass transition temperature are other parameters that need to be considered in processing and manufacturing, especially regarding the properties of the final nanocomposites. The thermal expansion coefficient, the rate of expansion as a function of temperature, is calculated from a linear, volumetric, or area basis. The linear and volume TECs are shown below:

$$\alpha = \frac{1}{l}\frac{\Delta l}{\Delta T} \qquad \text{equation (1)}$$

$$\beta = \frac{1}{V}\frac{\Delta V}{\Delta T} \qquad \text{equation (2)}$$

Where l is the d-spacing parameter and V is the volume of the unit cell at low temperature.

Experimental results have shown that the linear TEC of native cellulose increases to 17×10^{-5} K^{-1} as temperature increase from room temperature to 200 ℃ along the axis, whereas the volumetric TEC still maintained the same value of 0.5×10^{-5} K^{-1}. For cellulose nanomaterial, a low TEC was observed due to the hydrogen bond network that is formed, along with the high crystallinity. This property can be applied to reduce the TECs of nanocomposites by reinforcing them with cellulose nanoparticles, leading to less thermal expansion at high temperatures. A study by Nakagaito *et al.* demonstrated that an MFC-reinforced phenol formaldehyde resin had a lower TEC of $10^{-5}K^{-1}$ with the addition of 40 wt% MFCs, compared with a TEC of 6×10^{-5} K^{-1} for the pure matrix [48]. Another thing that needs to be mentioned is the thermal stability of the cellulose nanomaterial, which determines the further processing of CNC nanocomposites, as well as their applications. Kim *et al.*

reported that the decomposition of cellulose crystallites in 1-hour isothermal treatment did not happen at 300℃[49] and completed at 340℃. However, after an acid hydrolysis step, the thermal stability of cellulose nanocrystals decreased due to the introduction of sulfuric groups. The previous work studied by Petersson *et al*. showed that the degradation temperature of CNCs prepared by MCC reduced from 320℃ to 240℃ in the nitrogen flow atmosphere[50].

2.1.5 Chemical modification of nanocellulose

Cellulose nanomaterials as a reinforcing filler in polymeric matrix have been extensively researched, and the dispersibility of nanoparticles in the polymer is critical to the physical and chemical performance of the final product. However, due to their inherent hydrophilicity, it is not easy to uniformly disperse CNCs in water-insoluble polymer. The aggregation caused by hydrogen-bonding induced in the nanocomposite is challenging for CNC-reinforced polymeric materials. To solve this problem, a chemical modification strategy is always used to introduce functional groups that can prevent self-aggregation and enhance dispersibility. The abundant hydroxyl groups of cellulose particles provide the possibility of green modification through chemical reactions to broaden the functions of the material.

"Green" modification has been investigated in the last decade, as harmful solvents will restrict the disposal of cellulosic nanocomposites. Several researchers have presented more ecofriendly, solvent-free, biocompatible, and biodegradable processes to modify CNC surfaces. During the CNC extraction process, CNCs can obtain different functional groups after acid hydrolysis. Sulfuric acid, which is the most commonly used acid for extraction, provides sulfuric groups for CNC particles. Hydrochloric acid has also been used to hydrolyze CNCs, only removing the amorphous cellulose and adding hydroxyl groups onto the CNCs' surface[51]. 2,2,6,6-tetramethyl-piperidinyl-1-oxyl (TEMPO) has also been reported as a treatment media to provide carboxylic acid groups. In addition to functional groups introduced onto CNC surfaces in the hydrolysis process, chemical modification can usually be classified into two categories: non-covalent surface modification and covalent surface modification.

2.1.5.1 Non-covalent surface modification

There are usually two ways to realize a non-covalently bound surface modification: adsorption of surfactant and utilizing the presence of negatively charged functional groups on CNCs. Thus, the modifiers and cellulose nanocrystal particles are connected through electrostatic attractions, hydrogen bonding interactions, or Van der Waals forces. Salajkova *et al.* have reported research on using electrostatic interactions to connect positively charged groups such as quaternary ammonium salts with long alkyl, phenyl, glycidyl, and diallyl groups onto TEMPO treated CNCs[52] To improve dispersibility and stability in nonpolar polymer, Heux *et al.* showed that incorporating Beycostat NA (BNA), a phosphoric ester of polyoxyethylene(9)nonylphenyl ether[53], onto CNCs increased the uniformity of their distribution in hydrophobic polymer. Recently, Torres-Rocha *et al*. reported using the block copolymer PPEGMA-b-PBuVIm and PS-b-PBuVIm to increase the compatibility of CNCs with hydrophobic polymer and their dispersibility in organic solvents[54].

2.1.5.2 Covalent surface modification

Covalent surface modification is a favorite method to achieve desired properties due to the excellent reactivity of CNC. It is generally realized through reactions with the hydroxyl groups on the CNC surface. It can be categorized into three types (shown in Fig.5): 1. the substitution of hydroxyl groups with small molecules such as TEMPO hypochlorite oxidation, epoxide, anhydride, chlorosilane, and halogenated acetic acid;2. “graft onto” strategy with a coupling agent (e.g., PEO grafted onto CNC); 3. “graft from” strategy with ring opening polymerization, atom transfer radical polymerization, and single-electron transfer living radical polymerization. (e.g., PCL grafted from CNC).

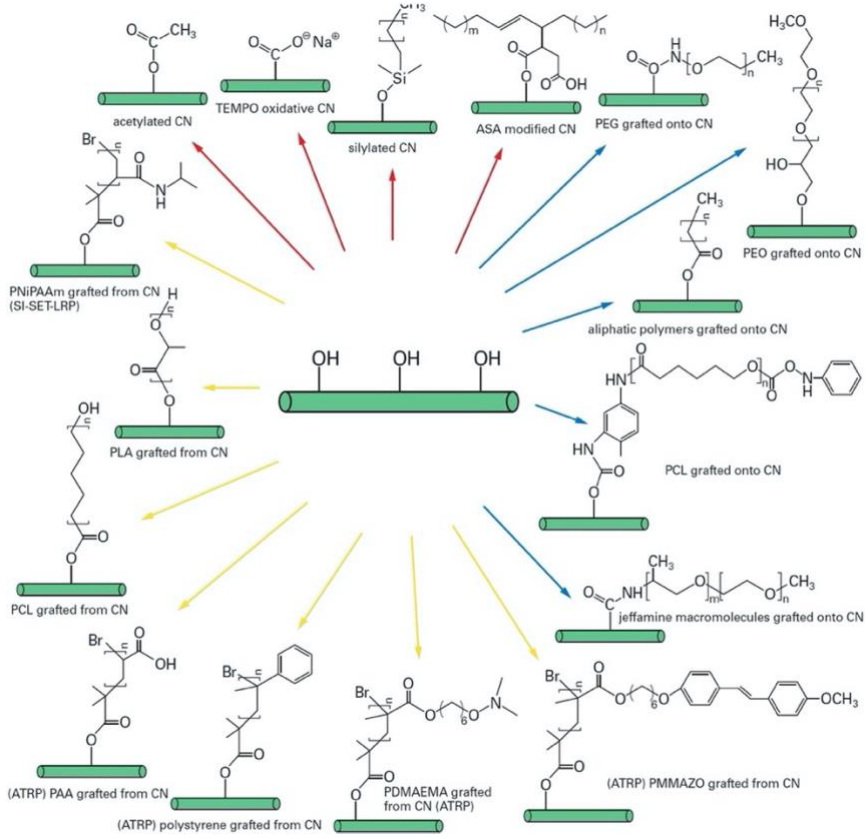

Figure 5. Commonly used examples of chemical modification of CNC[55].

2.2 Polyurethane

Polymers have been extensively used as promising materials in various industries due to their high transparency, flexibility, and durability, as well as their light weight and excellent mechanical performance, and can be seen in numerous aspects of our daily life. The versatility of polymers allows them to be applied in a wide range of products, including food packaging, textiles, electronics, aerospace, biosensors, and solar cells. Polyurethanes (PUs) are an important group that exhibits great mechanical and chemical properties due to their structure and the components used to fabricate them. Over the past three decades, use of polyurethane in a variety of applications has intensified due to its comfort, cost-effectiveness, energy efficiency, and potential environmental friendliness.

Polyurethane was first invented by German chemist Otto Bayer and his co-worker in the 1930s, then vastly improved and modified according to various requirements. Polyurethanes are obtained by the reaction of isocyanates $(R\text{-}N{=}O)_n$ and polyols$(R'\text{-}OH)_n$ to form urethane groups (-NH-

COO-)[56]. Therefore, a typical PU material always consists of functional groups containing urea, aliphatic or aromatic hydrocarbons, esters, ethers, and amides[57]. These functional groups enable PU to have properties of both thermosets and thermoplastics, combining softness, flexibility, rigidness, and toughness, giving PU the potential to replace metal, plastic, and rubber in general industrial manufacturing. After years of investigation and improvement, PUs can be applied in solar cells, textiles, biomedical devices, electronics, vehicles, and several other engineering products. Importantly, PU can be tailored to specific applications, such as coatings, adhesives, sealants, and elastomers, with desired properties like waterborne, thermoplastic, thermoset, rigid, or flexible[58]. Fig. 6 demonstrates commonly used categories of PUs, where the mechanical properties are determined by the combination of isocyanates and polyols[58]. Fig. 7 presents the structure-property relations between chain stiffness, interchain, crystallinity and degree of branching depending on the type of PU used. Normally, rigid foams have the highest degree of branching and chain stiffness, possessing excellent mechanical properties.

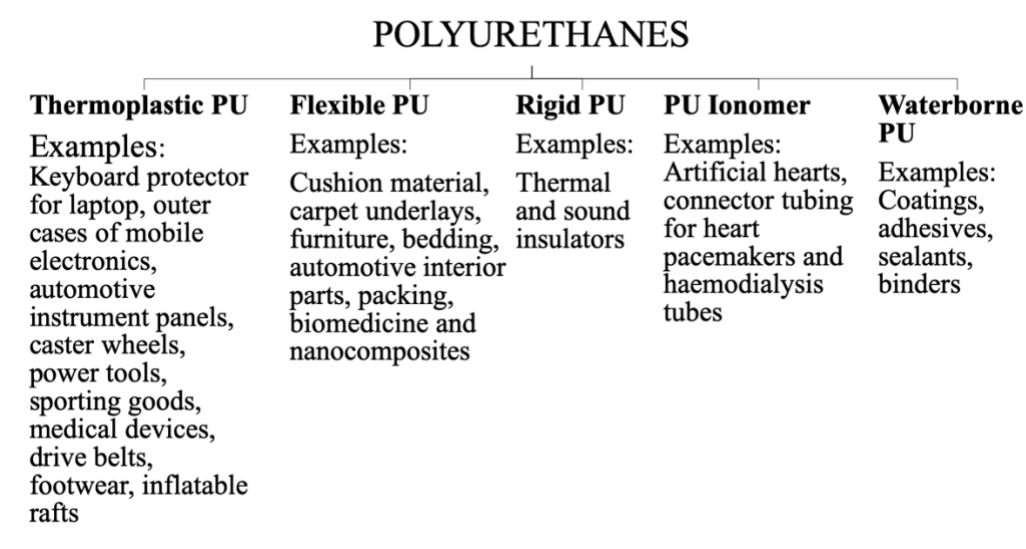

Figure 6. Categories of polyurethane most commonly used, along with their applications[59].

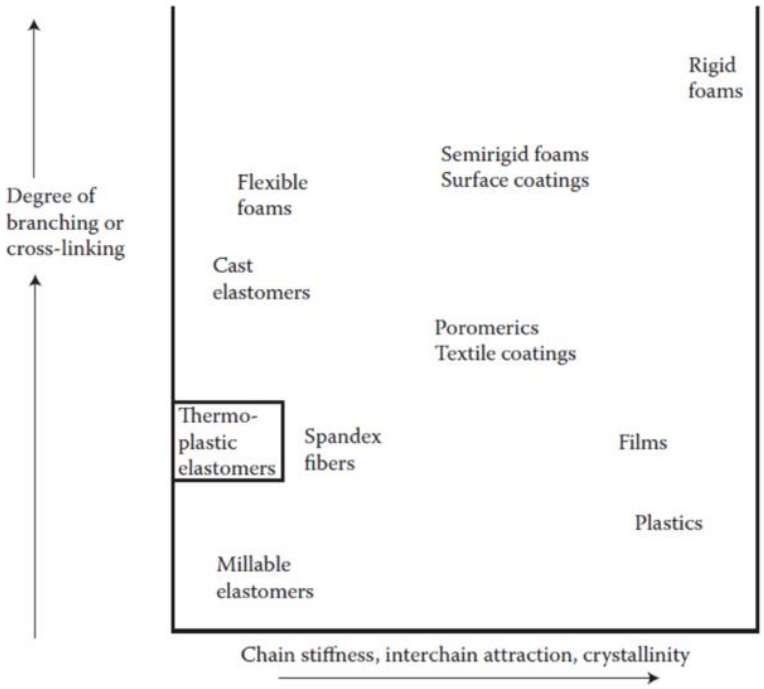

Figure 7. The structure-properties relationship between chains and cross-linking[58].

2.2.1 Chemistry of PU

PU is synthesized by polyols, diisocyanates, and chain extenders, which leads to the formation of strong covalent bonds like C-C, C-N, O-H, N-H, and C=O. These bonds always come from compounds including phenolics, unsaturated polyester, and epoxies[60]. The energy required to break the covalent bond has an influence on the degradation behavior and thermal properties of the PU product. Also, the exhibited properties rely on the secondary bonds present, for instance, van der Waals forces, hydrogen-bonding interactions, and dipole interactions. Fig. 8 illustrates the reaction to synthesize thermoplastic PU. The resulting polyurethane chain contains rigid regions and the soft regions; long chains from polyols serve as soft segments contributing to elasticity and flexibility, whereas short chains and high cross-linking from diisocyanates or chain extenders serve as hard segments. The different combinations of polyols and polyisocyanates and the incorporation of additives provide additional characteristics and expand the possibilities of PU.

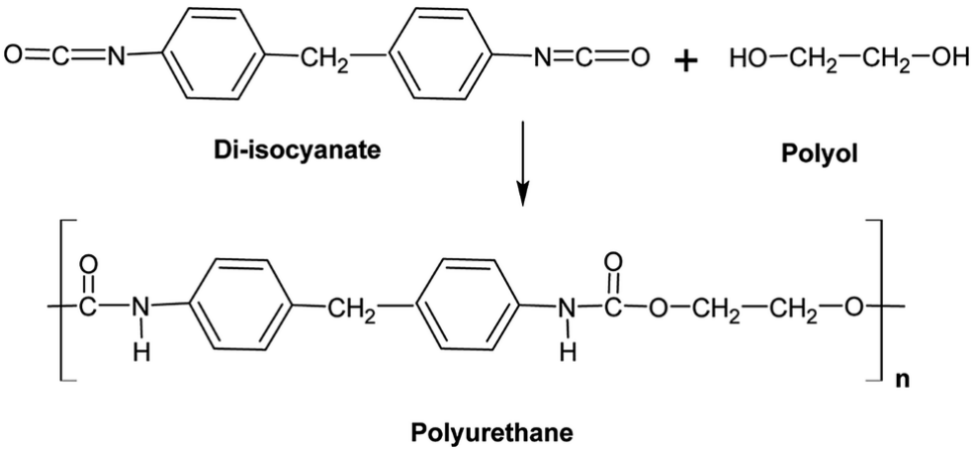

Figure 8. The common route for PU synthesis[59].

2.2.2 Types of polyurethanes

2.2.2.1 Polyurethane Foam (PUF)

Among all kinds of PU consumption, polyurethane foams account for 67% of the global PU market share in 2016 and took up half of the polymeric foams market[61]. There are two main types of polyurethane foam (PUF), rigid polyurethane foams and flexible polyurethane foams, which can be applied in a wide range of fields according to their features. Rigid polyurethane foams are one of the most common multi-purpose and energy-efficient insulation materials. One of the advantages of rigid polyurethane foams is that they are multi-purpose and save energy, allowing them to be used in many areas such as isolation, sealant, residuals with fewer energy costs compared to other forms of PU. Therefore, these foams have been used in walls, windows, roofs as insulators and sealants to maintain a stable temperature and reduce noise.

The preparation of rigid polyurethane foams can be realized by the reaction of hydroxyl groups and isocyanates, producing the urethane linkage, urea groups, and CO_2[62]. Urethane and urea moieties are correlated with the stiff segments of polyurethane foam, while polyols constitute the soft segments. Therefore, the higher the isocyanate content, the more rigid segments there are, making PUF stiffer. However, methylene diphenyl diisocyanates and toluene diisocyanate, two well-known diisocyanates, are harmful to the environment and health, which is still one major limitation of rigid polyurethane foams.

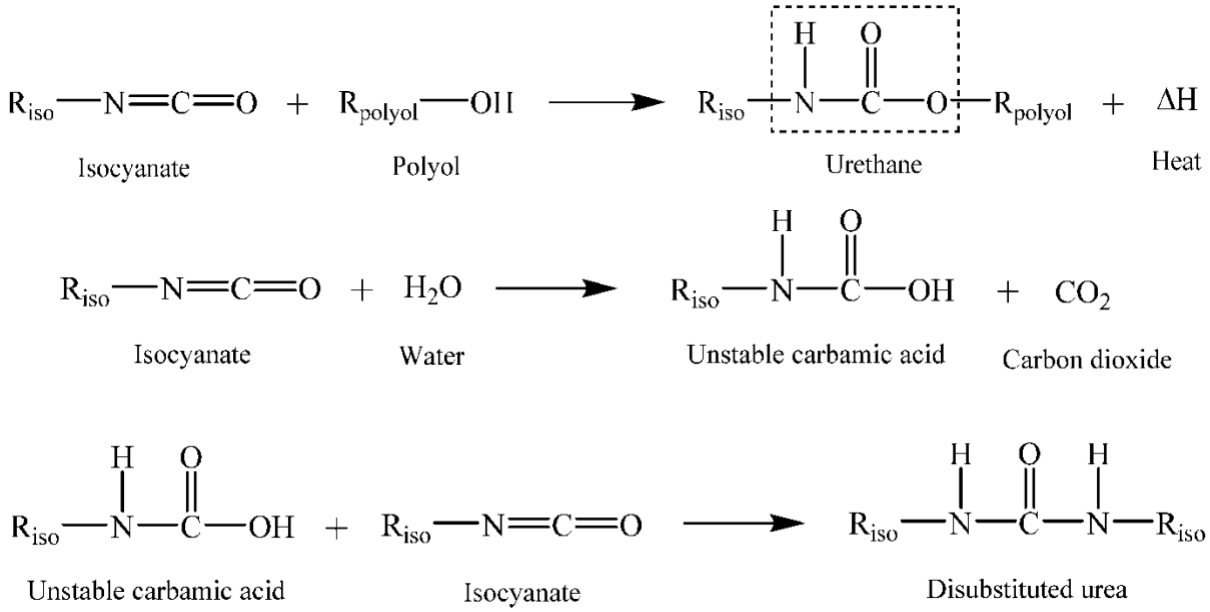

Figure 9. The reaction scheme of urethane production and isocyanate with water[68].

Flexible polyurethane (FPU) foams consist of several block copolymers whose flexibility is rooted in the phase separation of the flexible and rigid regions. They can be classified as flexible PU based on a series of physical properties; for instance, in respect of density, durability, rigidity, tear resistance, surface elasticity, etc[64]. FPUs can be used in a wide range of commercial and engineering products such as furniture, packing material, automotive interior parts and biomedicine[65,66].

The microstructure and morphology of FPUs are decided by several factors in terms of the mobility of urea groups, degree of cross-linking after the reaction, etc. Also, when the NCO/OH ratio is reduced, the cross-linking density is lower, obtaining a highly flexible PU foam. Another factor is the incorporation of soft chain segments from the chain extender, which results in a lower T_g. However, the high combustibility of FPUs is a problem for disposal, as they can emit large amounts of CO_2, NO_x, and HCN. As such, better recyclability and flame retardancy properties need to be discovered.

2.2.2.2 Thermoplastic PU (TPU)

Thermoplastic PU represents another category of polyurethane that exhibits great flexibility, transparency, mechanical properties, abrasion, and impact resistance. Similar to other

thermoplastic polymer materials, TPU can be processed by extrusion, blow molding, compression, and injection moulding equipment[67]. The chemical structure of TPU consists of stiff segments in a continuous phase of soft segments. Typically, polyesters or polyethers with molecular weights of 1,000-10,000 g/mol are the source of the long, flexible soft segments, whereas the hard segments consist of 4,4'-methylene diphenyl diisocyanate (MDI) or its hydrogenated form (HMDI), connected by various chain extenders[67]. The thermodynamic incompatibility of these two components accounts for immiscibility between hard segments and flexible segments, producing a microphase-separated polymer. This resulted in an elastomer with outstanding physical and chemical properties: excellent tensile strength, wear resistance, crack resistance, intrinsic lubricity, and biocompatibility[68,69]. Strong intermolecular hydrogen bonds are also formed, which are attributed to the urea moieties in hard segments; these segments provide a superior tensile strength to the material, while the soft segments, with a lower T_g, contribute to the polymer's flexibility and elasticity[70].

Usually, there are two methods to synthesize TPU. The first type, one-step reaction, involves mixing raw material with proper ratios together in a mold of the desired shape to realize the reaction. As for the two-step reaction approach, the polyol and diisocyanates are reacted first to produce a prepolymer terminated by the isocyanate group, followed by reacting with chain extenders as a short diol. Both approaches have their own benefits; the one-step reaction can form a more random block polymer with a high polydispersity (PDI), whereas two-step polymerization generates a polymer with a high molecular weight but low polydispersity. The one-step synthesis is a more suitable for coatings, automotive, building, adhesives, and textile applications[70].

2.2.2.3 Waterborne polyurethane

Waterborne PUs (WPU), like many other waterborne polymers, have received increasing attention and are seen as a promising alternative to solvent-based coatings due to their excellent performance, versatility, and biocompatibility[71]. Increasingly restrictive environmental legislation regarding volatile organic compounds (VOCs) motivated the development of these high-performance waterborne coatings. WPUs are principally used in wood coatings, fabric coatings, leather coatings, fiberglass sizing, and automotive interior coatings.

Waterborne polyurethanes consist of two key components: the primary structure and the hydrophilic or amphiphilic emulsifier. The commonly employed emulsifiers are divided into two types, external and internal, which govern the properties of polyurethane hydrophilicity. The diol generally serves as an emulsifier due to its ionic groups, such as carboxylic, sulfonate, or quaternary ammonium salts[71]. Therefore, WPUs possess both the good dispersibility of ionomers and the great mechanical properties of PUs. The performance of water-based polyurethane dispersion depends highly on the polyols, isocyanates, ionomers, and chain extenders employed in the synthesis. As polyurethane is hydrophobic in nature, it is the incorporation of hydrophilic segments into the polyurethane chain that enable the dispersion of polyurethane in water.

2.2.3 Synthesis of waterborne polyurethane

There are several methods for synthesizing water-based PU, for instance, pre-polymer or emulsification, acetone process, hot melt, etc. Isocyanate-terminated (NCO) pre-polymer is normally employed in synthesizing WPU in the pre-polymer/emulsification approach due to its inactivity in water. The chain extension happens in the heterogeneous phase and the diisocyanates disperse in the aqueous phase. To ensure the method is prepared successfully, the temperature should be kept lower than the critical point where NCO groups react with water. It is critical to precisely control the viscosity and functionality of the mixture as well. The first step in synthesize is the reaction of prepolymer, usually medium molecular weight polymer, with polyols containing polyester and polyether. Next, the ionomer is introduced to the aqueous mixture as an internal emulsifier. An organic solvent like N-methyl-2-pyrrolidone (NMP) is then added to decrease the viscosity and achieve dispersion in water. The steps involved in the pre-polymer approach are demonstrated in Fig. 10.

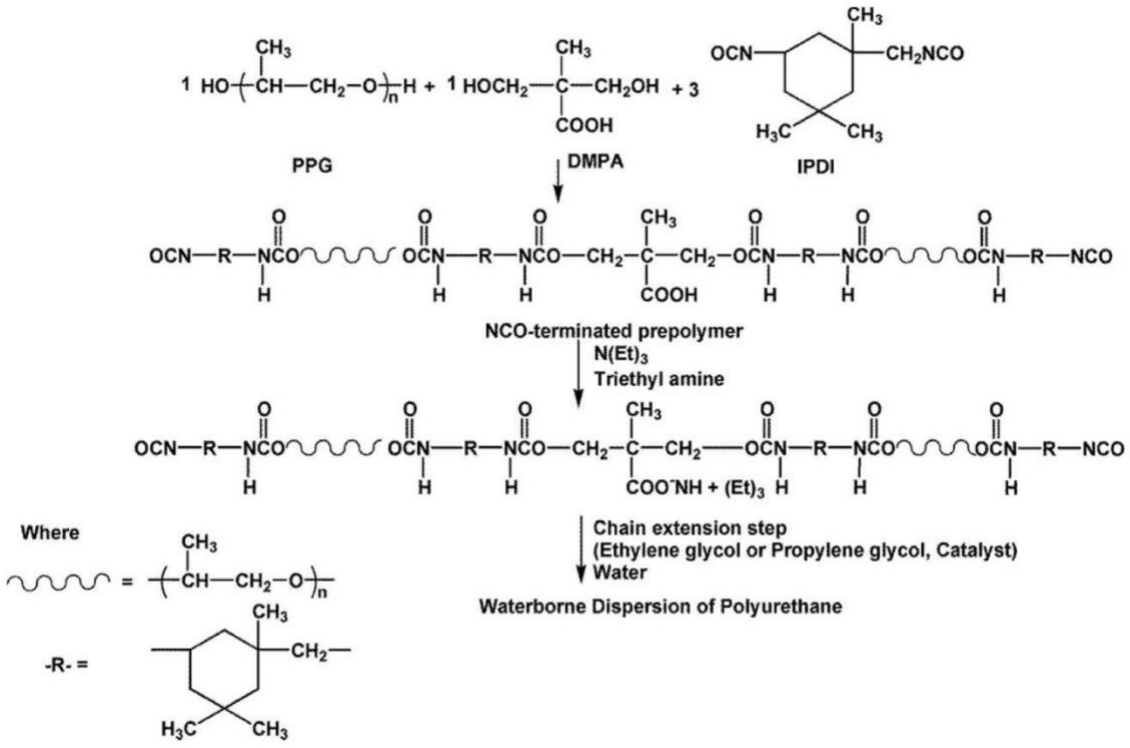

Figure 10. The reaction scheme of fabricating WPUs via pre-polymer method[72].

The acetone process is another method that is also broadly used for WPU preparation. The acetone process is usually carried out in a homogeneous solution for formation of polyurethane. Acetone is suitable to serve as the liquid medium because it is not reactive to isocyanate, it is inert regarding the polyurethane-forming process, and its boiling point is relatively low which means it is easily removed by a solvent evaporation step. Another benefit of acetone is that it lowers the reaction rate of the chain extension step, helping to control the viscosity (which, as mentioned before, is important to the synthesis). Acetone is also a suitable choice in the chain extension step to obtain a solvent-free product; however, the usage of high quantities of acetone and the additional distillation step lead to extra energy and commercial costs, which is not desirable economically for large-scale production[73,74]. The acetone process is generally applied in industrial manufacturing of waterborne polyurethane. The prepolymer approach is usually applied for the preparation of coating material, whereas the acetone approach is typically for adhesive applications.

Hot melt is a solvent-free method for the preparation of polyurethane dispersion. The prepolymer with NCO groups is reacted with urea to form biuret (-(HN-CO-)$_2$N-) groups. This prepolymer is then dispersed in water and reacted with formaldehyde. Then, a condensation reaction forms polyurethane-urea[58,75]. The hot melt method is always employed to synthesize WPU with low molecular mass. In this process, the control of formaldehyde reaction is challenging; side reactions of urethane groups can and do happen. Therefore, this process produces polyurethane dispersions with polymeric performance that is significantly different from those synthesized with the acetone process.

2.2.4 Components in PU synthesis

2.2.4.1 Isocyanates

Isocyanates are indispensable components in the synthesis of polyurethane. They can be categorized as difunctional or heterobifunctional and aromatic or aliphatic compounds. Aliphatic isocyanates are extensively used in waterborne polyurethane synthesis due to their poor reactivity with water, ultraviolet stability, and resistance to hydrolytic degradation. In contrast, aromatic isocyanates can provide better mechanical properties due to the benzene ring, with the most commonly used ones being methylene diphenyl diisocyanate (MDI) and toluene diisocyanate (TDI). MDI and TDI are widely applied in the production of polyurethane foams and elastomers. To solve the issues of toxicity and volatility, isocyanates may be modified by reacting with polyols, which decrease their freezing point, making the material easier to handle. Environmental issues caused by diisocyanates are always a concern in the research and further application of waterborne polyurethane. Potential alternatives or substitutions have been less investigated than polyols. However, a new type of non-isocyanate polyurethanes (NIPUs) has been reported[76] that use cyclocarbonate oligomer instead of toxic isocyanate. This type of NIPU has better chemical resistance, less water sensitivity, lower porosity, and higher thermal stability with potential applications as sealants, coatings, and foams[77].

2.2.4.2 Polyols

Polyols used in WPU synthesis can be generally classified into polyesters or polyethers. Various polyols that can be used lead to different mechanical properties. Polyols with high M_w of 2000-

10000 are utilized for the preparation of soft, elastic, and flexible PU, whereas polyols with lower M_w and high functionality are more frequently used in the synthesis of rigid PU. PUs obtained from polyether polyols are known to have excellent physical properties such as flexibility and stretchability, excellent resistance to impact, and low temperature of hydrolysis as well, with their low costs a further asset. WPUs produced by polyesters have great solvent, cutting, and abrasion resistance. To combine the beneficial physical properties and increased tensile strength, one common method is to mix two types of polyols. Researchers reported a new synthesis route for poly (ether ester) polyols, demonstrating that the resulting PU products have superior physical properties and better hydrolytic stability compared with PUs prepared by polyester or polyether polyols alone[78].

2.2.4.3 Catalyst

The selection of catalyst determines the reaction rate of isocyanates and polyols. There are two categories of commonly used catalysts: amine catalysts and metal compounds. The amine catalyst has the ability to accelerate the urethane, urea, or isocyanate trimerization reactions. Amine compounds incorporated into PU contain tertiary amines, for instance, dimethyl cyclohexylamine (DMCHA), dimethylethanolamine (DMEA), 1,4-diazabicyclo [2,2,2] octane (DABCO), and triethylenediamine (TEDA). Typical metal complex catalysts include zinc, tin, lead, bismuth, and mercury. However, there is research that has demonstrated that both amine and metal catalysts are toxic and hard to remove from PU products.

2.2.4.4 Other components

In addition to the primary components described above, other components are also involved in the preparation of waterborne polyurethane. The most important of these is the chain extender or crosslinker, which provides better physical properties of resulting elastomers, coatings, or adhesives; these substances are always terminated with hydroxyl or amine groups. For the crosslinker, hard segment urethane usually servers in this role, connecting the domains of flexible segments in rigid polyols. Sometimes, the chain extender can decide the chemical properties, heat resistance, wear resistance, and tensile properties. Another important component is the ionic group, which is the key to enable water-based polyurethanes. The concentration of ionomer (anionomer, cationomer, and zwitterionomer) incorporated in PU governs the water solubility or dispersibility,

higher concentrations of ionomer enhance the solubility, while lower concentrations of ionic groups can improve the dispersibility. Surfactants are another potential component, and are normally applied to modify the properties of foam PU polymers. The introduction of surfactant can emulsify the liquid phase, regulate the cell size, and stabilize the cell structure. Some defects such as sink marks, uneven surfaces, or pinholes can be solved by adding a surfactant, and air releasing and degassing can be achieved as well. However, side effects from surfactants have been observed, such as decreased resilience against delamination and corrosion. Table 2 lists the most common components that are frequently applied in classical PU synthesis and the reasons for their inclusion.

Table 2. Components frequently involved in PU synthesis and their functions.

Additives	Purposes
Isocyanate[79]	Responsible for the PU reactivity and curing properties
Polyols[80]	Provides soft segments, offering flexible elastic polyurethanes
Catalysts[81]	Accelerates the reaction between the diisocyanates and polyols and optimizes the reaction conditions
Plasticisers[67]	To decrease product rigidness
Cross-linkers/chain extenders[82,83]	Network modification of the PU molecule and offer mechanical support that will enhance the material properties

2.3 Vitrimer material

2.3.1 Epoxy resin

There are two types of polymers: thermoplastic and thermosetting. Thermoplastic polymers (e.g., polyethylene, polyvinyl chloride, etc.) are linear macromolecules whose molecular chains are not chemically bonded to each other. The thermoplastic material will melt with increasing temperature and become rigid when cooled down. This process is a physical change and can be repeated, i.e., repeated heating and cooling for reprocessing. However, thermoplastic polymers have poor thermo-mechanical properties and cannot be used in many fields. Thermoset materials (e.g., epoxy

resins, silicones, etc.) are the opposite, with excellent mechanical properties, pressure resistance, and thermal stability. However, thermosetting materials become stiff due to cross-linking reactions (chemical reactions) during the first processing and molding, and this change is irreversible. The cross-linked three-dimensional network structure has the property of being insoluble and infusible. Therefore, once the thermoset material is processed and molded, it cannot be processed again, and its issues related to aging, recycling, and damage not only cause waste of resources but also make disposal difficult.

Epoxy resins are a class of three-dimensional cross-linked thermosetting polymers that cannot be reprocessed after curing and molding. Epoxy resin refers to a molecule containing two or more epoxy groups, and the curing agent can form a three-dimensional cross-linked network of the compounds. Epoxy resin molecular weight is in the oligomer range, in contrast to cured epoxy resin, which is sometimes also known as epoxy prepolymer. There are many types of epoxy resins, and they can be divided into glycidyl ether, glycidyl amine, glycidyl ester, and alicyclic resins according to their chemical structure (shown in Fig. 11). Among them, bisphenol A diglycidyl ether epoxy resin, occupies about 80% of the market share, mainly because bisphenol A diglycidyl ether cured products have the advantages of good adhesion, low curing deformation rate, good stability, good mechanical properties and excellent electrical properties. The uncured epoxy resin is a polymeric prepolymer with thermoplastic properties; it has almost no use value and cannot be used directly alone. Only after cross-linking reactions with various curing agents at room temperature or under heating conditions, forming a three-dimensional cross-linked insoluble and non-fusible thermosetting polymer, can the epoxy resin become an applied material (with the properties of common materials) and demonstrate a value for use.

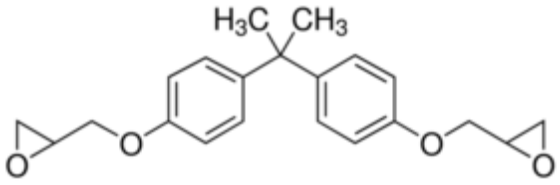

Figure 11. Figure 11. Chemical structure of BADGE.

Commonly used curing agents include amines, anhydrides, carboxylic acids, etc. Most curing agents require higher temperatures (above 100℃) to cure and cross-link with the epoxy prepolymer; only a small number of amine-based curing agents can be cross-linked at room temperature. High temperature curing goes through two stages: the first is pre-curing to a gel state or slightly above the gel state; the second is to continue curing at high temperature to the fully cross-linked state. The induction effect causes the oxygen atom of the epoxy group to be enriched with more negative charges and the terminal carbon atom to be enriched with more positive charges. The resulting dissociation of positive and negative charges allows the epoxy group to undergo addition reactions with both anhydrides (electrophilic reagents) and amines (nucleophilic reagents), resulting in ring-opening polymerization of the epoxy group. Most curing agents are involved in the addition polymerization reaction, i.e., the curing agent itself becomes part of the final three-dimensional network structure.

2.3.2 Vitrimer material

In recent years, researchers have introduced ester exchange reactions into acid-cured epoxy resin systems, resulting in a third type of polymer that is insoluble, but can flow: vitrimers, which combine vitreous and polymer and exist between thermoplastics and thermosets. In 2011, French chemists Leibler *et al.* introduced ester exchange dynamic covalent bonding into the crosslinking network of epoxy resins obtained by reacting epoxy prepolymers with acids or anhydrides[84]. At high temperatures, rapid ester exchange reactions cause the topology of the network to change and rearrange, resulting in a viscoelastic and fluid material.

When the temperature is higher than the ester exchange temperature in the system, the topology of the cross-linked network changes, making the material flow at high temperatures, enabling capabilities for recycling and repairing damage. However, many of the current vitrimers (including ester exchange, urethane exchange, and complex decomposition reactions) do not possess excellent mechanical strength and are elastomeric at room temperature, limiting their use in load-bearing structural materials.

In a similar vein, since the introduction of microencapsulation technology by White *et al*., research on self-healing has developed rapidly in the last 20 years[85]. Self-healing techniques are divided into two main categories: external and intrinsic. The external self-healing method is realized by phase transformation from solid to liquid of a repair agent in the matrix. When materials are cured under certain treatments such as heating, light, humidity, and catalysts, the repair agent can flow out from the matrix and then solidify to heal the cracks and damages. The biggest problem with external self-healing is that it cannot achieve repetitive repair at the same damage point. Although the hollow fiber and micro-vein fiber systems developed later have some repetitive repair capability, the addition of such brittle fibers encapsulated with repair agents greatly reduces the physical strength of the vitrimer materials and limits their long-term and heavy-duty applications. This idea was first proposed by Hayes *et al.* in 2005, and a linear thermoplastic copolymer of bisphenol A and epichlorohydrin was synthesized[86,87], which had almost the same structure as bisphenol A and was easy to blend into the epoxy resin matrix. By adding 20 wt% of the copolymer, the material could be restored to 75% of its original properties after fracture; amounts as low as 5 wt% of the copolymer already demonstrated repair-capable properties, but with a very low repair efficiency.

2.3.3 Dynamic covalent network

The cross-linked network of vitrimer contains exchangeable chemical bonds. Exchangeable links are dynamic covalent bonds, which are stable in general but can be reversibly broken and regenerated under specific conditions[88]. When dynamic covalent bonds are used in the synthesis of polymeric materials, the resulting dynamic covalent polymers (DCPs) can exhibit stability similar to that of polymers composed of conventional nonreversible covalent bonds under certain conditions, but also have dynamic properties like supramolecular polymers under certain stimuli, i.e., structural and compositional reorganization can take place under appropriate conditions, even after polymerization. A variety of dynamic covalent bonds have been applied to the synthesis and application of polymeric materials, such as ester bonds, disulfide bonds, imines, Schiff bases, etc[89-104]. While the chemical structure and material properties remain intact, the exchange reaction between different cross-linking points changes the topology of the network, which can be called covalent adaptable networks (CANs)[88,105,106].

CANs can be further divided into two types by their mechanism of exchange. One type of dissociative CANs presented in Figure 10a is those with reduced crosslinking sites (first broken, and then generated at different sites), which temporarily decrease in crosslinking site density under certain conditions, as if the polymer network is depolymerizing. The most typical example of this class is the crosslinking network based on the Diels-Alder reaction, which is a reversible reaction; the temperature of the forward ring formation reaction is relatively low, and increasing the temperature results in a reverse decomposition reaction that exhibits a significant increase in the rate of bond breakage and reformation. As such, when a material containing the Diels-Alder reaction is heated, the cross-linking point density decreases due to the reverse movement of the reaction; the molecular chain segments are unimpeded and move quickly, the topological network rearranges rapidly, and the viscosity drops abruptly. However, after cooling down, the crosslinking points are recreated and the final crosslinking point density is almost the same as the initial one, so that the material has the initial mechanical properties (e.g., strength, hardness, and tensile properties) again.

The other type of associative CANs presented in Fig. 12b is associative CANs, which exhibit fixed crosslinking sites, where the crosslinking point density remains constant as the network changes. Only after new covalent bonds are formed do the former covalent bonds break, and therefore the network does not decouple. This network is like a dynamic body that keeps the structure and properties of the material intact during the exchange reaction. In 2011, Leibler and coworkers synthesized a vitrimer based on the associative CANs mechanism by adding transesterification catalyst to an epoxy/acid or epoxy/anhydride polyester-based system, realizing a thermally triggered transesterification system[84]. The new network exhibited a gradual decrease in viscosity with rising temperature, which is a performance distinctive to vitreous silica[107].

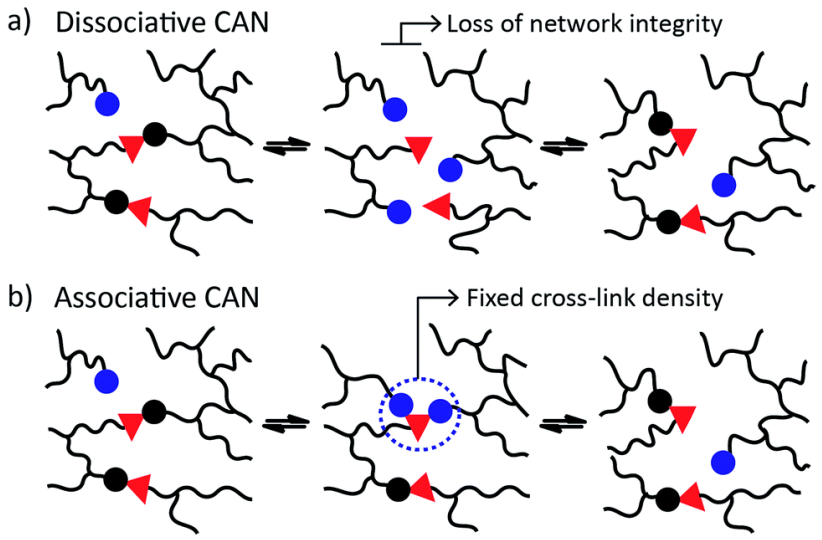

Figure 12. Mechanism of two types of CANs[108].

2.3.4 Epoxy resin-based vitrimer

For vitrimer materials, the topological network of epoxy resin-based vitrimers are fixed when below a certain temperature; however, above this temperature, the rapid ester exchange reaction allows the topological network to show viscoelastic behavior. There are usually two characteristic transition temperatures. The first temperature is similar to the T_g in that it allows polymer chain segments to change reversibly between rubbery and glassy states, correlated to the onset of long-range, coordinated molecular motion.

In addition to the T_g, there is also a temperature similar to T_g that results from the cross-link exchange reaction and rearrangement of the topological network. This temperature is defined by Leibler as the topology freezing transition temperature (T_v); to determine this temperature, according to Leibler, the transition of a topological network is usually considered to occur when the viscosity of material reaches 10^{12} Pa[84,109].

Similar to amorphous polymers, vitrimers undergo a transition between glassy, elastomer, and viscoelastic flow states with increasing temperature. The relation between the two temperatures detailed above can be categorized into two types. For most vitrimeric systems, T_v is higher than T_g. In these systems, when T is lower than T_g, the vitrimer is in a glassy state, and neither the molecular chains nor the chain segments can move; only the atoms (or groups) of the molecule are

vibrating at their equilibrium positions. When the temperature rises above T_g, the molecular chains cannot move, but the chain segments start to move to the rubbery state and exhibit elastic behavior; when temperature rises above T_v, the molecular chains become mobile and the exchange reaction is accelerated. When the time required for the exchange reaction is shorter than the time required for material deformation, the topology of the cross-linked network can be rearranged and begins to flow, similar to the viscous flow state of amorphous polymers, which is dominated by cross-linking movement kinetics that conform to the Arrhenius equation as the temperature increases, i.e., its viscosity decreases linearly with the increase of temperature.

For the second type of system, the T_g is higher than T_v. For these systems, when the temperature is between T_g and T_v, the exchange reaction is difficult to proceed because the polymer chain segments are still fixed; when the temperature continues to rise above T_g, the polymer chain segment movement allows the exchange reaction to occur rapidly. In this case, the viscosity of the glassy polymer is controlled first by the diffusion law, exhibiting Williams-Landel-Ferry behavior for thermoplastic polymer melting. With further heating to a certain T, the exchange kinetics change from diffusion controlled to exchange kinetic controlled, which conforms to the Arrhenius law (presented in Fig. 13).

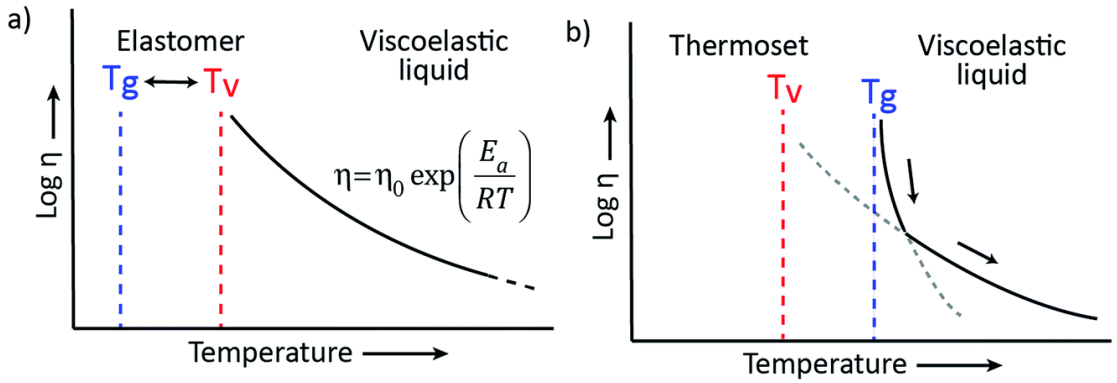

Figure 13. The representation of the viscoelastic behavior of vitrimer with a) T_v>T_g. b) T_g>T_v.[108]

When designing the synthesis of glassy polymers, it is usually important to consider both transition temperatures and the factors that affect them, such as crosslinking density, rigidity of the reacting monomer, the kinetics of the exchange reaction (catalyst content, type, etc.) and density of exchangeable bonds or groups. In order to achieve a wide range of applications, glass-like

polymers should have a wide temperature range for use like traditional thermoset materials, where the network can be reconstituted only in a specific temperature range.

2.3.5 Vitrimers chemistry

2.3.5.1 Carboxylate transesterification

Ester exchange reaction is a reaction between an ester and alcohol (or acid or ester) under catalyst (acid or base) or heating conditions to produce a new ester and new alcohol (or acid or ester), as shown in Fig. 14. Ester exchange reactions catalyzed by alkaline catalysts (e.g., amines, organophosphorus catalysts) are characterized by mild reaction conditions, fast reaction rates, low dosage, and less corrosiveness to the reactor vessels than acid catalysts. Therefore, alkaline catalysts are currently the most widely used catalysts for ester exchange reactions. While the conditions of base-catalyzed ester exchange reactions in past studies were usually harsh and required enhanced reflux of alkali (e.g., potassium methanol) in toluene to complete the reaction, the ester exchange reactions in recent studies are catalyzed by special alkaline catalysts (e.g., 1,5,7-triazabicyclo[4.4.0]dec-5-ene (TBD), $Zn(OAc)_2$, etc.) and can occur rapidly at high temperatures.

Leibler originally developed the concept of vitrimers on the basis of the ester exchange reaction. For this original concept, BADGA is cured with an anhydride or aliphatic dibasic acid (molar ratio 1:1) in the presence of an ester exchange catalyst ($Zn(OAc)_2$, $Zn(acac)_2$) to obtain thermosetting epoxy resins. One portion of the epoxy group reacts with one portion of the carboxyl group to produce one portion of the ester group and one portion of the hydroxyl group, leading to a large number of ester bonds and hydroxyl groups in the three-dimensional network, both of which will undergo ester exchange reactions during curing and any reprocessing processes after molding. The obtained glass-like polymers have the same excellent properties as ordinary thermosets at room temperature due to the very slow ester exchange reaction; however, at high temperatures (above T_v), the rapid ester exchange reaction causes the structural rearrangement of the cross-linked network, thus realizing the reprocessability, recyclability, and weldability of the thermosets after molding[110,111].

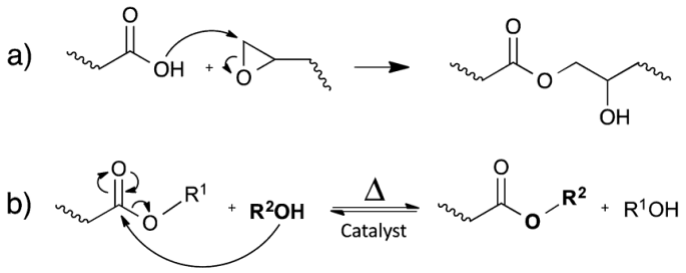

Figure 14. a) the reaction between epoxides and carboxylic acids. b) the catalytic transesterification[109].

Hillmyer *et al.* have synthesized and prepared isocyanate-based ester exchange glass polymers[112]. In this system, $Sn(Oct)_2$ was employed as a catalyst to catalyze both the polymerization and the ester exchange reactions. Because the cross-linking network possesses a large number of ester groups or potentially higher catalyst activity compared to epoxy resin-based vitrimer, the relaxation time of isocyanate-based vitrimer is extremely short. The ratio between isocyanate and hydroxyl groups can be arbitrary, and the relaxation time is still very short even when there is only a very small amount of free hydroxyl groups. It can be seen from this system that, in addition to the number of free hydroxyl groups, the content of ester bonds also greatly affects the relaxation time[112].

2.3.5.2 Transamination of vinylogous urethane

Prez *et al*. reported a vinylogous urethanes class of vitrimer that can undergo transamination reactions without catalyst[113,114]. This class of vitrimer can be made by spontaneous condensation reactions of acetoacetates with secondary amine monomers. From a thermodynamic perspective, the C-N bond exchange reaction is similar to that of amide or ammonia ester bonds, since the exchange process generates C=C intermediates, and the C=C bond forms an electronically conjugated structure with the carbonyl group (vinylogy principle). Therefore, the excess free amine in the crosslinking network can undergo transamination when the equivalence ratios of the reaction materials are different (Fig. 15). Because of the higher density of polyurethane in the system and the lower activation energy (60 kJ/mol), the relaxation time of poly(m-vinylamine) vitrimer is much shorter than that of epoxy resin glass polymers (~3 min relaxation at 150℃)[114].

Despite the excellent properties of vinylogous urethane vitrimers, the excessive amounts of amines in the cross-linked network make their stability vulnerable to oxidation, which is a potential threat to the long-term application of the material.

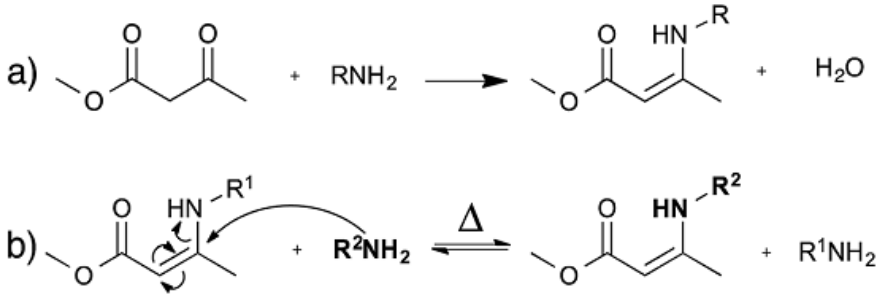

Figure 15. Synthesis of vinylogous urethane[109].

2.3.5.3 Transalkylation of triazolium salts

Recently, Drockenmuller *et al.* reported a novel vitrimer material based on a transalkylation reaction[115]. These polymers were synthesized by a one-pot polyaddition of α-azide-ω-alkyne monomers with bifunctional alkylating reagents (e.g., dibromo- and diiodo alkane or alkyl mesylates) followed by a simultaneous cross-linking step, as shown in Fig. 16. The resulting cross-linked networks contain long chain with substituents of 1, 2, 3-triazolium salts, triazolines, and alkyl halides. The activation energy of the exchange reaction of the triazolium salt glass polymer is 140 kJ/mol, and the stress relaxation time follows the Arrhenius law. The relaxation time of the network is short (30 min) when the temperature is at 130℃; when the temperature is increased to 200℃, the relaxation time is shortened further to only a few seconds. The relaxation time of triazolium salts vitrimer can be controlled by different counter ions, which lead to a faster stress relaxation ($Br^- >> I^- > MsO^-$). At present, the mechanism of the transalkylation reaction is not clear, with Fig.16 illustrating the speculated possible mechanism.

Although the polymerization reaction of triazolium salt polyionic network has the advantages of being simple, solvent-free, catalyst-free, one-pot synthesis, and the potential of forming conductive polyionic materials, the issues of low scalability, high cost, and hazardous raw materials (azides, alkylating reagents) of these vitrimers are not conducive to large-scale production compared to the previous two classes of vitrimers.

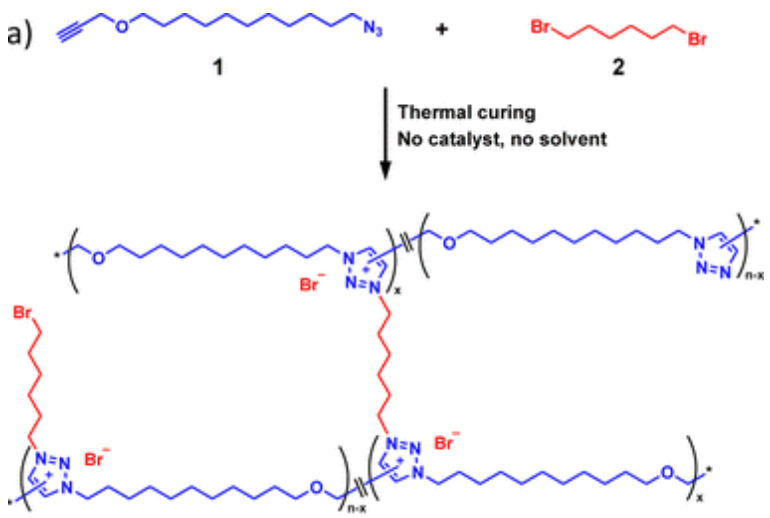

Figure 16. Polymerization of α-azide-ω-alkyne monomers with bifunctional alkylating reagents[115].

2.4 Polymer nanocomposites

Considering solvent-free polyurethane, its mechanical properties, heat stability, and hydrolytic strength are decreased compared to conventional polyurethane. As such, nanoparticles have been incorporated as reinforcing agents to obtain better chemical and physical properties from water-based polyurethane. Hydrogen bonds and van der Waals forces are mainly involved in the polymer chain, determining the cohesive energy, which includes inter-and intra-molecular hydrogen bonding interactions between polymer chains. The cohesive energy density (CED) can be estimated by:

$$c = \frac{\Delta H_{vap} - RT}{M/\rho} \qquad \text{equation (3)}$$

Where M is the molecular weight, R is the gas constant, ΔH_{vap} is the vaporization heat, ρ is density, and T is the absolute temperature. The higher cohesive energy density comes with higher polarity, which means the polymers have stronger intermolecular hydrogen bonding interactions with materials such as cellulose. The squared root of the CED, also known as the Hildebrand solubility parameter, is also used to estimate the solubility of polymers. The introduction of polar agents or functional groups increases the intermolecular hydrogen bonding, leading to better mechanical properties. Another factor that also affects the performance of nanocomposites is crystallinity. The degree of crystallinity depends on the intermolecular forces and the stiffness of the backbone chain due to better packing density and the increasing number of secondary bonds.

Both higher crystallinity and stronger intermolecular forces benefit the physical strength of the material. In contrast, a large size of side groups makes the polymer harder to arrange along the crystal growth direction, reducing the crystallinity[25].

2.4.1 CNC nanocomposite processing

Since nanocellulose tends to self-aggregate because of the hydroxyl groups on the surface, recent researchers have focused on optimizing the methods of fabricating cellulosic nanocomposites. The main methods are melt processing, in situ polymerization, and solvent cast and evaporation.

2.4.1.1 Melt processing

Melt processing (extrusion, or resin transfer molding) is widely applied in many types of bio-nanocomposites, like PBAT-grafted nanocomposites[116], PLA-based nanocomposites[117], etc. This process requires high external forces to facilitate the dispersion of nanoparticle materials into the melted thermoplastic polymer[118]. The main drawback of this approach is caused by the surface property of CNCs, which leads to aggregation in non-polar matrices, resulting in poor wettability and the formation of agglomerates. Additionally, the low thermal stability of CNCs impairs the usage of this approach, as melt processing requires high temperatures[119], especially for thermoplastic polymers. Some studies have tried a protective approach via a chemical modification to improve thermal stability of the CNC. Another attempted protective method tried covering the nanoparticles with matrices before melt processing, which can avoid contact of the nanoparticles with air. It is important to avoid contacting air under high temperatures during the processing, as this can improve the dispersity of nanoparticles in the polymer matrix.

2.4.1.2 *In situ* polymerization

In situ polymerization is the latest and most promising method among all the methods for the preparation of CNC-reinforced nanocomposites. The polymerization is usually carried out in a solvent that allows both the CNCs to disperse and the monomers to dissolve, which may involve a prior casting method[120]. It has been reported that PCL[19] and PBS[121] can be grafted onto CNC surfaces through this method. In this process, the CNCs were initially mechanically dispersed into an unpolymerized solution containing the monomer to obtain a uniform suspension[122]. In some

cases, the functional groups modified onto the CNC surface can serve as monomers themselves, which can then react with other monomers[123]. Computer simulations have shown that the interfacial strength of nanofiller reinforced composites obtained through covalent bonds is much higher than that through van der Waals-interacting system[124,125]. The feasibility of the *in situ* polymerization method is restricted by the thermal decomposition behavior of CNCs, since the polymerization process is usually carried out under high temperatures that are over the decomposition temperature of nanocellulose. Another issue of the *in situ* polymerization method is that the presence of modified CNCs will affect the ability of the macromolecules to diffuse, resulting in a low degree of polymerization. *In situ* polymerization can also be employed to fabricate hydrogels, where a work reported by Zhou *et al.* shows the introduction of CNCs enhanced both toughness and strength[126,127]. As part of their findings, CNCs with a lower aspect ratio benefited the transition from solution to gel, suggesting CNCs with a high surface area promoted the network formation.

2.4.1.3 Solvent and casting

The solvent casting method is usually achieved by dispersing the nanocrystals in solvent with the polymer matrix. Afterwards, the final nanocomposite can be obtained after the liquid is evaporated. This allows the preparation of materials with well-controlled thicknesses at lower temperatures using very little nanofiller. CNC nanocomposites prepared by the solvent casting method can exhibit the best mechanical properties provided by CNC particles. However, this method is usually only suitable for laboratory scales.

The polymer matrix can be water-soluble or non-water-soluble. A limited kind of hydro-soluble polymer can be mixed with CNC dispersion directly; the resulting interaction between CNCs and the polymer matrices is strong due to the polarity of the two components. However, when non-water-soluble polymers (non-polar) are utilized, additional solvents are needed to dissolve the matrix. The hydrophilic nanocellulose will not be compatible with hydrophobic polymers or non-polar solvents, resulting in a poorly-dispersed mixture. The solvent exchange approach can allow the CNC to be compatible with non-polar polymer matrices. Generally, CNCs are in water, which is exchanged to acetone, and then to an organic solvent such as toluene[128], DMF[129] and pyridine[130].

Chapter 3 Mechanical and tribological properties of PU/CNC composites

3.1 Introduction

Polymeric coating materials are a promising application for polyurethane, especially biodegradable PU. As a surface coating material, it will inevitably be exposed to sunlight, rain, plants, animals, minerals, air pollutants from nature, and even corrosive chemicals. Nowadays, coating materials are frequently applied to every kind of surface, such as wood, metal, and plastics, for better scratch, corrosive, and abrasion resistance. The surface coatings are usually in the form of liquid dispersions with good stability and homogeneity, uniformly spreading on the surface of physical structures to form a stable, cohesive, solid, and adherent thin film. However, a large number of polymeric coatings are petroleum-based, which could cause environmental issues and recycling difficulties. Alternatives for polyols and polyisocyanates such as vegetable oil, castor oil, lignin, and tannic acid have been extensively investigated for more environmental-friendly and sustainable PU products. Compared with solvent-based polyurethane, waterborne polyurethane (WPU) coating systems are greatly preferred due to their low volatile organic compounds (VOCs), good compatibility, ease of applicability, and ease of removal.

It is necessary to note that water-based PU does not present superior mechanical performance or thermal stability in wet conditions compared to solvent-based PU. To obtain WPU with improved properties, nanoparticles are used as reinforcement agents to be introduced into the polymer matrix. In this study, cellulose nanocrystals (CNCs) were incorporated into commercial WPU dispersions to obtain coating films with enhanced mechanical strength, tribological properties, and thermal stability. In this study, a series of aqueous polyurethane nanocomposites were fabricated by mixing varying amounts of CNC dispersions with waterborne polyurethane to realize a uniform PU/CNC dispersion. The cellulosic nanocrystals in the aqueous polyurethane can form a “concrete-steel” structure, where the CNC particles play a role in rigid segments in the nanocomposites system. The selection of processing methods is the main challenge and critical to the quality of final nanocomposites products.

As mentioned previously, there are several commonly applied methods for processing polymer nanocomposite such as in situ polymerization, casting and evaporation, layer-by-layer lamination, and melt processing. One of the shortcomings of introducing CNC particles into the polymer matrix is the self-association caused by surfaces hydroxyl groups on CNCs. Over decades of exploration, avoiding aggregation is still a difficulty for the preparation of CNC-reinforced nanocomposites due to the strong hydrogen bonding interactions. CNC dispersion is a great solution to overcome aggregation, in which CNC-CNC interactions can be replaced by CNC-solvent interactions during wetting. Since both CNCs and polyurethane are in a dispersed form, the cast and evaporation method is a suitable, low cost, and eco-friendly method to prepare PU/CNC composite. The cast and evaporation method can provide the best mechanical reinforcing effect for nanocomposites because of the longtime processing periods. Dispersibility of CNC particles in the polymer matrix determines the performance of nanocomposite. Due to using water-dispersible polyurethane, directly mixing the aqueous suspension of CNCs offers the desired shape and a uniform thickness after evaporation of water, if the mixture is dried under a controlled atmosphere.

This project aims to fabricate a CNC-reinforced WPU coating that can provide improved mechanical performance. Since water-based polyurethane is frequently used as a coating material, several tests were carried out to characterize mechanical and tribological performance such as tensile tests, scratch tests, friction tests, and micro-indentation tests to examine the effect of CNC particles on the coatings. After various characterizations, the optimal CNC content was selected, which displayed a good dispersion of nanoparticles in the PU matrix and resulted in improved tensile strength and excellent scratch resistance.

3.2. Experiment

3.2.1 Material

CNC powder was provided by CelluForce Inc. (Montreal, Canada) and used as received. The cellulose nanocrystals were pretreated with sulfuric acid in the acid hydrolysis process. Water-based polyurethane (WPU) (UD-303) was purchased from Bond Polymers International with a solid content of 35%.

3.2.2 Preparation of PU/CNC nanocomposite films

CNC powder was dispersed in deionized (DI) water at a concentration of 10 mg/ml. To ensure the CNC dispersion is well-dispersed, the mixture was stirred at 300 rpm overnight at room temperature until no visible aggregate was left, then followed by bath sonication for 20 min. The CNC dispersion was added to WPU at various ratios followed by brief vortex stirring. To make sure CNCs were uniformly dispersed in WPU, the dispersion was sonicated for 15 min, followed by degasification carried out in a centrifugal mixer. The PU/CNC nanocomposite solid films were prepared by casting PU/CNC dispersions onto petri dishes and glass slides, then naturally dried at room temperature for 24h for further test. To investigate the effects of the humidity and temperature on the surfaces, different drying conditions were attempted. The dispersion was also dried in a humidity chamber at 60 ℃ and 30 % relative humidity and at 60 ℃ and 95% relative humidity, as well as in a fridge at 4 ℃ and 20 % relative humidity. The thickness of the films varied from 0.15 to 0.25 mm. The PU/CNC composites with various CNC content were labeled as PU/CNC-1, PU/CNC-3, PU/CNC-5, PU/CNC-7, PU/CNC-9, and PU/CNC-11, with the number at the end corresponding to the wt% of CNC incorporated into the WPU.

3.2.3 Characterization

Tensile tests were conducted on a Universal Material Tester(UMT-2mt, Center for Tribology, Inc.), equipped with a 10 kg load cell. The tensile test was performed at room temperature with a gauge length of 7 mm and a crosshead speed of 2 mm/s. The specimens were cut into dumbbell shapes with a dimension of $20\times5\times t$ mm^3, where the thickness, t, was measured for each sample and varied from 0.15 to 0.25 mm. The friction tests were carried out on the same UMT machine equipped with a 1 kg load cell, mounted with a PDMS probe. The PDMS probe moved at a constant speed of 1 mm/sec against the surface of solid film back and forth under a constant preload (F=1, 2, 3, 4, 5 g). The real-time friction force and real-time preload were measured with a 2-dimensional sensor at 200 Hz frequency. Although a constant preload force is initially set to be applied to the friction system, there is a small deviation from the initial preload (<0.5% for steady-state sliding) due to the viscoelastic deformation of the PDMS probe and the interfacial adhesion between the film surface. Therefore, the coefficient of friction is calculated by dividing the measured real-time friction force by the real-time preload. The rolling friction test was performed by a self-made set-

up, where the neat WPU and PU/CNC with 3 and 5 wt% CNC dispersion were casted on four 5 cm rubber wheels of hardboard cart. The cart was then rolled down freely from a 100 cm long steel slope with 25° angle. To minimize the error of the experiments, each sample was tested 10 times and the duration was recorded for each run. The scratch tests were performed on the same UMT machine. The scratch indenter was a 1 mm diameter stainless steel ball, which was mounted to a 1 kg load cell. The steel probe moved toward the film surface at a constant speed of 5 μm/sec until a normal force of 1 g was reached. The indenter kept moving horizontally along the film surface at a sliding velocity of 0.1 mm/sec while the normal force increased linearly from 10 to 800 g. The maximum force was selected because the glass slides would break at higher preloads.

The water contact angle measurements were performed by a custom-made sessile drop setup in ambient environment at room temperature. The water was dispensed with a micro-size needle through a syringe pump (New Era Pump System Inc.) in the shape of a 3 μL droplet. The images of droplets were recorded after they were stable for 5 seconds. The contact angle measurement was controlled by a custom-made LabVIEW program. Pristine polyurethane and PU/CNC composite samples were analyzed by FTIR (ATR-FTIR Nicolet 6700, Thermo Scientific Inc) to obtain IR spectra. The transparent film was fixed on a metal holder horizontally to allow the light to transmit through it, and the spectrum was scanned from 500 to 4000 cm^{-1} in transmittance mode with 32 scans. Air was used as a background for the FTIR test.

The thermal properties were characterized by Thermogravimetric analysis (TGA 500, TA Instrument). The results were measured from room temperature (~20℃) to 800℃ with a heating rate of 10 ℃/min under nitrogen flow. The weight loss and degradation temperature were recorded during the test for the analysis of the thermal stability of CNC reinforced polyurethane.

3.3 Results and discussion

3.3.1 The effect of drying conditions

The films obtained from various temperature and humidity conditions are presented in Fig. 17-20. It can be seen that the surfaces are affected by the drying conditions. The films dried naturally at room temperature are clear and transparent with several shrinkages, while the films dried at 60 ℃

30 % humidity also show smooth surface and minor wrinkles at the edges without visible aggregates. However, when the humidity was increased to 95 % (the upper limit of the humidity chamber), the solid film became blurry on its surface. In contrast, when the PU/CNC dispersion was placed in a fridge to slow down the evaporation, the film products are cleared and smoother on their surfaces. From these differences on the film appearance, the humidity and temperature are critical to the formation of the PU/CNC composites. We also conducted tensile tests on the film samples; however, their mechanical properties exhibited similar values of strength and strain. The biggest problem that was caused by drying conditions is the drying time. When the dispersion was dried at room temperature, it took from 10 h to overnight to obtain the solid film (depending on the exact room humidity), whereas dispersions at lower temperatures or higher humidities always needed 3-5 days to become fully dry. This long processing time is not desirable in practical manufacturing, and as such, in this study the dispersion was only dried in ambient air at room temperature for the solvent casting and evaporation.

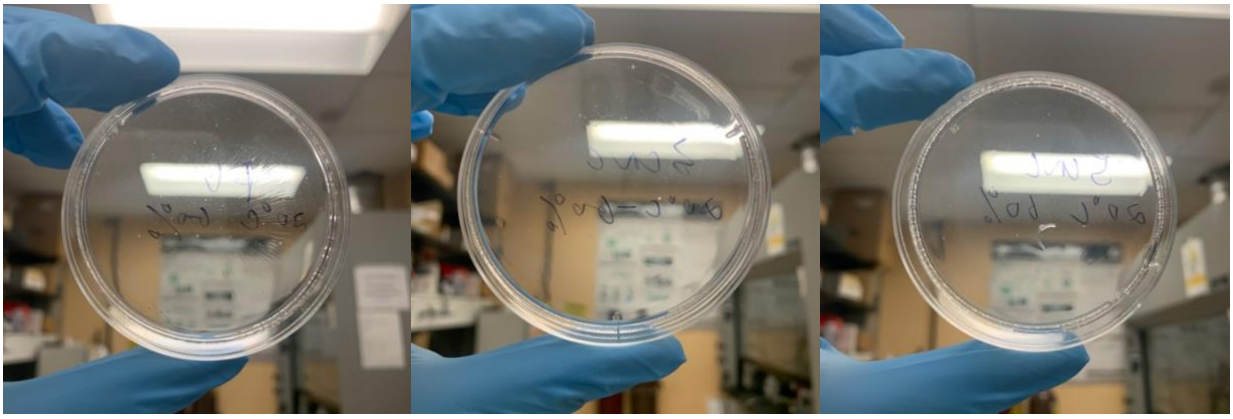

Figure 17. The films obtained from drying in room temperature

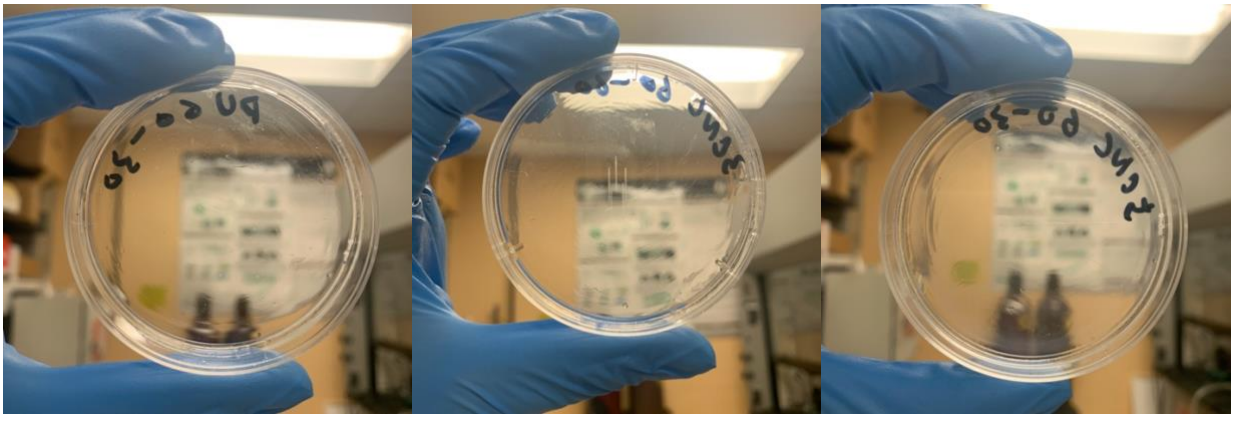

Figure 18. The solid films dried in the humidity chamber at 60 ℃, 30 % humidity.

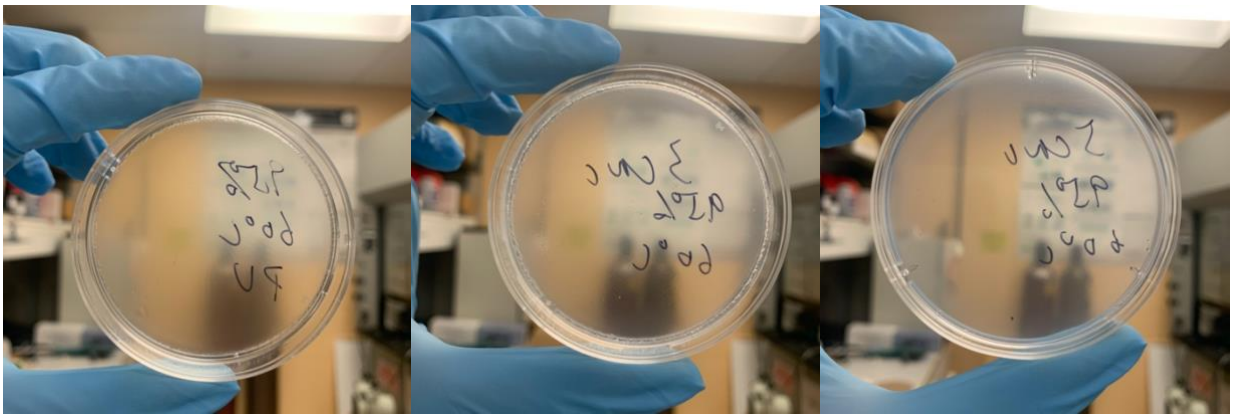

Figure 19. The solid films dried in the humidity chamber at 60 ℃, 95 % humidity.

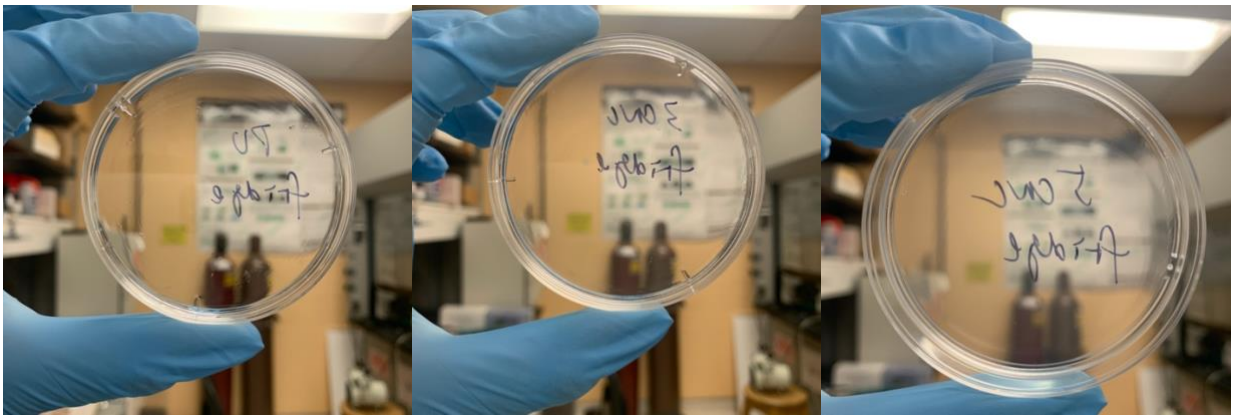

Figure 20. The solid films dried in the fridge at 4 ℃, 20 % humidity.

3.3.2 Tensile tests

The mechanical properties of PU/CNC nanocomposites were characterized by tensile tests, with results shown in stress-strain curves presented in Fig. 17b. The mean values of strain at break and tensile stress versus CNC content in the WPU matrix are shown in Fig.17a. The mean values of Young's Modulus and toughness are calculated from the stress-strain curves, demonstrated in Fig. 17b and 17c. Obviously, there are two deformation behaviors observed in all curves. The stress changes rapidly at low strain, and the Young's modulus was determined from the slope of the initial linear region.

Table 3. the mean values of tensile strength of PU/CNC composites

PU/CNC sample	Strain at break (%)	Stress (MPa)	Young's Modulus (MPa)	Toughness (J/m^2)

Neat WPU	1321.1	19.6	16.7	138.8
PU/CNC-1	1267.5	21.5	19.2	145.9
PU/CNC-3	1356.6	25.8	34.5	194.6
PU/CNC-5	1174.7	27.2	57.6	186.6
PU/CNC-7	1005.2	27.8	90.3	177.3
PU/CNC-9	881.0	25.2	100.5	145.8

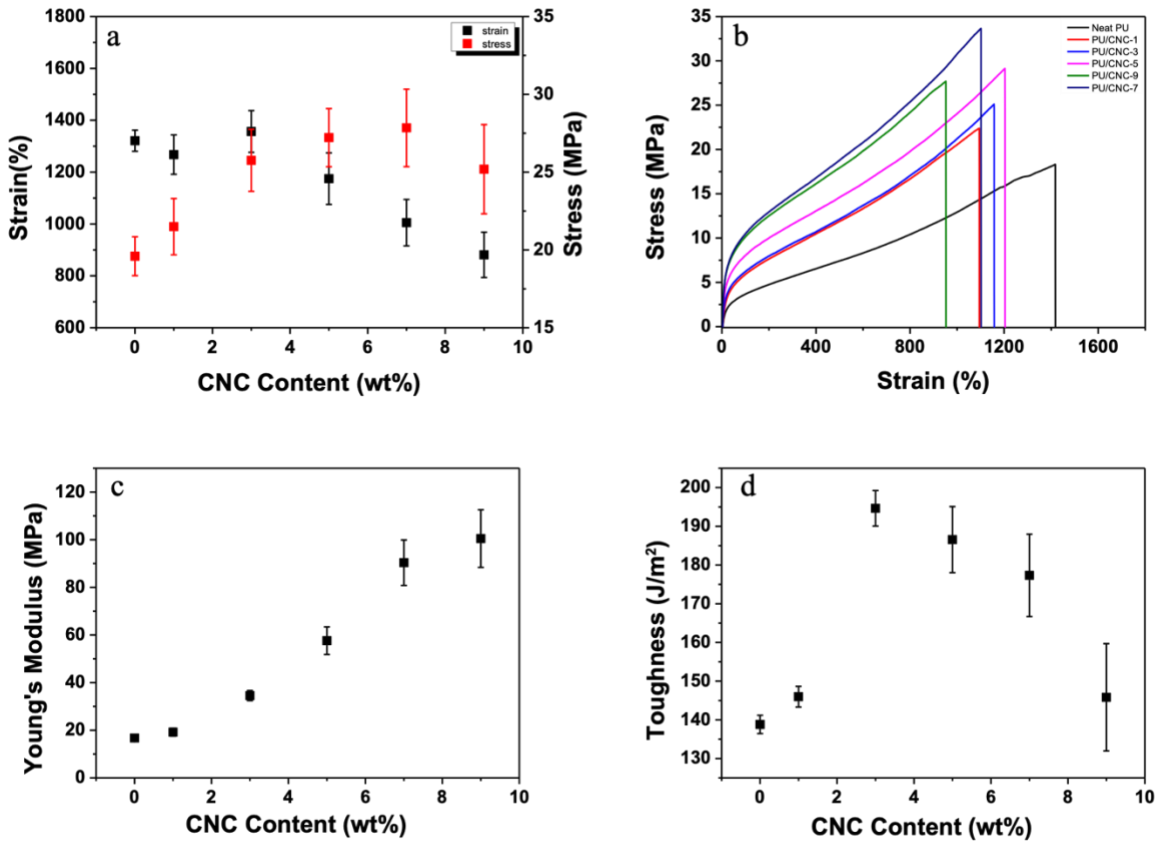

Figure 21. a) tensile stress change along with CNC content, b) the typical strain-stress curves of PU/CNC composites and c) Young's modulus and d) toughness for nanocomposites with various CNC content.

As expected, the values of tensile strength and Young's modulus increased with increasing CNC content. When the PU is incorporated with 7 wt% CNC, the strength reaches its maximum value of 28 MPa. For low amounts of CNC, the values of strain at break remain almost the same to that of pristine WPU. However, as the CNC content is increased further, the values of strain at break drop significantly.

The measured Young's modulus shows a great increase with the introduction of cellulose nanocrystals. The modulus of 9 wt% PU/CNC nanocomposites film reaches a maximum value of 100 MPa, which is 5 times higher than that of neat WPU. This confirms that CNC particles were well-dispersed in the WPU matrix, as well as the homogeneous morphology of the film composites. The increasing tensile strength and decreasing strain at break indicate that the incorporation of CNCs into the WPU matrix contributes to a strong interaction between CNC particles and the matrix, which also results in stiffer elasticity. Initially, the hydroxyl groups on the CNC surface form strong hydrogen bonding interactions with the WPU segments. However, when the CNC content is further increased, non-participating CNC particles tend to self-agglomerate. The increase of Young's Modulus could be attribute to both the strong inter-and intra-hydrogen bonding, which also leads to higher hardness and rigidness.

3.3.3 Scratch test

The improved mechanical strength and stiffness make PU/CNC nanocomposite a promising material for thin film coating in packaging, soft electronics, or wearable devices. In order to investigate the scratch resistance of PU/CNC films, we employed scratch tests using the UMT. Fig. 18 presents a typical scratch track of induced damage with increasing preload under the microscope, showing the change in normal preload, lateral force, and friction coefficient along with time. The point where the curves start to show vibrations denotes the failure point of the film. For the neat WPU as shown in the picture, the film shows snag points after the scratch starts at 530 g, providing an average scratch resistance for the WPU film. With the introduction of CNC particles, the hydroxyl groups on the CNC surface should interact with NCO groups in the WPU chain, and any deformation would go through several stages, including fully recoverable elastic, time-dependent viscoelastic, and nonrecoverable plastic deformations[131]. When a small amount of CNCs, 1 and 3 wt%, was incorporated into the WPU matrix, the film shows the first break at around 600 g for PU/CNC-1 and PU/CNC-3 without delamination. When the normal force keeps increasing over 600 g, the probe leaves dotted damage on the film surfaces.

For the WPU with 5 wt% of CNC, the strength and rigidity greatly increased, as we mentioned before, to the point that there are no visible failure points that occurred on the surface. When the normal force increased linearly from 10 to 800 g during the sliding process, the film damage

transferred from plowing at 10-580 g to stick-slip behavior for 620-750 g, ending with a snag point at 766 g. However, when CNC content increased to 7 wt%, the snag point occurs at 680 g, which could be caused by the excessive amount of CNC, as too large an amount of CNC is not well dispersed in the WPU matrix; this result also matches the decreasing strength and strain observed in tensile tests. Another potential reason for the decreasing scratch resistance could be the low adhesion properties of PU/CNC-7 film on the glass slide.

It is worth noting that a huge drop in the friction coefficient can be observed in all the curves of coefficient of friction (COF) versus time, which could be caused by the static friction force when the metal probe started sliding. Then the change in COF becomes stable when the normal force increases, which can be caused by the elastic deformation of the films. This will be discussed in the next section.

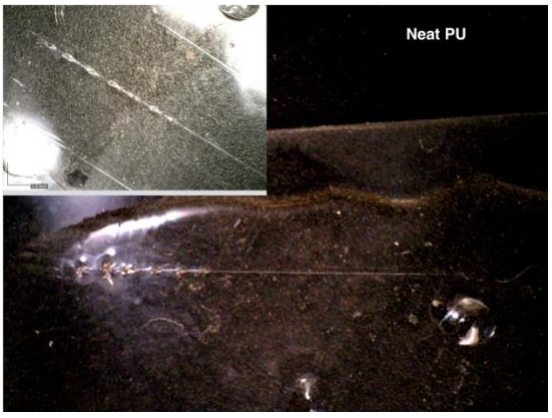

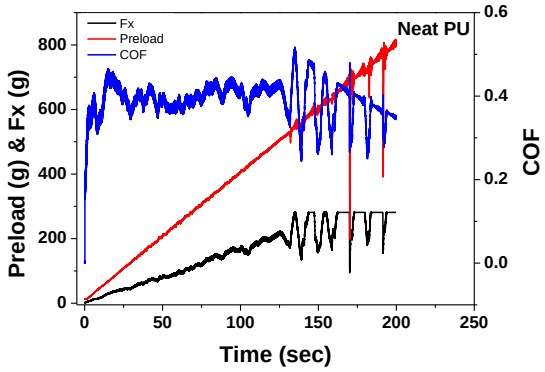

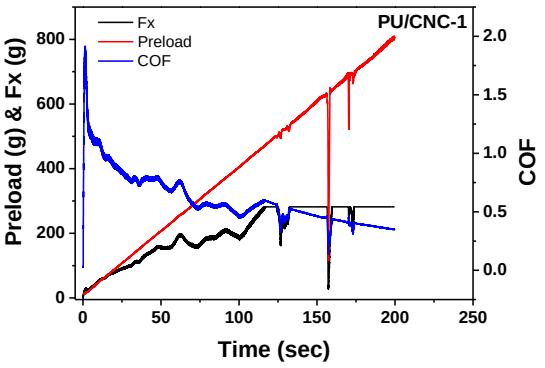

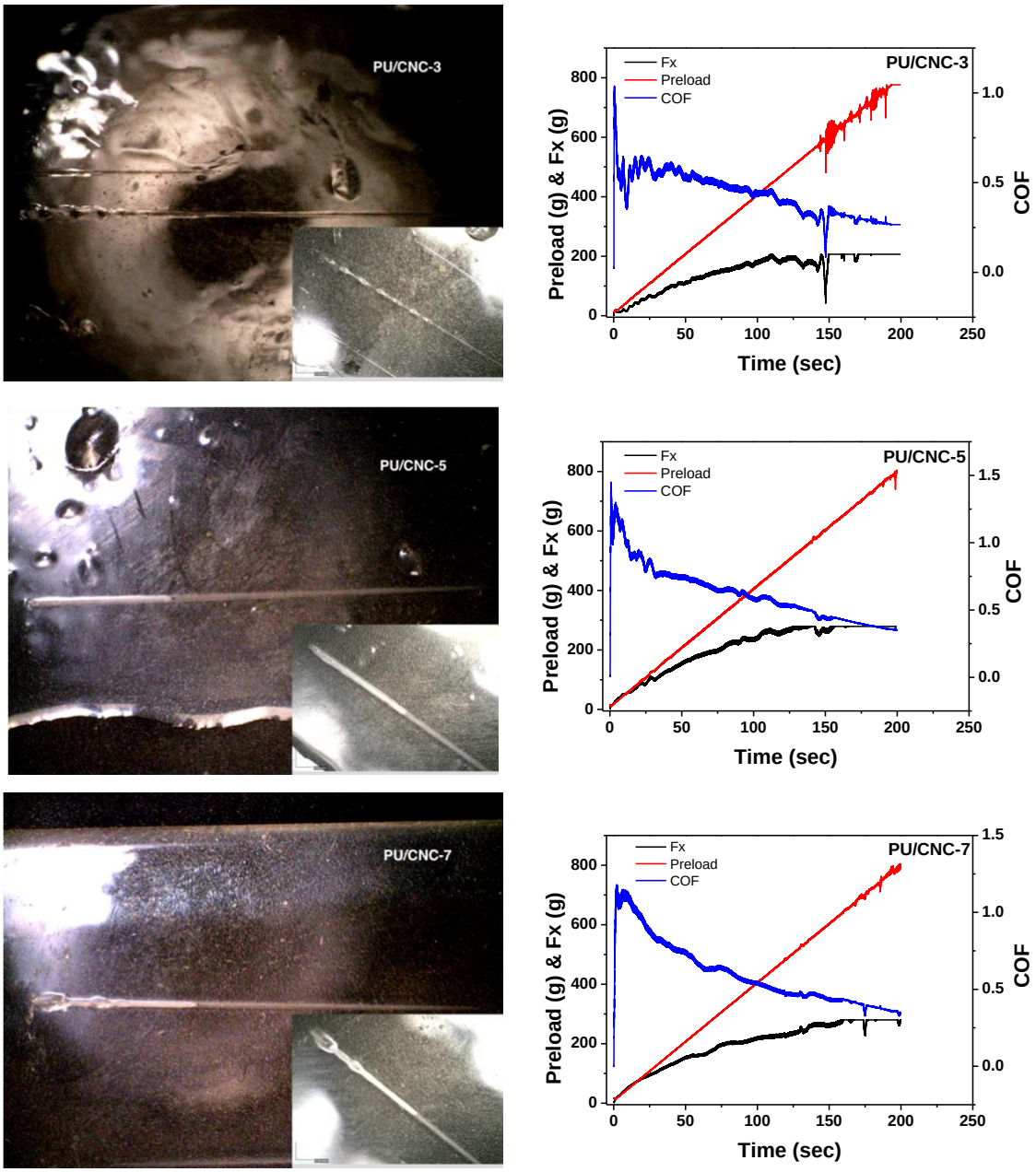

Figure 22. Images of film surfaces after scratch test and typical curves of preload, lateral force and COF versus scratch time. Insert: zoom-in images of the damage at the end of the scratches.

3.3.4 Friction test

Along with the scratch test, the friction properties of a coating material are important in any applications of CNC-reinforced nanomaterial where normal and lateral forces are also involved. The plots of lateral force as a function of displacement for the PDMS probe on PU/CNC-7 film coated on glass under different preloads are shown in Fig. 23. The average friction force did not

show any decrease with the repeat of five cycles, which suggests the coating on a glass was be damaged by the sliding movement.

Fig. 24 demonstrates the relationship between COF and friction force with increasing friction force. The COF was calculated by dividing the real-time lateral force by the real-time applied force during sliding. The mean COF values are listed in Table 4. From Fig. 24 we can see that the COF for all WPU composites decreased gradually with an increase in preload. When CNC was incorporated with the WPU matrix, the coefficient increases significantly, which is much clearer at higher preloads. However, when the CNC content reaches 11 wt%, the COF starts to drop to be even lower than that of neat WPU.

To investigate the relationship of friction force and adhesion between PDMS and PU/CNC, we applied Amonton's law (equation 4), where μ_A is the coefficient of friction. As mentioned above, the friction coefficient μ_A at a low preload force of 1 g was remarkably higher than that at a high preload force, which suggests the effect of molecular adhesion on friction[138]. To identify the adhesion properties, Bowden and Tabor's theory, which introduced the adhesion component to Amonton's law, was fitted well to the friction behavior, which included the molecular adhesion effect[139].

$$F_f = \mu_A F_N \qquad \text{equation (4)}$$

$$F_f = \mu_B F_N + \sigma A \qquad \text{equation (5)}$$

It is important to note that the coefficient μ_A in equation 4 is not the same as μ_B in equation 5. μ_A can be calculated by Amonton's law for each data point in Fig. 24, and may vary under different forces, whereas μ_B is determined from the slope of each fitting line in Fig. 25, independent of the preload. From Fig. 25, we can tell that equation 5 is more applicable for the PU/CNC thin film coating on glass, which means there is high effect from molecular adhesion between PDMS and PU/CNC composites. Applying Bowden and Tabor's theory to the detailed information of the friction tests of PU/CNC film, μ_B and σA were obtained for the PU/CNC films, with values summarized in Table 5. Comparing neat WPU films to those incorporating cellulose nanocrystals particles, the μ_B or friction coefficient shows an obvious increase from around 1.7 to around 3, whereas σA or adhesion component reduced for all film composites. This could suggest that the introduction of CNC particles may deteriorate the adhesion effect of WPU material. Since the

introduction of CNC can both enhance and reduce the friction coefficient, it could be useful as a way to tailor these properties according to various application requirements.

Table 4. Friction coefficient (μ_A) between PDMS and PU/CNC films.

COF	Preload (g)				
	1	2	3	4	5
Neat WPU	4.31	3.17	2.91	2.40	2.32
PU/CNC-1	4.18	3.86	3.43	3.49	3.24
PU/CNC-3	4.40	3.49	3.30	3.24	2.78
PU/CNC-5	4.33	3.86	3.24	3.07	2.75
PU/CNC-7	4.92	4.03	3.63	3.45	3.14
PU/CNC-9	4.01	3.56	3.25	3.00	2.86
PU/CNC-11	3.15	2.62	2.13	1.89	1.88

Table 5. Adhesion component and friction coefficient (μ_B) between PU/CNC films and PDMS

Samples	μ_B	σA	R^2
Neat WPU	1.78	2.82	0.979
PU/CNC-1	3.03	1.44	0.993
PU/CNC-3	2.50	2.18	0.972
PU/CNC-5	2.34	2.59	0.977
PU/CNC-7	2.73	2.53	0.992
PU/CNC-9	2.54	1.87	0.993
PU/CNC-11	1.48	1.94	0.984

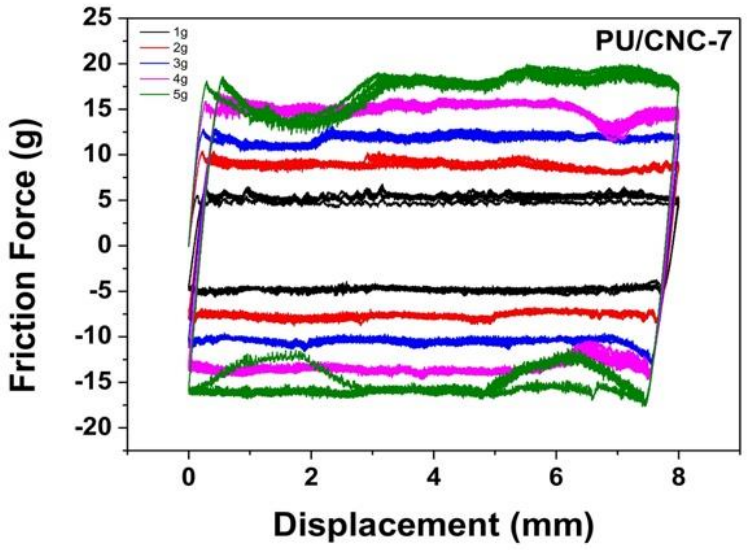

Figure 23. Plots of friction force versus lateral displacement under various preloads during five sliding cycles on PU/CNC-7.

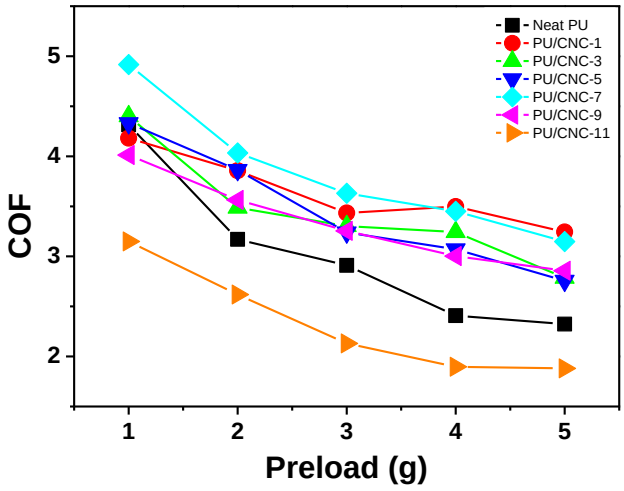

Figure 24. Evolution of the COF for PU/CNC composite under increasing preload.

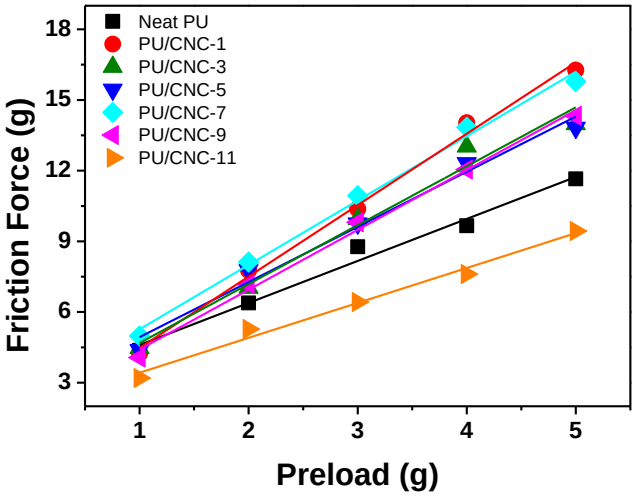

Figure 25. Evolution of the friction force for PU/CNC composite under increasing preload.

The increase in COF enables the film to be employed as an anti-slip material coated on floors, wheels, wooden boards, steel, or plastics, to reduce abrasion from excessive movement. The rolling friction test can be a direct and practical method to illustrate the real application of the PU/CNC composite coatings. When the distance and weight are constant, a shorter travel time can be interpreted as a lower friction force. Since the weight of the whole set up used is the same and the cart traveled over the same distance, a longer time means smaller velocity and higher friction force between coating and surface. With the incorporation of CNCs, the time increased from 0.98 sec for neat rubber wheels to 1.08 sec for PU/CNC-5. The 10% increase confirmed the effect in increasing the friction for the better resistance, it can be a potential material for anti-slip applications.

Figure 26. Schematic of rolling friction test.

3.3.5 Water contact angle test

Water contact angle measurement is an effective method to quantitatively evaluate the hydrophobicity or hydrophilicity of materials. The trend of the change of contact angle with the increase of CNC content is shown in Fig. 27.

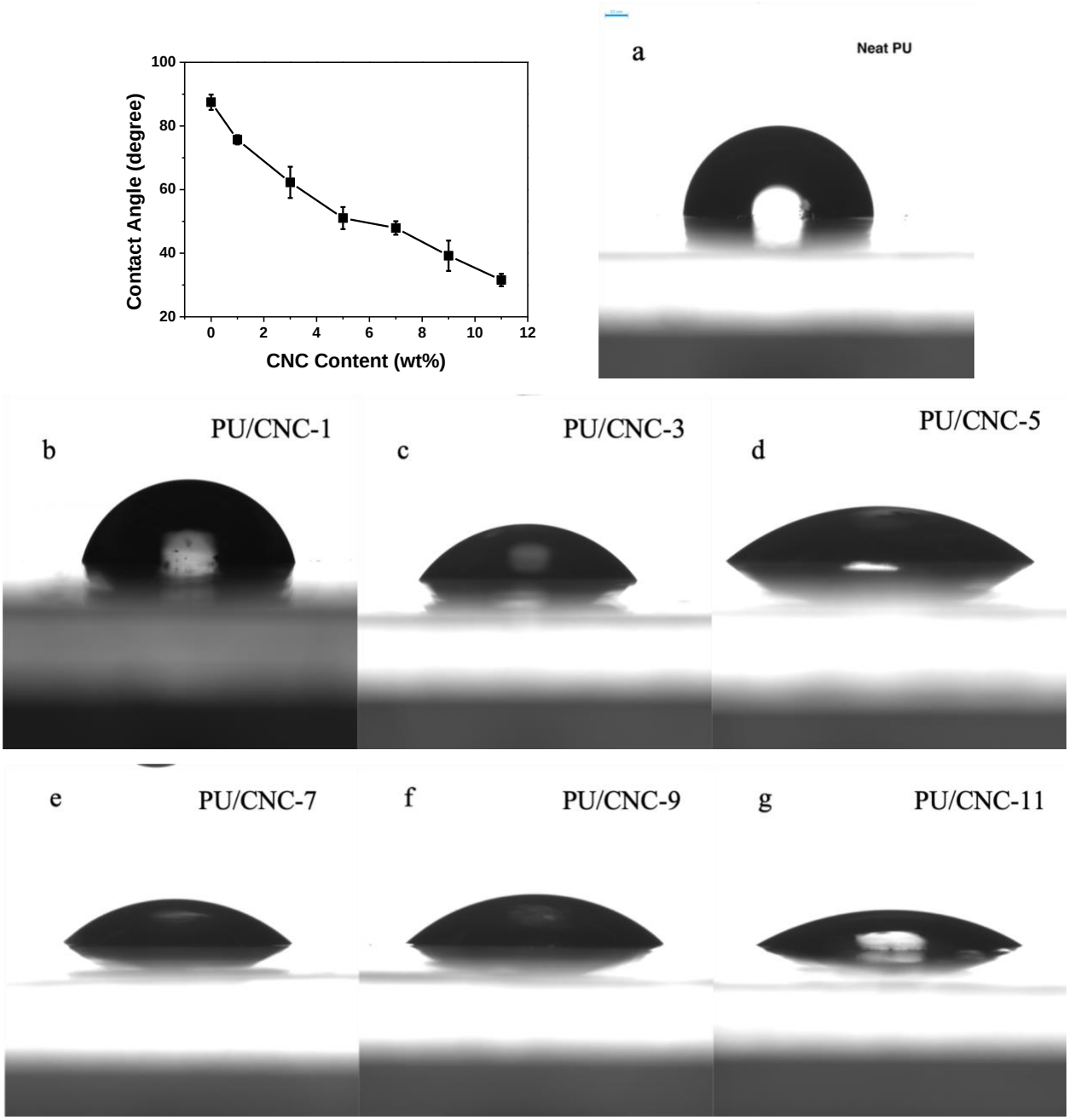

Figure 27. Evolution of contact angle with CNC content; the images obtained of contact angles for a) WPU and WPU reinforced with b) 1wt% CNC; c) 3wt% CNC; d) 5wt% CNC; e) 7wt% CNC; f) 9wt% CNC; g) 11wt% CNC

As the amount of CNCs in the PU/CNC composites increased, the contact angle decreased dramatically, reaching as low as 32˚ for the PU/CNC-11 nanocomposites. Figure 27a presents the image of the water droplet on a neat WPU surface. For neat WPU, the contact angles were always around 90˚, denoting a relatively hydrophobic film surface. From the images obtained during the contact angle measurements, the introduction of CNC significantly reduced the hydrophobicity of WPU film. As known before, CNC is a hydrophilic material due to the abundant hydroxyl groups on its surface. The decrease in contact angles suggests that the CNC particles are well dispersed in the WPU matrix, as they are influencing the surface chemistry of the film.

3.3.6 Fourier Transform Infrared Spectroscopy (FTIR)

The structural properties and chemical bonding interactions of CNC-reinforced WPU were studied by FTIR characterization. The FTIR spectra of neat CNCs are presented in Fig. 28a and those of PU/CNC nanocomposites are presented in Fig. 23b. The peak at around 3332 cm^{-1} is the stretching peak of N-H from urethane groups. There is no other characteristic peak showing at 2280 and 2360 cm^{-1}. The lack of these peaks suggests that the WPU material does not contain any NCO residuals, which can come from diisocyanates, an important component in synthesizing waterborne polyurethane. The band of urethane N-H and C-N stretching would be seen at 1537 $cm^{-1,}$ and the strong absorption of the C=O bond was visible at 1716 cm^{-1}. This suggests the presence of phase mixing of the rigid and flexible segments in WPU. However, as CNC content in the WPU increased, the density of the band gradually reduced and shifted toward a higher wavenumber. This might be caused by the CNCs influencing the hydrogen bonding between N-H and C=O groups and improving the separation of hard and soft regions due to the interactions between CNCs and polyurethane. Compared with pristine WPU, there is also no new peak appearing in the range of 1100-1715 cm^{-1}, indicating that no new chemical bond was formed in the material. As a comparison, the absorption of NH stretching at around 3330 cm^{-1} shows a shoulder peak, which is attributed to the OH stretching vibration of CNC[132].

The peak at 1580 cm^{-1} that could be seen in the spectra of CNC and all PU/CNC composites could be the hydroxyl bonded carbonyl, demonstrating a strong interaction of hydroxyl groups on the CNC surface and carbonyl in the WPU matrix. Additionally, it is worth noting that the increased transmittance band at 1183 cm^{-1} was related to the formation of the allophanate crosslinking

effect[133,134]. With the increasing amount of nanocellulose crystals, the higher density of this band further confirms that the isocyanates do not react with CNC and that its growing amount in the system leads to the formation of more crosslinks.

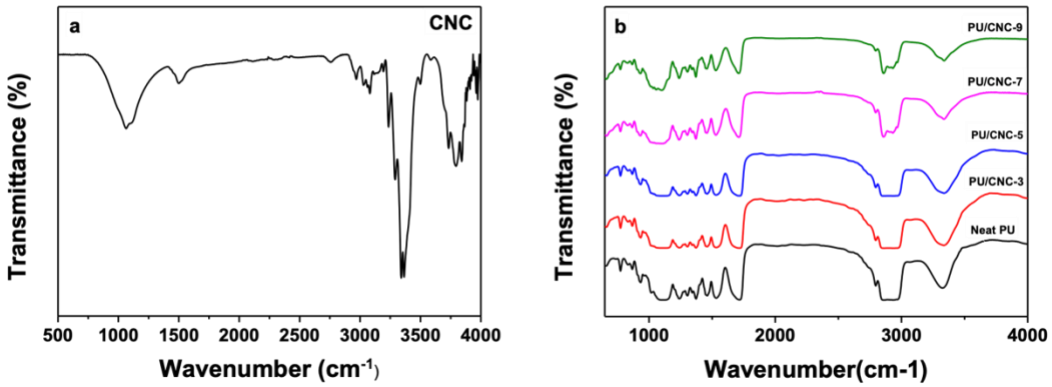

Figure 28. FTIR spectra of a) neat CNC and b) PU/CNC composites.

3.3.7 Thermogravimetry Analysis (TGA)

It is important to examine the influence of CNCs on the thermal stability of WPU composites. This is because CNCs have a relatively weak thermal stability, which can restrict the application of the PU/CNC nanocomposites. TGA was performed to obtain the thermal degradation profiles of the native WPU and CNC-reinforced composites, with results demonstrated in Fig. 29. Under nitrogen flow, CNCs exhibit two-stage degradation; the first step corresponds to the evaporation of water molecules at around 100 ℃, the second is related to thermal degradation of the CNC chains, i.e., dehydration, depolymerization and decomposition of glycosyl[135]. For all samples with WPU, the thermal decomposition behavior depends more on the thermal properties of WPU, which is a three-stage weight loss. The first stage of degradation was shown at around 270 ℃, which is related to the loss of the urethane group, then the second stage happened at urea bond decomposition. Finally, the third stage is degrading the soft segment in he WPU chain. From the curves of weight percentage against temperature, the neat WPU started to lose weight at around 276.4 ℃, with a peak weight loss at 385.7 ℃. WPU with 1 wt% CNCs shows an early onset at 324.15 ℃ and peak loss at 394.17 ℃. With increasing CNC content, the onset temperatures are 307.13 ℃, 313.16 ℃, and 298.7 ℃ for PU/CNC-3, PU/CNC-5 and PU/CNCN-7, respectively, with respective peak weight losses at 389.92 ℃, 409.02 ℃ and 404.77 ℃.

When the WPU composites were incorporated with the CNC particles, all the samples showed increasing onset temperature and peak degradation temperature, which confirms improved thermal stability of CNCs in the WPU matrix. The increase in stage three, the degradation of the urea group, is because of the high crystallinity of CNCs and great interaction between the rigid segments. Also, the components that are decomposed in the first two stages can form a charred layer, which protect the soft segments in WPU.

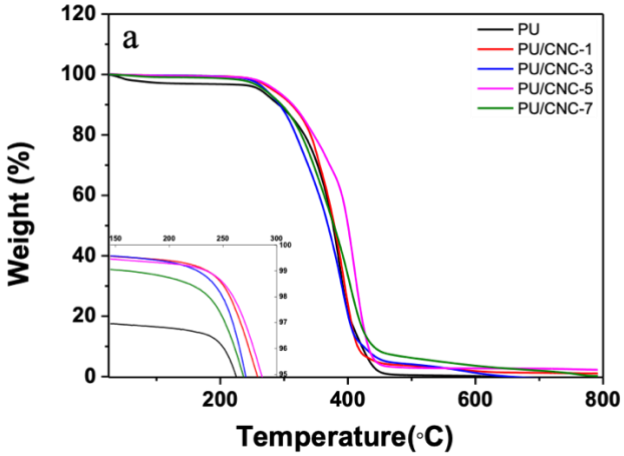

Figure 29. the TGA of PU/CNC composites.

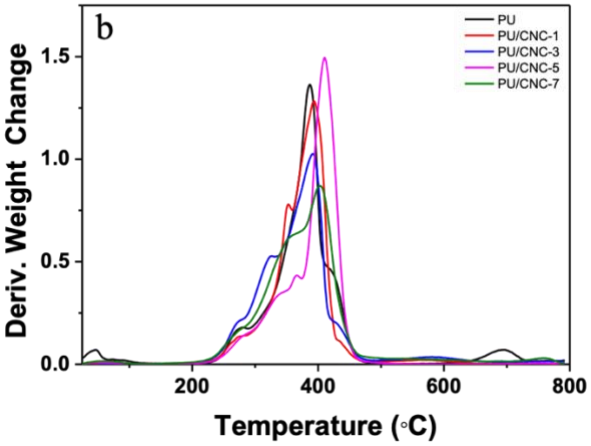

Figure 30. the derivative weight change of PU/CNC composites

3.4 Conclusion

In this project, the introduction of CNCs improved the mechanical properties in terms of tensile strength, Young's modulus, and toughness with a compromise of decreasing strain. The WPU

matrix with 7 wt% CNC can provide the best tensile strength with a relatively good strain. As for the tribological properties, the PU/CNC composites have a higher friction coefficient with a small amount of CNCs. On the other hand, the presence of CNCs enhanced the scratch resistance of WPU composites. The improvement in friction and scratch resistance allows the PU/CNC to have more applications as a coating material. The hydrophobicity of the WPU matrix is also affected by the hydrophilic nature of CNC, resulting in a reduction in the contact angle from ~90˚ for pure WPU to ~31˚ for PU/CNC-11. This change can make PU/CNC composites more water favorable and can be further applied in water-soluble systems. As for the thermal properties, the introduction of CNCs does not reduce the thermal stability. In fact, the PU/CNC-5 sample exhibits improved thermal stability with a peak decomposition temperature of 409.02 ℃ compared to 385.7 ℃ for neat WPU. The glass transition temperatures also gradually increased with the CNC content up to 7 wt%, which confirms the strong interaction between WPU matrix and CNCs. In summary, it is reasonable to say that PU/CNC composites can be a potential environmental-friendly multifunctional material with excellent thermal and mechanical properties.

Chapter 4 Preparation and characterization of CNC reinforced vitrimer material [1]

4.1 Introduction

Epoxy resin has excellent stability, corrosion resistance, electrical insulation, high adhesion, and other properties, and is widely used as coatings, adhesives, electrical and electronic materials in mechanical and electronic, aerospace, marine construction, automotive, military, metallurgical, and light industries, along with other fields. Since cured epoxy resin is a 3-dimensional cross-linked structure, it is insoluble and infusible. Once they are processed and molded, they are difficult to re-process and reuse. In 2011, Leibler *et al*. introduced a reversible transesterification reaction into epoxy resins to obtain epoxy resin-based glassy polymer (vitrimer), which enables thermosetting epoxy resin-based vitrimers to be reshaped and reprocessed after molding, attracting a series of research interests in the reprocessing of epoxy resins.

In the presence of an ester exchange catalyst, high temperatures induce a rapid ester exchange reaction, which leads to a continuous breaking and reorganization of the ester bonds, resulting in a change in the topological network and enabling the reshaping and reprocessing. However, the ester exchange reaction realized by thermal conditions will deteriorate the mechanical properties of the material, which limits its potential application. Commonly, the introduction of nanosized particles is a cost-effective and directive method to improve the strength, toughness, modulus, and thermal properties of a material. As such, the research of polymeric nanocomposites has been gaining much interest from academic and industrial communities.

Cellulose is the most abundant organic polymer on earth, and its excellent psychical and chemical properties make it a promising material as a reinforcing agent. In its nanocrystalline form, the reactivity of CNC provides more possibilities for chemical modification to fit the many increasing requirements in many scientific fields. Typically, CNC is in a powder form and is not compatible with the hydrophobic vitrimer system, so chemical modification is needed to make CNC adapt into vitrimers. These chemical modifications can be always achieved by “graft onto” or “graft from” methods, where the grafted polymer can control the properties of the final material. Aliphatic

[1] In this chapter, Fig 31-35 are provided by Dr. Jian Sun, with who a manuscript is being prepared.

polyesters are one of the most versatile groups of biodegradable polymers; they can be applied in biomedical, food packaging, three-dimensional printing, and other uses, and have been successfully applied to modify many cellulose derivatives.

In this project, we employed the "grafting from" method to graft polycaprolactone (PCL) to CNCs, which contains both ester and hydroxyl groups, and then incorporated the modified CNCs into the vitrimer system. A series of characterizations such as tensile tests, swelling tests, indentation tests, DSC, and TGA were performed to characterize the enhanced mechanical and adhesive properties of CNC-vitrimers.

4.2 Experiment

4.2.1 Material

Pentaerythritol tetrakis(3-mercaptopropionate) (PETMP), bisphenol A diglycidyl ether (BADGE), ε-caprolactone (ε-CL), polycaprolactone diol (PCLOH), triazabicyclodecene (TBD), 3-mercaptopropionic acid, 1,8-Diazabicyclo[5.4.0]undec-7-ene (DBU), tin(II)ethylhexanote ($Sn(Oct)_2$) were all purchased from Sigma-Aldrich. Cellulose nanocrystal was provided by CelluForce Inc. Thionyl chloride ($SOCl_2$), potassium iodide (KI), potassium carbonate (K_2CO_3), magnesium sulfate ($MgSO_4$), and sodium bicarbonate ($NaHCO_3$) were provided by Sigma-Aldrich. Dimethylformamide (DMF), ethyl acetate, toluene (99.8%), dichloromethane (99.5%), acetone (99%), and heptane (99%) were used as received.

4.2.2 Fabrication of CNC-vitrimer

4.2.2.1 Synthesis of PCL-SH

The synthesis of polycaprolactone dithiol (PCL-SH) was realized by a two-step procedure (Fig. 31). The first step is the synthesis of polycaprolactone dichloride (PCLCl) from PCLOH. To a solution of polycaprolactone diol (PCLOH, 20.0 g, 10.0 mmol, Mn ~2000) in CH_2Cl_2 (100 mL) was added $SOCl_2$ (2.97 g, 25.0 mmol). The mixture was stirred at 60°C for 24 hours. After cooling, the mixture was carefully extracted with CH_2Cl_2 (3×50 mL) by adding deionized water (50 mL). The organic layer was washed with $NaHCO_3$ (saturated aqueous solution, 50 mL) and hydrochloric

acid (1 M) and dried over $MgSO_4$. The solvent was removed in a vacuum and the residue was dried in a vacuum oven for 24 h at 80 °C to give a light yellow solid PCLCl (17.4 g, 85.4%).

Next, PCLSH was prepared from the PCLCl. To a solution of PCLCl (10.0 g, 4.9 mmol) in DMF (100 mL) was added 3-mercaptopropionic acid (1.168 g, 11.0 mmol), DBU (0. 336 g, 2.2 mmol), KI (0.360 g, 2.2 mmol) and K_2CO_3 (1.658 g, 12.0 mmol). The mixture was stirred at 95 °C for 24 h. After cooling, DI water (50 mL) was carefully added and the mixture was extracted with ethyl acetate (3×50 mL). The organic layer was washed with hydrochloric acid (1 M) and NaHCO3 (saturated aqueous solution, 50 mL) and dried over $MgSO_4$. The solvent was removed in a vacuum and the residue was dried in a vacuum oven for 24 h at 100 °C to give a light brown solid PCLSH (8.7 g, 81.6%)

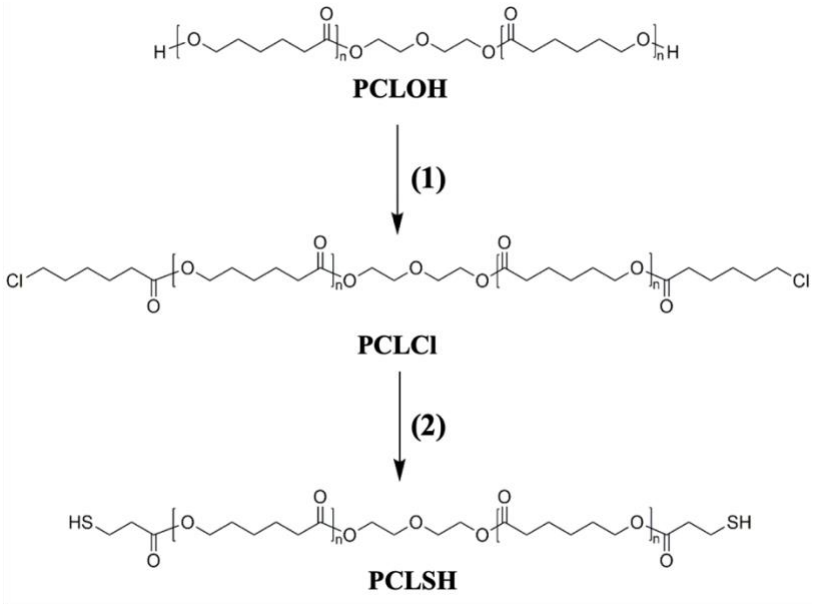

Figure 31. Synthesis of PCLSH. Reagents and conditions: (1) $SOCl_2$, CH_2Cl_2, 60 °C, reflux; (2) 3-mercaptopropionic acid, DBU, KI, K_2CO_3, DMF, 95 °C, reflux.

4.2.2.2 Synthesis of PCL grafted CNC

The PCL chains were grafted from CNC by ring-open polymerization (ROP) method adapted from Habibi *et al*[19]. The solvent exchange of CNC was performed by wet transfer with acetone followed by several successive centrifugation and redispersion operations with dry toluene. A solution of CNCs (1.0 g) in toluene (100 mL) was stirred at 110 °C for 30 min under nitrogen. Then, a mixture of ε-caprolactone (ε-CL) (5.0 g), Sn(Oct)2 (0.2 mL) and citric acid (0.2 g) in toluene (20 mL) was

added dropwise. The ring-opening polymerization was allowed to proceed for 24 h and was stopped by the addition of a few drops of dilute aqueous hydrochloric acid (1M). After precipitation by the addition of hexane, the modified PCL-CNC was subjected to centrifugation. To remove the free PCL chains, the obtained PCL-CNC was purified by Soxhlet extraction with dichloromethane (DCM) for 24 h and then allowed to disperse in toluene.

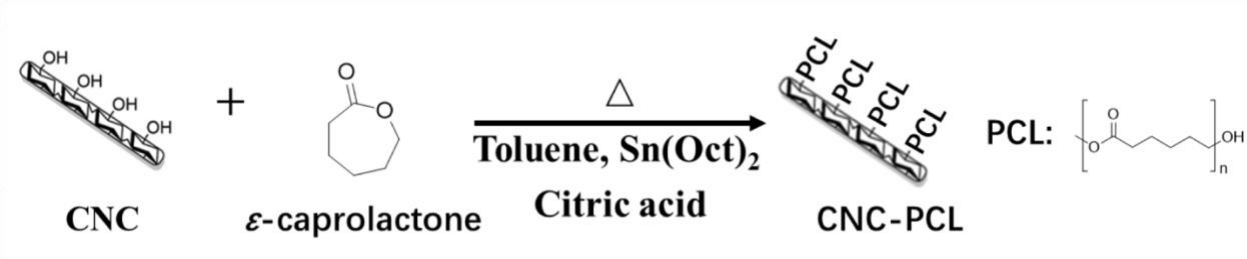

Figure 32. Chemical modification of CNC. Reagents and conditions: Wet transfer; ε-CL, $Sn(Oct)_2$, citric acid, toluene, 110 °C reflux.

4.2.2.3 Preparation of CNC-vitrimer

To prepare the CNC-vitrimer composite, BADGE and PCLSH were preheated prior to weighing. 0.071 g (0.145 mmol) of PETMP, 0.25 g (0.734 mmol) of BADGE, and 0.9587 g (0.44 mmol) of PCLSH were mixed in toluene (0.5 mL), and varying contents of PCL-CNC dispersion were added into this mixture (0 wt%, 5 wt%, 10 wt%, 15 wt%, 20 wt%). To ensure all components mixed well, the mixture was kept in the oven at 80 °C for 10 min, followed by sonication for 15 min. After sonication, 0.15 mL of catalyst TBD is added to the polymer mixture. Subsequently, the final mixture was bath sonicated for 20 min, then poured into a glass mold. The samples were heated at 100 ℃ for 2 h to remove residual toluene, then heated up to 140 ℃ to realize the polymerization. The samples with different PCL-CNC content were labeled as vitrimer, PCL/CNC-5, PCL/CNC-10, PCL/CNC-15, PCL/CNC-20 (with the number corresponding to the wt% of PCL-CNC added).

4.2.3 Characterization

The adhesive properties were characterized by a custom-made micro-indentation set-up equipped with a PDMS probe. The vitrimer samples were fixed on glass slides, which were themselves attached to the bottom of a petri dish. The probe approached at a constant speed of 1 µm/sec to reach the set preload (from 1 g to 5 g) and then held for 30 seconds between the loading and unloading period. To investigate the adhesive properties above the glass transition temperature,

the samples were tested at room temperature, 40, 60, 80, and 100 ℃. Force and displacement data were recorded by a custom-made LabVIEW program. The test was run 5 times for each sample.

Dynamic mechanical analysis was performed on the vitrimer composite samples using the TA instrument (DMA Q800). The samples with the dimensions of 20×5×~0.85 mm^3 were tested in dual cantilever mode with temperatures ranging from room temperature to 180 ℃ and a frequency of 1 Hz. The storage modulus and tan delta were recorded for analysis. The stress relaxation tests were conducted on the TA instrument (DMA Q800). All samples had dimensions of 20×5×~0.85 mm^3. After temperatures reached equilibrium, a constant 10% strain was applied, and the stress was recorded over time. Tests were also undertaken to investigate the reprocessability of the vitrimer composites. Tensile tests were performed on samples with a size of 20×5×~1 mm^3 by the same TA instrument (DMA Q800) under a temperature of 70 ℃. After each sample broke, it was cut into pieces and fixed on glass slides for reprocessing in an oven with a temperature of 150 ℃. The tensile tests were repeated 3 times to compare the mechanical properties.

The water contact angle measurements were performed by a custom-made sessile drop setup in ambient environment at room temperature. The water was dispensed with a micron-sized needle through a syringe pump (New Era Pump System Inc.) in 3 μL droplets. The images of droplets were recorded after they were stable for 5 seconds. The contact angle measurement was controlled by a custom-made LabVIEW program. For swelling tests, vitrimer samples were cut into square pieces with dimensions of 5×5×~1 mm^3. The specimens were soaked in water and toluene respectively. The initial masses of samples were measured before the test started. The weight change was measured every half hour for the first two hours, then measured every hour until the mass did not show a large change. The tests were conducted at room temperature, 40, 60, and 80 ℃. After samples were soaked in water and toluene for two days, samples were dried in the oven at 80 ℃ overnight. Gel content was calculated from the mass after drying divided by the initial mass.

The thermal properties were characterized by Thermogravimetric analysis (TGA500, TA Instrument). The results were measured from room temperature (~20 ℃) to 600 ℃with a heating rate of 10 ℃/min under nitrogen flow. The weight loss and degradation temperature were recorded

during the test for the analysis of the thermal stability of CNC reinforced vitrimer, which was performed by a differential scanning calorimeter (Q2000; TA Instruments). For each run, around 10 mg sample was weighed, then sealed in an aluminum pan. The test was run under nitrogen flow with a heating rate of 10 ℃ /min from room temperature to 200 ℃. The specimens were held at 150 ℃ for 5 min then cooled to -90 ℃ at a cooling rate of 10 ℃/min, then heated up to 150 ℃ again with a heating rate of 10 ℃ /min, holding for 10 min.

4.3 Results and discussion

4.3.1 Characterization of PCL-CNC

A series of characterizations was applied to check the modification on the CNC surface. The water contact angle is a direct method to demonstrate the difference between neat CNC and PCL-grafted-CNC (PCL-CNC). Fig. 33 showed the water droplets on the glass slides coated with neat CNC and PCL-CNC. The water droplet on the neat CNC surface suggested a hydrophilic feature with a contact angle of around 24°. After the grafting of PCL, the film became hydrophobic with a contact angle of around 87°, and the droplet remained unchanged in shape for a much longer period. The shift in hydrophobicity of the CNCs confirmed the ring-opening polymerization and successful grafting.

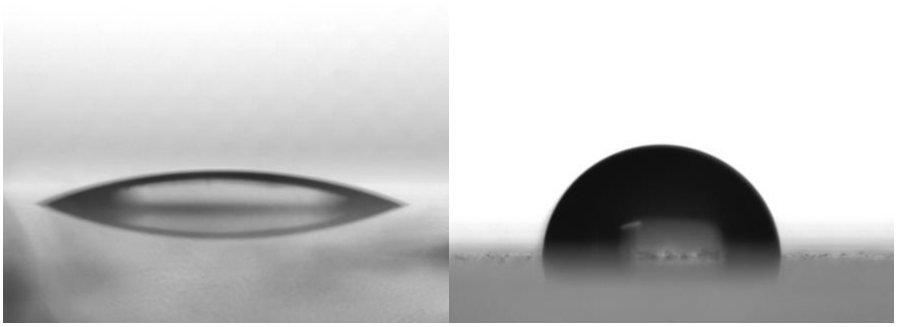

Figure 33. Water droplet on a glass substrate coated with the film of (a) CNC (24.0 ± 2.0°) and (b) CNC-PCL (86.7 ± 1.0°).

The FTIR analysis further confirmed the successful modification of CNC. The FTIR spectra of unmodified CNC and PCL-CNC are presented in Fig. 34. It is obvious that after modification there is an intense new peak at around 1726 cm^{-1}, which is related to the carboxyl groups' (C=O) stretching frequency. Moreover, a lower band intensity at 3330 cm^{-1} was also observed, suggesting the PCL successfully grafted from CNC[19].

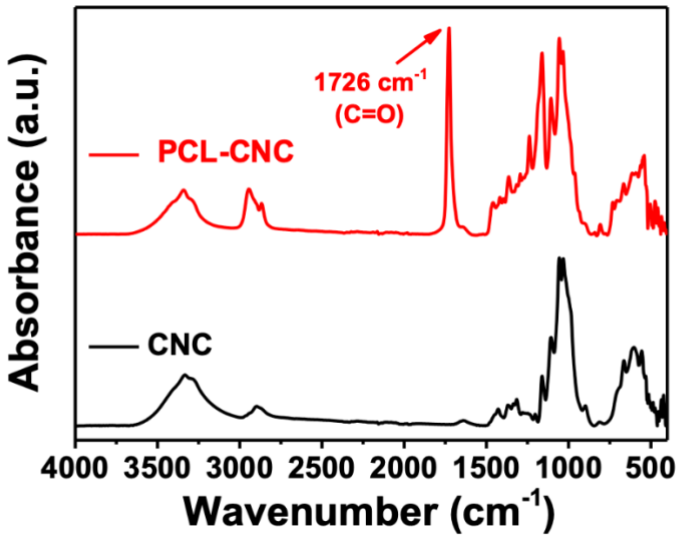

Figure 34. ATR-FTIR spectra of CNC and PCL-CNC.

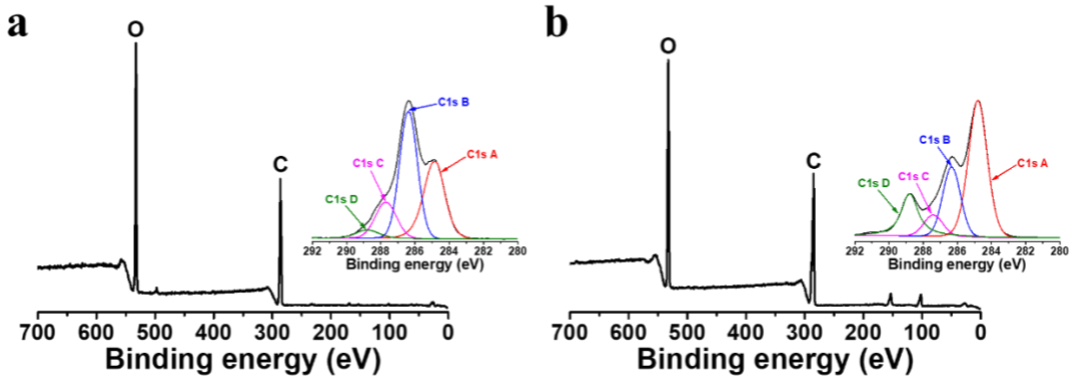

Figure 35. XPS spectra of (a) CNC and (b) PCL-CNC. Insets: high-resolution carbon spectra: C1s A: C–C/C–Hx, 284.8 eV; C1s B: C–OH, 286.4 eV; C1s C: O–C–O, 287.7 eV; C1s D: O–C=O, 288.8 eV.

Table 6. Proportions of carbon atoms involved in various chemical bonds for CNC and PCL-CNC

	C1s A C-C/C-H_x (%)	C1s B C-OH (%)	C1s C O-C-O (%)	C1s D O-C=O (%)
CNC	34.62	46.21	15.34	3.83
CNC-PCL	50.62	23.65	7.67	18.06

X-Ray photoelectron spectroscopy was applied to determine the elements and investigate the carbon-based band. The XPS spectra of unmodified and PCL-grafted CNC are presented in Fig. 35; both show that CNC and PCL-CNC are predominated by oxygen and carbon atoms. In the insert, the high-resolution spectra can be resolved into several peaks, showing the carbon atoms involved in the chemical composition. The four peaks are classified into C-H and C-C, C-OH, O-C-O, and O=C-O by the carbon bonds involved in PCL and/or CNC. The proportion of each carbon-based bond is calculated and summarized in Table 6. The existence of carbon with three bonds to oxygen in the pure CNC might be attributed to the residual cell wall polysaccharides that possess carboxylic groups and are linked to cellulose[19]. The increasing ratio of carboxylic groups in CNC-PCL results from PCL grafted from the ending hydroxyl groups of CNC.

4.3.2 Adhesive properties

One of the features of vitrimers is the rapid change in their viscosity when the temperature exceeds the glass transition temperature (T_g). There are still few studies about the adhesive properties of vitrimer materials, so we applied micro-indentation tests to investigate the adhesion between a vitrimer film (~1mm) and a PDMS probe. In this test, only pure vitrimer was used. Fig. 36 shows the typical curves of preload force vs displacement and time for indentation tests of the vitrimer under different temperatures between room temperature and 100 ℃. It is obvious that the indentation curves changed drastically as the temperature and preload grew, indicating that the pull-off force and the loading and unloading hysteresis increased with rising temperature. Furthermore, in curves of force vs. time shown in Fig. 36b, different relaxation behaviors were observed for samples at different temperatures. The pull-off force during separation is a characteristic parameter of the adhesive interactions between the vitrimer and the PDMS probe; we used it to assess the effect of temperature on the adhesion properties of the vitrimer. The pull-off process occurs gradually, rather than suddenly snapping off the probe; we attribute this behavior to the gradual peeling of the vitrimer from the PDMS probe[136].

From Fig. 37 it is obvious that the pull-off force increased significantly with the rising temperature, especially when it became higher than the glass transition temperature. At higher temperatures, the pull-off force exhibited a significant increase when the applied forces increased from 1 to 5 g, whereas it maintained the same values across all preloads when tested at room temperature. When

the temperature was increased higher than the T_g the curves followed the same trend: increasing rapidly with the increase of preload, then plateauing when the preload force increased further. In the curves of pull-off force vs. time, we can see significant stress relaxation behavior in a constant loading period for temperatures from 60 ℃ to 100 ℃, which confirmed the viscoelastic behavior of vitrimer composites.

Table 7. The pull-force (g) of vitrimers peeling of PDMS at different temperature.

Preload	RT	40℃	60℃	80℃	100℃
1g	0.327	0.516	1.033	1.182	1.138
2g	0.301	0.505	1.187	1.381	1.343
3g	0.266	0.575	1.494	1.682	1.420
4g	0.309	0.671	1.603	1.841	1.649
5g	0.301	0.825	1.626	1.868	1.815

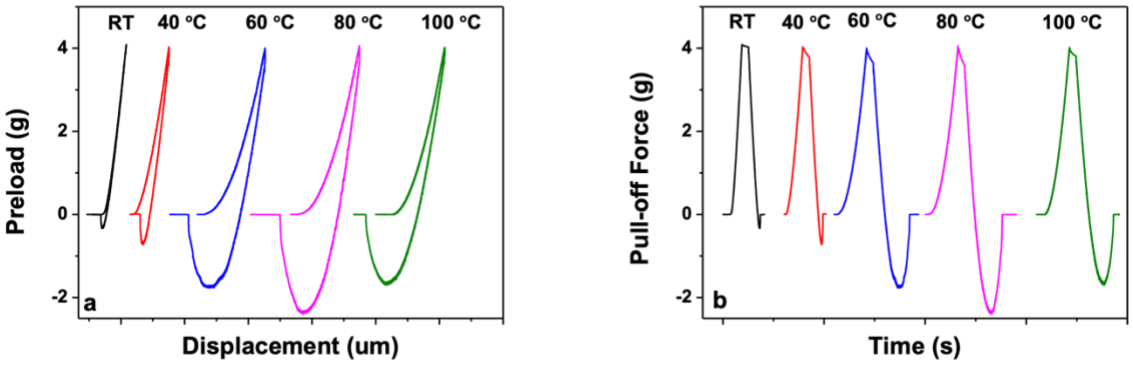

Figure 36. Plots of forces vs a) displacement and b) time for vitrimer with 4 g indentation force.

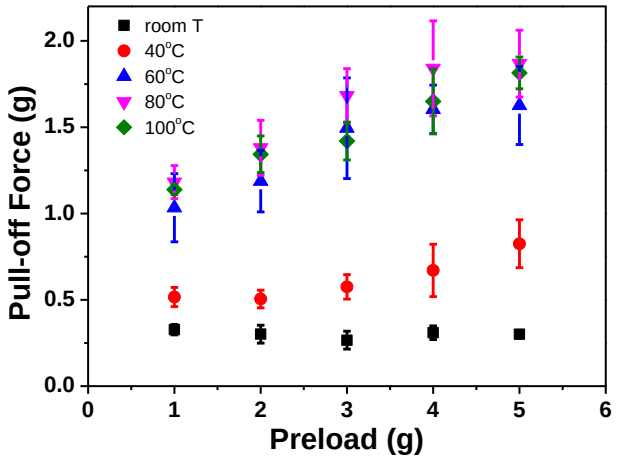

Figure 37. Evolution of pull-off force under different indentation forces at different temperatures.

4.3.3 Thermal stability

4.3.3.1 Differential scanning calorimetry (DSC)

Differential scanning calorimetry was applied to measure the crystallization temperature (T_c) and melting point (T_m), calculated the melting enthalpy (ΔH_m) and crystallization enthalpy (ΔH_c). The results are summarized in Table 8, and the DSC curves of CNC-vitrimer composites are presented in Fig. 38. The PCL-CNC sample exhibits melting and crystallization temperatures of 55.2 ℃ and 31.95 ℃, respectively, which align with literature values[19]. For the vitrimer material, the melting point increased, starting from the melting point of pure vitrimer of 36.6 ℃, as PCL-CNC increased, becoming closer to the melting point of PCL at around 50 ℃, further confirming the increasing presence of PCL. With the introduction of PCL-CNC, there is a shift in the melting temperature towards higher temperatures. This results from the interaction of PCL-CNC, as increasing amounts of ester groups in CNC-vitrimer composites require higher temperature to realize the transesterification. The crystallization temperature was also obtained from the cooling period, presented in Fig. 38. Similar to the melting point, there was also an increase in crystallization temperature due to the high crystallinity of PCL. Therefore, the crystallinity of CNC-vitrimer composited increased with higher loading of PCL-CNC, which shows better filler-matrix compatibility. All the samples exhibited higher melting and crystallization enthalpies except PCL/CNC-5, which corresponds to the result in DMA.

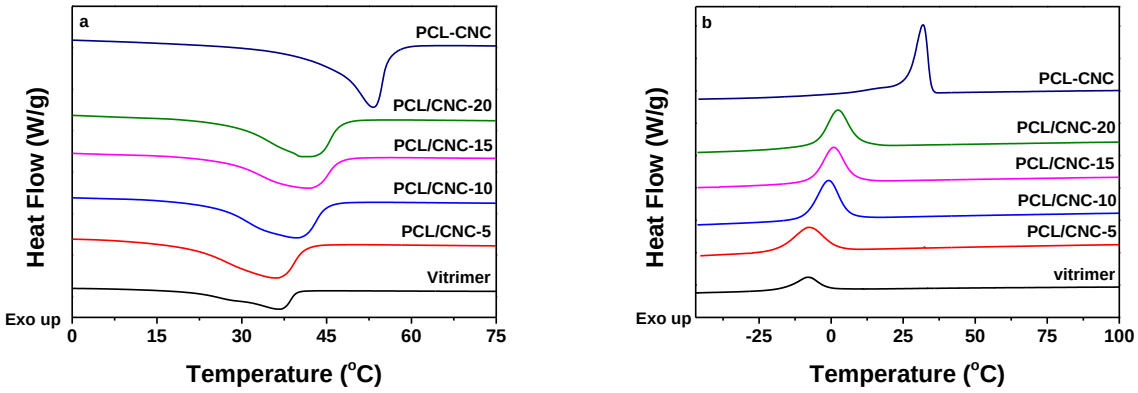

Figure 38. DSC thermogram of CNC-vitrimer composites during a) heating and b) cooling.

Table 8. DSC data of CNC-vitrimer samples; melting (T_m) and crystallization (T_c)temperature, enthalpies of fusion (ΔH_m) and crystallization (ΔH_c)

Sample	T_c (°C)	ΔH_c (J/g)	T_m (°C)	ΔH_m (J/g)
Vitrimer	-8.19	37.23	36.64	36.18
PCL/CNC-5	-7.77	31.89	35.84	34.83
PCL/CNC-10	-0.73	37.89	39.71	35.22
PCL/CNC-15	0.82	39.64	41.50	35.58
PCL/CNC-20	2.23	39.51	40.80	37.24
PCL-CNC	31.95	45.63	55.20	46.17

There is an interesting feature shown in the curves of DSC analysis (Fig 39). For the pure vitrimers, the peak for the crystallization appeared twice in both the cooling and heating period at the same temperature. However, with the incorporation of PCL-CNC, the crystallization appeared only once for all CNC-vitrimer composites. It is still unknown what caused it, we hypothesize that the additional PCL-CNC affects the network structure of vitrimer composites, which would then influence the nucleation and crystallization behavior.

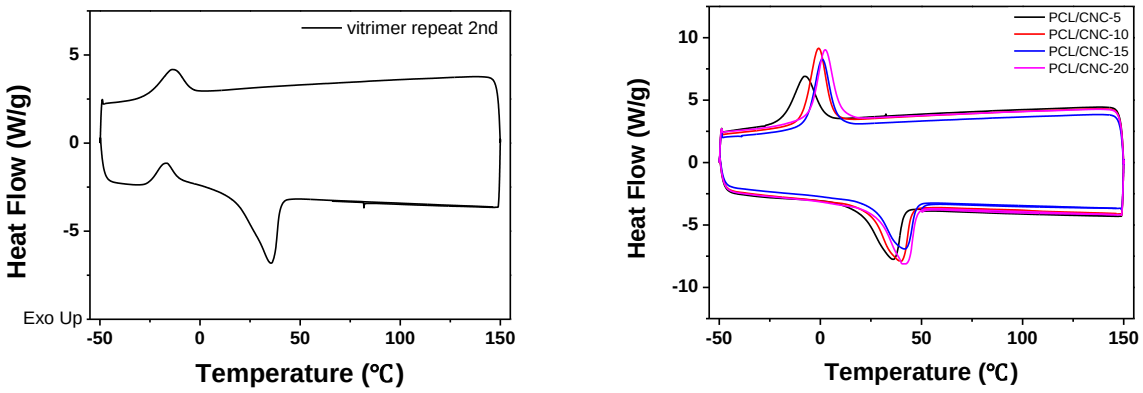

Figure 39. DSC curves of pure vitrimer and PCL-CNC grafted vitrimer composites.

4.3.3.2 Thermogravimetric Analysis (TGA)

The thermal decomposition behaviors of CNC-vitrimer composites were investigated by thermogravimetric analysis and differential thermogravimetry, with the results demonstrated in Fig. 40. Overall, the CNC-vitrimer composites show great thermal stability that are not affected by the incorporation of PCL-CNC. There are two stages for the thermal degradation behavior of PCL-CNC. First, the PCL grafted onto the CNC surface degraded at around 225 ℃ due to its low molecular weight. Then another maximum weight loss appeared at 400 ℃, corresponding to the degradation of CNC. The 5% weight loss temperature for CNC-vitrimer composites is around 325-350 ℃, which is higher than PCL-CNC (250 ℃). The CNC-reinforced vitrimer composites exhibited similar onset temperatures at around 375 ℃ compared to the pure vitrimer. This may result from the successful incorporation of PCL-CNC into vitrimer composites by *in situ* polymerization, as PCL is successfully integrated into the three-dimensional network, demonstrating improved thermal stability. The maximum rate of weight loss of all CNC-vitrimer only occurred at 408-422 ℃, confirming that all PCL-CNC was incorporated into the vitrimer composites.

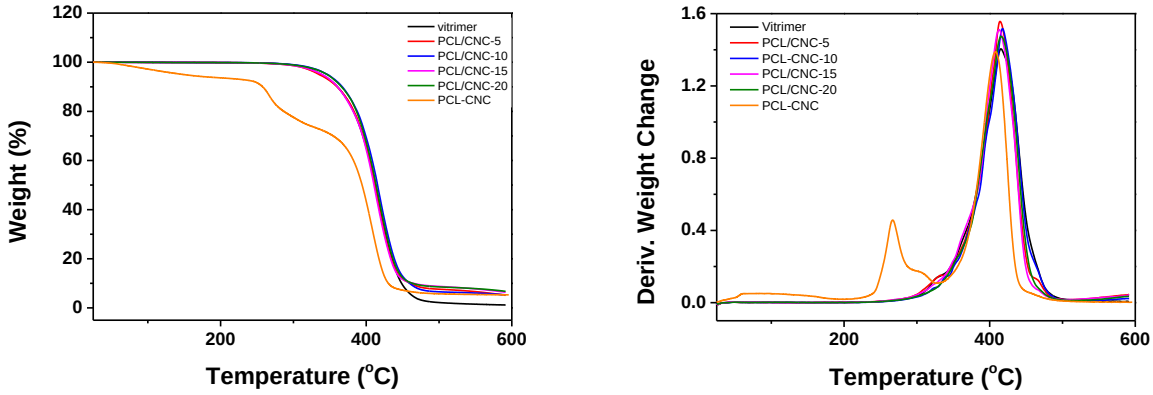

Figure 40. TGA curves of PCL grafted CNC and CNC-vitrimer composites

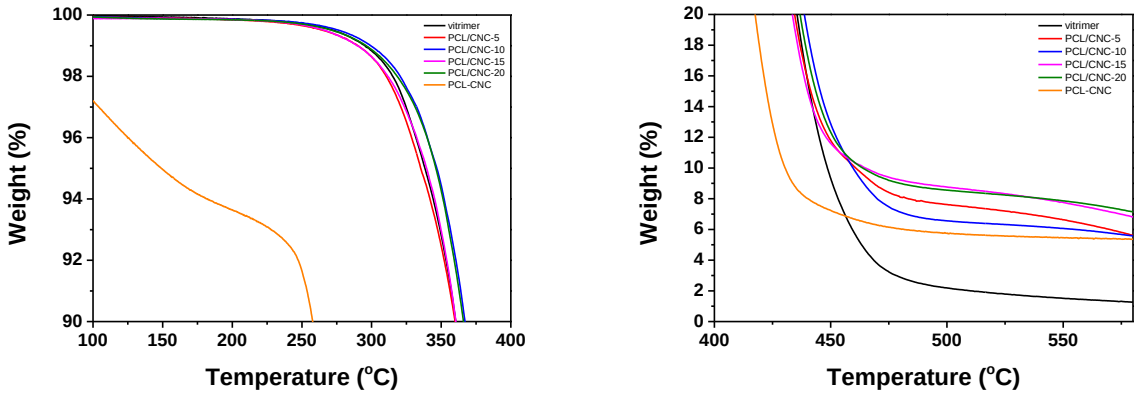

Figure 41. The TGA curves if CNC-vitrimer composites.

4.3.4 Water resistance

4.3.4.1 Water contact angle test

The surface wettability of vitrimer with and without PCL-CNC was characterized by water contact angle tests. The change in water contact angle with the PCL-CNC content is presented in Fig. 42. The addition of PCL-CNC decreased the contact angle of the CNC-vitrimer composite from ~90° to ~85°, due to the hydrophilicity of CNCs. Thus, the introduction of PCL-CNC has minimal effects on hydrophobicity of CNC-vitrimer compared to pure vitrimer.

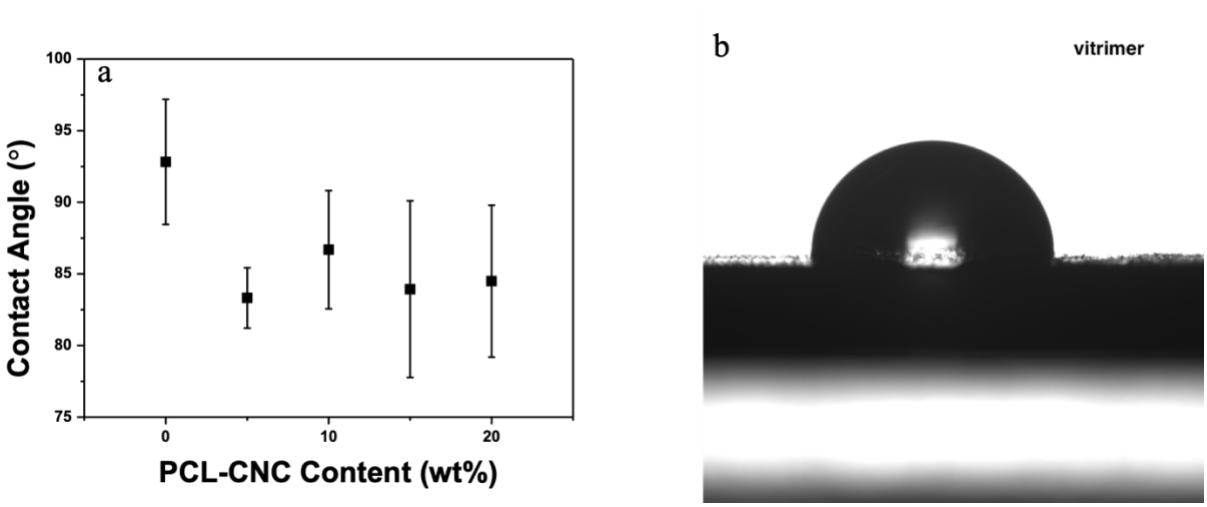

Figure 42. a) The evolution of contact angle of CNC-vitrimer with PCL-CNC content. b) The images of the contact angle of pure vitrimer composites during the test.

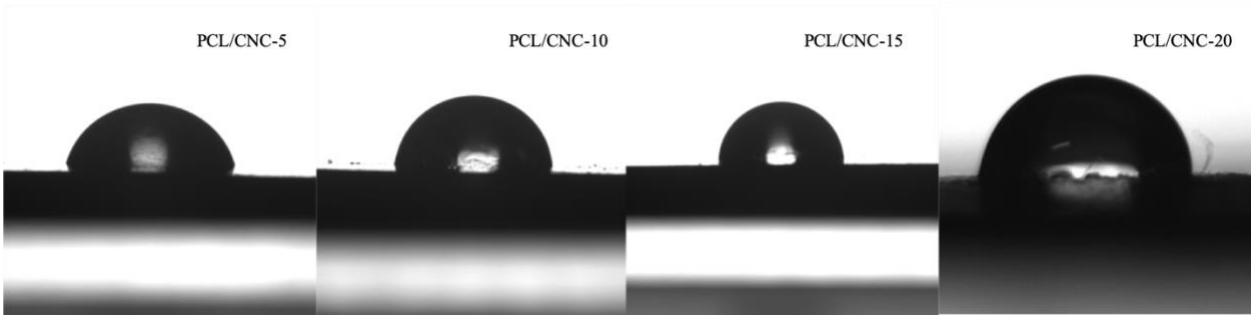

Figure 43. The images of contact angle of CNC-vitrimer composites during the test.

4.3.4.2 Swelling test

The mass change ratio of all CNC-vitrimer composites in water and toluene over time at different temperatures are demonstrated in Fig 44. The samples only swelled without dissolving in the solvent, which matches the insoluble nature of vitrimers, further confirming the three-dimensional network of the CNC-vitrimer composites. It is clear that samples soaked in toluene show a great increase in mass compared to samples soaked in water. Also, among all swelling test conditions, the samples swelled the most at 40 ℃.

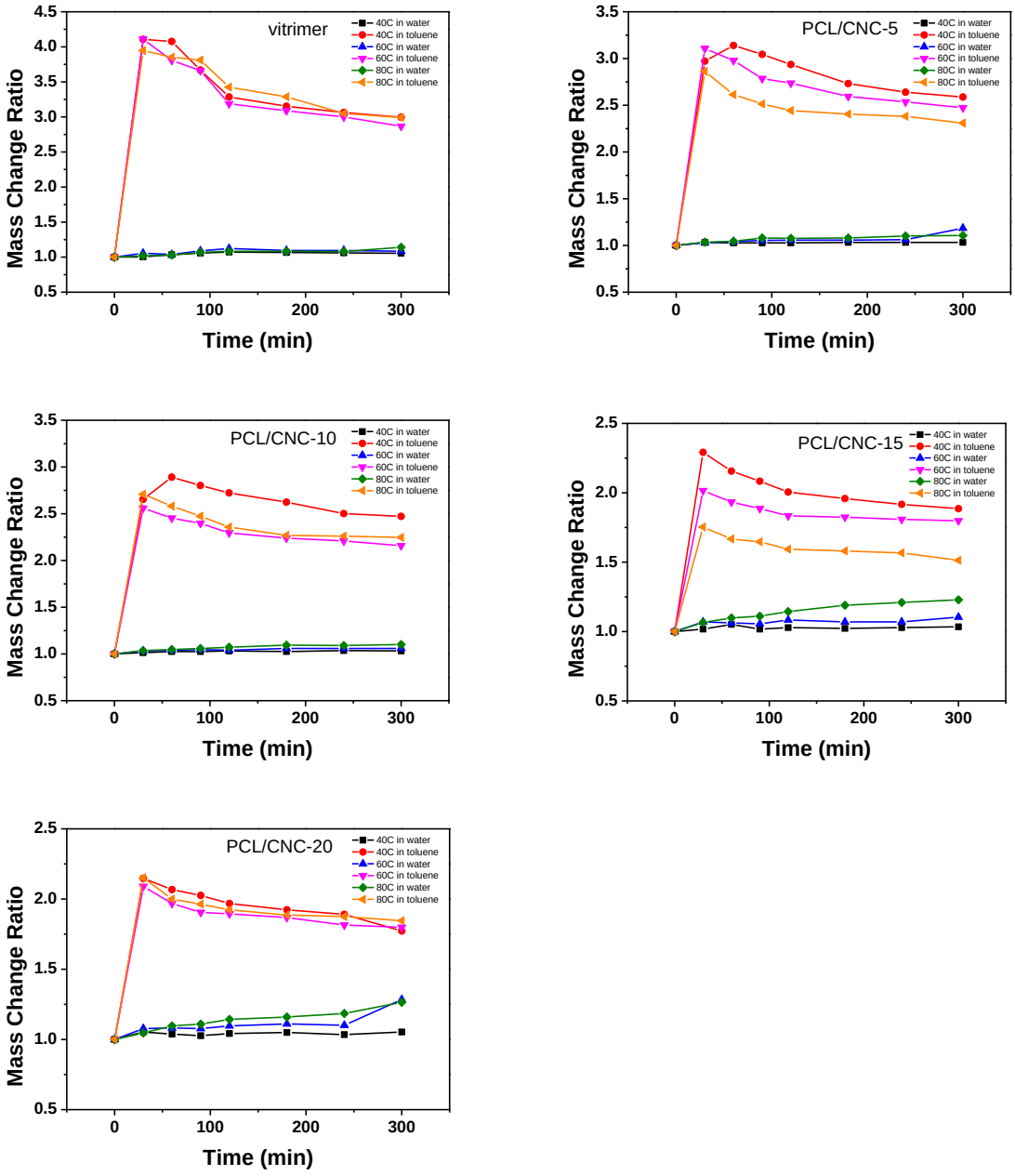

Figure 44. the mass change ratio of CNC-vitrimer in water and toluene at different temperatures.

With the introduction of PCL-CNC, the mass change ratio decreased from the peak value of 4.1 for pure vitrimer to 2.2, suggesting PCL-CNC forms a denser crosslinking network and absorbs less solvent. In addition, the presence of higher loading (15 and 20 wt%) of CNC slightly increased the water absorption when tests were conducted at 80℃ for one and half hours, which is opposite to the swelling behavior of the samples in toluene. The low water uptake, even above the T_g, allows

this vitrimer and the CNC-vitrimer composites to be applied underwater. One observation of note is that the mass of samples soaked in toluene for longer timescales gradually decreased. This might be caused by small molecules that did not participate in the polymerization dissolving into the solvent. The gel contents after the swelling test listed in Table 9 confirmed the weight loss in the swelling tests. This suggests we might further develop the structure of CNC-vitrimer composites and optimize the experiment conditions for transesterification.

Table 9. The gel content of CNC-vitrimer composites after swelling in toluene and water.

Gel Content	40 ℃		60 ℃		80 ℃	
	In water	In toluene	In water	In toluene	In water	In toluene
Vitrimer	0.98	0.56	0.99	0.55	1	0.51
PCL/CNC-5	0.98	0.64	0.98	0.55	0.91	0.61
PCL/CNC-10	0.99	0.55	0.99	0.52	1	0.48
PCL/CNC-15	0.98	0.52	0.96	0.54	0.96	0.43
PCL/CNC-20	1	0.53	1	0.48	0.96	0.49

4.3.5 Thermo-mechanical properties

4.3.5.1 Dynamic mechanical analysis (DMA)

To characterize the effect of PCL-CNC on the mechanical properties of the vitrimer composites, DMA was used to obtain the curves of storage modulus and tan delta of vitrimer with and without PCL-CNC, presented in Fig. 45. For the vitrimer without PCL-CNC, the storage modulus could reach around 80 MPa. With the various concentrations of PCL-CNC, the storage modulus improved significantly and reached its peak value of 220 MPa for vitrimer incorporated with 15 wt% PCL-CNC. However, when the content of PCL-CNC increased to 20 wt%, the storage modulus reduced to around 150 MPa, which is attributed to aggregation of CNC at higher content resulting in deteriorated interactions with the vitrimer matrix. The addition of PCL-CNC into the vitrimer matrix also slightly affects the glass transition temperature (T_g) of the CNC-vitrimer composites, with this shift trending towards higher temperatures with growing PCL-CNC content. The T_g of CNC-vitrimer composites are summarized in Table 10. The increase in T_g resulted from the incorporation of PCL-CNC, due to it possessing a higher melting point than pure vitrimer. Also,

the increasing amount of crystallinity in vitrimers with the addition of PCL-CLC would limit the chain mobility, which could also cause the increase in T_g.

Table 10. the mean values of mechanical properties of CNC-vitrimer composites

Samples	T_g (℃)	Young's modulus (MPa)	1st Strain (%)	1st Stress (MPa)	2nd Strain (%)	2nd Stress (MPa)	3rd Strain (%)	3rd Stress (MPa)
Vitrimer	45.1	93.43	66.29	0.078	53.06	0.058	54.48	0.081
PCL/CNC-5	46.2	127.78	137.51	0.284	106.15	0.297	98.70	0.195
PCL/CNC-10	50.9	163.99	163.87	0.407	107.84	0.427	85.61	0.305
PCL/CNC-15	55.2	224.16	118.55	0.487	80.26	0.359	66.87	0.304
PCL/CNC-20	55.3	145.45	81.00	0.472	61.63	0.385	39.77	0.255

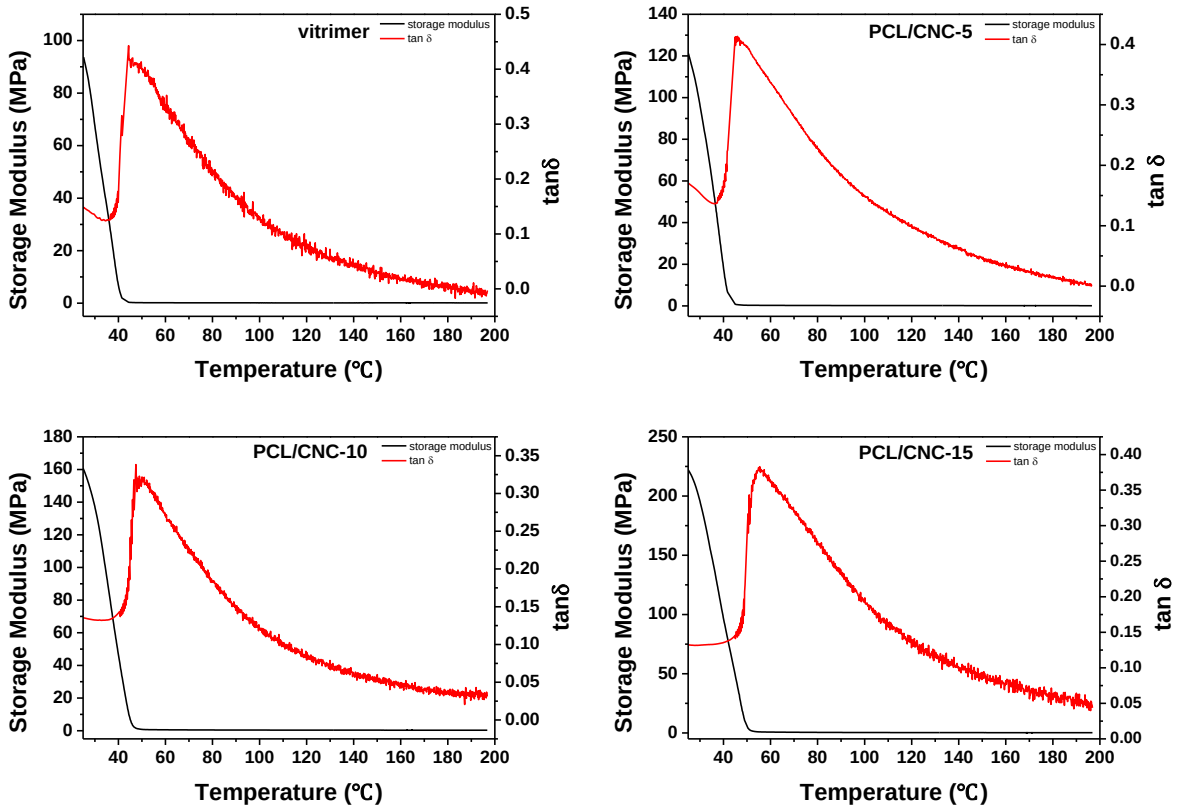

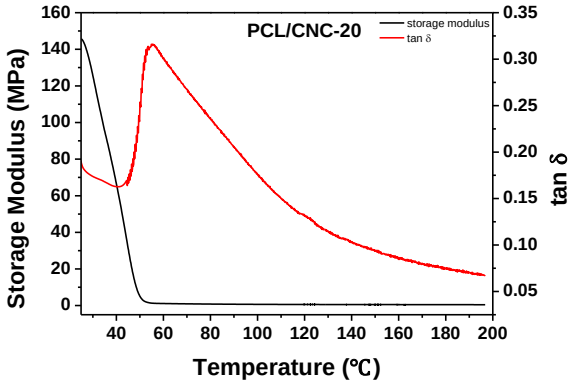

Figure 45. Storage modulus and tan delta for CNC-vitrimer composites as a function of temperature.

4.3.5.2 Stress relaxation

As a typical feature of vitrimer materials, the stress relaxation behavior, which is caused by dynamic cross-linking exchange reactions and rearrangement of the network, is commonly investigated to characterize the thermo-mechanical properties of CNC-vitrimer material. The characteristic relaxation time (τ) of vitrimers is defined as the time when the normalized stress is lower than 1/e (36.8%) of the initial stress or modulus. As shown in Fig. 46, the vitrimer and CNC-vitrimer composites all completely released their deformational stress at temperatures of 150-180 ℃. The relaxation process is relatively slow at 150 °C and 160 °C, and is significantly faster at 170 °C and 180 °C. Furthermore, PCL/CNC-5 vitrimer releases its deformational stress more quickly than the other composites under the same conditions.

The whole stress relaxation process shows rapid relaxation for a short period of time at the beginning, followed by a longer slow relaxation process[138]. The initial rapid relaxation is caused by the relaxation of the normal cross-linked polymer as a result of the partial response to external forces of the chain segments between the small unit and the cross-link point. The forces applied to the specimen are gradually able to overcome the internal frictional resistance to the thermal motion of the small unit structure, and the molecular chain conformation is continuously adjusted to the thermal motion of the chain segments. The subsequent long-term stress relaxation is caused by the breakage and reorganization of the cross-linked sites, which occurs in the high temperature region where the increased activity of the catalyst and the increased rate of ester exchange accelerates the breakage and reorganization of the cross-linked sites. The relaxation is initially dominated by the

normal cross-linking polymer relaxation and then by the transesterification reaction. Combining the Maxwell model and the generalized Maxwell model:

$$\sigma(t) = \sigma_1 + \sigma_2 \quad \text{equation (6)}$$

$$\varepsilon_0 G(t) = \varepsilon_0 G_1 e^{-t/\tau_1} + \varepsilon_0 G_2 e^{-t/\tau_2} \quad \text{equation (7)}$$

$$\frac{G(t)}{G_0} = \frac{G_1}{G_0} e^{t/\tau_2} + \frac{G_2}{G_0} e^{t/\tau_2} \quad \text{equation (8)}$$

Where σ is the strain, ε is the stress, G is the shear modulus, and τ is the relaxation time.

We can simplify equation (7) to

$$y = A_1 e^{-t/\tau_1} + A_2 e^{-t/\tau_2} \quad \text{equation (9)}$$

Where τ_1 we consider as the relaxation time of the corresponding external stress in the small molecules, and τ_2 is the time of stress relaxation induced by the chain break accelerated by the transesterification. By applying equation 9 to the curves of stress relaxation as a function of time, we can obtain τ_1 and τ_2 respectively; all the curves show excellent fitting results, with all R^2 larger than 0.995. Additionally, according to the definition of vitrimer by Leibler, at high temperatures, it fits the Arrhenius law:

$$\tau = \tau_0 \exp\left(\Delta E/RT\right) \quad \text{equation (10)}$$

Where R is the gas constant and ΔE is the activation energy.

In this case, we use τ_2 (presented in Table 11), which corresponds to the time of stress relaxation induced by transesterification. By plotting the curves of ln(τ) versus 1000/*T*, the activation energy for viscous flow can be obtained from linear fitting the curve to get the slope. The information for the fitting line was summarized in Table 11.

The stress relaxation behavior is associated with the rearrangement and transesterification of the network. From Table 11, the stress relaxation time (τ_2) gradually decreased with the increasing temperature, which suggests a viscoelastic behavior. We can see that with the incorporation of PCL-CNC, the stress relaxation time of vitrimer composites decreased from around 250 min to 180 min at 150 ℃ and from 184 min to 150 min at 160 ℃, indicating the composite has better dynamic properties than pure vitrimer at these temperatures. However, when the temperature increased to 180 ℃, the stress relaxation time of PCL/CNC-20 increased to 150 min compared to pure vitrimer stress relaxation time of 110 min.

Table 11. Stress relaxation time at different temperatures.

Samples	τ (150℃) (min)	τ (160℃) (min)	τ (170℃) (min)	τ (180℃) (min)	E_a (kJ/mol)
Vitrimer	247.9	184.5	152.2	117.8	38.67
PCL/CNC-5	194.6	148.1	121.3	98.4	35.84
PCL/CNC-10	250.7	193.6	161.8	132.1	33.54
PCL/CNC-15	215.7	178.8	153.4	128.5	27.24
PCL/CNC-20	184.9	173.5	163.6	152.3	10.21

The change in stress relaxation time with addition of PCL-CNC can be attributed to the extra ester and hydroxyl moieties, providing more cross-linking points for associative CANs, which benefits the transesterification reaction. However, excessive amounts of PCL-CNC contain more crystalline structures in the composites, limiting the chain movements of the vitrimer network. For practical applications, vitrimers with low τ_2 values are preferable, as they exhibit rapid stress relaxation and a rapid decrease in viscosity under heating conditions, thus accommodating the need for rapid processing. Additionally, the stress relaxation performance of vitrimer materials can also follow the Arrhenius equation at high temperatures (equation (10)). All vitrimer composites tested at 180 ℃ took around 130 min to achieve stress relaxation. However, when the temperature was decreased to 150 ℃, neat vitrimer shows a clear increase in stress relaxation time to around 250 min, whereas PCL/CNC-20 exhibits a smaller increase in stress relaxation time to 185 min. This comparison proves that the incorporation of PCL-CNC decreased the vitrimers sensitivity of temperature.

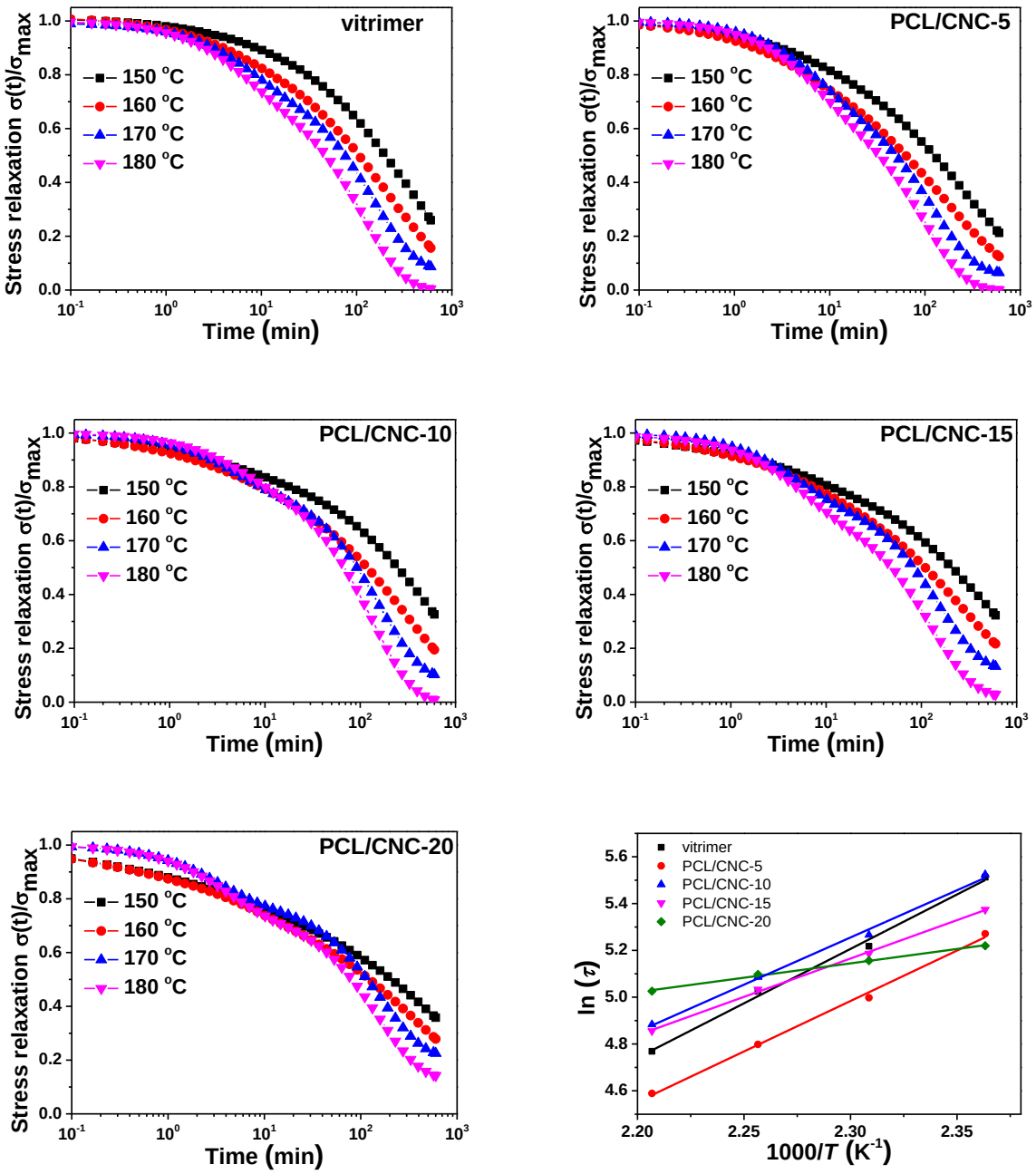

Figure 46. Normalized stress relaxation curves for neat vitrimer and CNC-vitrimer composites and linear fitting of the ln(τ) versus 1000/*T*.

For vitrimer materials, E_a characterizes the sensitivity of viscosity or stress relaxation behavior to temperature changes[137]. A higher E_a indicates the vitrimer is more sensitive to temperature changes at elevated temperatures, and also indicates the vitrimer will exhibit a rapid decrease in viscosity with rising temperatures. As presented in Table 11, the values of E_a decrease from 38.7 kJ/mol for

neat vitrimer to 10.21 kJ/mol for PCL/CNC-20, which means it is easier to realize the transesterification with higher loading of PCL-CNC due to the additional ester and hydroxyl groups. In the CNC-vitrimer system, the stress relaxation behavior can be associated with both the ester groups and crystallites in PCL-CNC. At low amounts of PCL-CNC, the hydroxyl groups on the CNC surfaces and ester groups on PCL chains dominate the CANs dynamics; however, with higher loading of PCL-CNC, the self-aggregation and crystallites in CNC limit the transesterification of vitrimer composites. The effect of CNCs can also be seen in the fitting lines for plots of $\ln(\tau)$ vs. $1000/T$, where the intercept of the fitting lines can reflect the characterization relaxation time (τ_0) of the vitrimer system without barrier[137]. The increasing τ_0 with increasing PCL-CNC content demonstrates that network rearranged slower, confirming the constraint on the chain mobility of CNC crystallites and aggregation. Therefore, CNC-vitrimer with more PCL-CNC became less sensitive to the temperature change. One may conclude that the segment mobility was mainly controlled by the concentration of PCL-CNC, as evidenced by the slight increase T_g. Therefore, the incorporation of PCL-CNC significantly increased the storage modulus of vitrimer composites.

4.3.6 Tensile mechanical properties

To verify that CNC-vitrimer can be reprocessed by the temperature-induced method and still maintain great mechanical properties, tensile tests were performed three times to break, reprocessing the vitrimer or CNC-vitrimer composite between each test. The strain-stress curves for each run were demonstrated in Fig. 47. The incorporation of PCL-CNC improved the strength of vitrimer composites under 70 ℃. When vitrimer matrix was incorporated with PCL/CNC, the tensile strength gradually increased, reaching the highest value of 0.4 MPa for PCL/CNC-10, then maintaining this value with higher loading of PCL-CNC. The increase in tensile strength is contributed to by the abundant hydroxyl groups on the CNC surface, leading to excellent hydrogen bonding interactions. The introduction of PCL-CNC enhanced the stain at break as well. The strain at break increased from ~66% for neat vitrimer to ~160% with the increase of PCL-CNC content to 10 wt%; when more PCL-CNC was added into the matrix, the CNC-vitrimer composites showed a decrease in the strain at break, which could be the result of the aggregation of CNC and crystallites limiting the mobility of the chains. These tensile test results correspond well to the performance observed from DMA characterization.

For the repeated tensile tests, after the first run, the samples were reformed by compressing and heating in the oven with 150 ℃, then the tensile tests were carried out under the same conditions. The vitrimer without PCL-CNC exhibited almost the same mechanical performance, showing similar values of strength and strain at break. However, the CNC-vitrimer composites all displayed reduction in both strength and strain after being repeated (Fig. 48). This change is most obvious in difference in the strain at break between the first test and second test. The decrease in mechanical performance might be attributed to reprocessing, in which the network and the crosslink were influenced by the external forces applied.

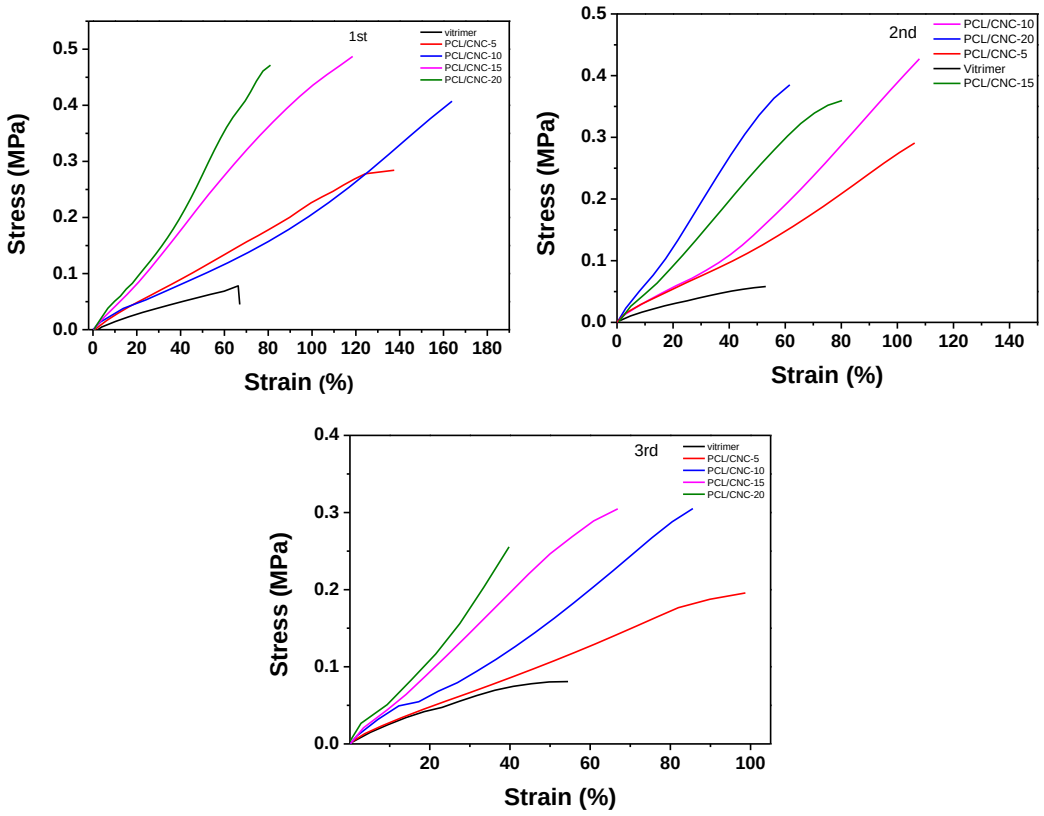

Figure 47. Typical strain-stress curves of CNC-vitrimer composites and after reprocessed for 2nd and 3rd times.

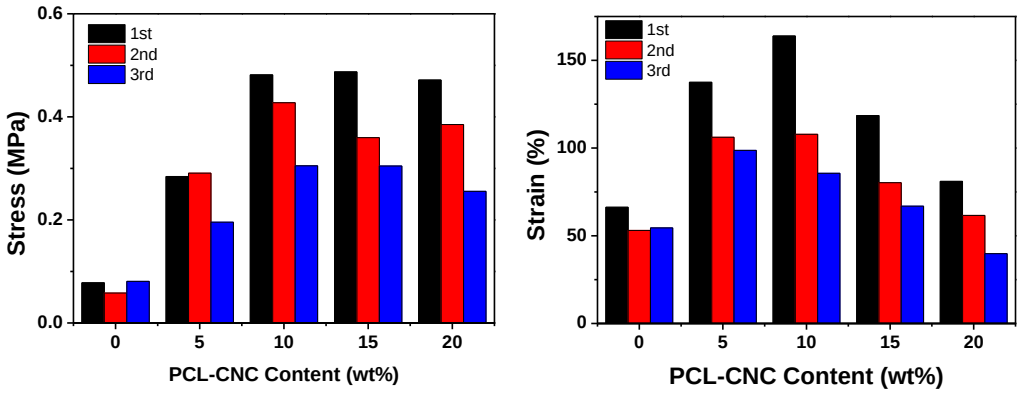

Figure 48. Values of stress and strain of vitrimers with varied PCL-CNC contents after reprocessing.

4.4 Conclusion

In this study, we applied PCL-grafted CNCs into a vitrimer matrix and investigated the effect of PCL-CNC on the mechanical, thermal, and thermo-dynamic properties. When the vitrimer matrix was incorporated with 15% PCL-CNC, the CNC-vitrimer composite exhibited the best storage modulus. The presence of PCL-CNC slightly increased the glass transition temperature of vitrimer composites from 45℃ to 55.82 ℃. The introduction of PCL-CNC also improved the tensile strength of the vitrimer composites both in the ambient environment and above its glass transition temperature. However, it is possible that PCL-CNC affected the mechanical strength after several reprocessing cycles. For the thermal stability, while the PCL-grafted CNCs do not possess as good a thermal stability as pure vitrimer, the CNC- vitrimer composites still maintained excellent thermal stability with the introduction of PCL-CNC, with an onset temperature of around 375 ℃ and peak temperature at around 410 ℃ for all vitrimer composites. The hydrophobicity of the vitrimer material was slightly influenced by the hydrophilic nature of CNC, which also affected the water absorption for the CNC-vitrimer composites with higher loading of PCL-CNC. The toluene swelling test demonstrates that there were some unreacted polymer molecules dissolved in the solvent, suggesting there is still potential for further research. The stress relaxation behavior is mainly controlled by the content of PCL-CNC; when a small amount of PCL-CNC was added into vitrimer matrix, the hydroxyl and ester groups accelerated the transesterification; however, when more PCL-CNC was incorporated into the matrix, the aggregation and crystals in CNCs limited the chain movement, leading to longer relaxation times.

Additionally, the lower E_a and shorter stress relaxation times provide CNC-vitrimer composites the ability to transfer faster from glassy state to rubbery state, which is an advantage for vitrimer materials in temperature-induced applications and expands their possibilities in 3D printing, electrical devices, and aerospace applications.

Chapter 5. Conclusion and recommendations

In this thesis, our main goal is to investigate the effect of introducing cellulose nanoparticles on the mechanical properties of composite material. First, PU/CNC nanocomposite films were successfully produced using the casting and evaporation method. The film products were clear and transparent, confirming CNC particles are well dispersed in the waterborne PU matrix. The tensile test proved the enhanced tensile strength, toughness, and Young's modulus, and decreasing strain at break with the increasing CNC content. The increased mechanical properties are attributed to the abundant hydroxyl groups on the CNC surface, which form strong hydrogen bonding interactions and limit the mobility of the PU chains. The FTIR characterization also shows the strong interactions between CNCs and PU. The incorporation of CNCs increased the friction coefficient and scratch resistance, suggesting the potential of the composites in serving as a coating material. As CNCs are hydrophilic, the contact angle of PU/CNC composites decreased to ~31º, resulting in a hydrophilic surface. Finally, the thermal stability slightly increased, with a 5% weight loss temperature of ~270 ℃ and maximum weight loss at ~400 ℃.

In the second part of this work, the vitrimer material showed good adhesion properties to PDMS when above its glass transition temperature. However, the vitrimer material also exhibited poor mechanical strength, especially above T_g. The CNCs were first grafted with PCL, since CNCs cannot be well dispersed into the vitrimer matrix. PCL-CNC was then added into vitrimer matrix through *in situ* method, showing obvious reinforcing effects in the vitrimer matrix with an improved storage modulus. For thermodynamic properties, increasing loading of PCL/CNC increased the T_g by ~10℃, and the melt point and crystallization temperature shifted towards those of pure PCL-CNC. The CNC-vitrimer composites presented good water resistance, with only a slight decrease in contact angles and minor swelling behavior in water, confirming the insoluble feature of vitrimer materials. Also, the tensile strength and strain at break increased dramatically, reaching a peak value of 163% for PCL/CNC-10 and 0.48 MPa for PCL/CNC-15 at 70 ℃ compared to 0.078 MPa and 66.29% for neat vitrimer, proving great mechanical reinforcing effect. The vitrimer also maintained good tensile strength after several reprocessing cycles. The thermodynamic properties also showed improvement in the stress-relaxation behavior. The stress relaxation time showed a decrease under all tested temperatures when PCL-CNC was added. The

E_a for the network arrangement and transesterification also decreased gradually from 38 kJ/mol to 10kJ/mol. The reduced relaxation time and active energy all demonstrate a faster transformation from glassy state to rubbery state, which can be more desirable for practical applications.

Overall, in this study, CNCs showed great reinforcing effect in both polyurethane matrix and vitrimer matrix by the casting and evaporation and *in situ* polymerization methods, respectively. The increased mechanical strength and Young's modulus provide more possible applications for waterborne polyurethane and vitrimer materials. Additionally, the better friction and scratch resistance make polyurethane more suitable for coating materials. The vitrimer system acquired better thermodynamic properties in terms of faster transesterification and lower activation energy.

As for the future work, since waterborne PU is commonly used as a coating material, the peeling test could be employed to evaluate the adhesion between films and different substrates. Besides, since the hydrophobicity of WPU is affected by the CNCs, water adsorption and swelling tests could be carried out to charaterize the water resistance behavior. Additionally, friction and tensile tests under water could be useful characterizations for underwater applications. For the CNC-vitrimer composites, the shape memory test can be applied, as this is key feature of vitrimer materials. The thermodynamic properties can be further investigated under different conditions such as varying frequency and stress to expand the possibilities of future applications. Additionally, the fabrication conditions can be optimized by adjusting the ratios of ingredients and synthesis time and temperature to achieve a higher gel content.

References

1. Heux, L., et al. “Structural Aspects in Ultrathin Cellulose Microfibrils Followed by 13C CP-MAS NMR.” *Carbohydrate Polymers*, vol. 40, no. 2, Elsevier Ltd, 1999, pp. 115–24, https://doi.org/10.1016/S0144-8617(99)00051-X.

2. Kargarzadeh, Hanieh, et al. “Recent Developments on Nanocellulose Reinforced Polymer Nanocomposites: A Review.” *Polymer (Guilford)*, vol. 132, Elsevier Ltd, 2017, pp. 368–93, https://doi.org/10.1016/j.polymer.2017.09.043.

3. “Comprehensive Cellulose Chemistry. Volume 1. Fundamentals and Analytical Methods By D. Klemm, B. Philipp, T. Heinze, U. Heinze, and W. Wagenknecht. Wiley: Weinheim, Germany. 1998. 260 Pp. $236.25. ISBN 3-527-29413-9.” *Journal of the American Chemical Society*, vol. 121, no. 37, American Chemical Society, 1999, pp. 8677–8677, https://doi.org/10.1021/ja9857514.

4. Nascimento, Diego M., et al. “Nanocellulose Nanocomposite Hydrogels: Technological and Environmental Issues.” *Green Chemistry: an International Journal and Green Chemistry Resource: GC*, vol. 2, no. 11, Royal Society of Chemistry, 2018, pp. 2428–48, https://doi.org/10.1039/c8gc00205c.

5. Habibi, Youssef, et al. “Cellulose Nanocrystals: Chemistry, Self-Assembly, and Applications.” *Chemical Reviews*, vol. 110, no. 6, American Chemical Society, 2010, pp. 3479–500, https://doi.org/10.1021/cr900339w.

6. Lu, Benlian, et al. “Cation Does Matter: How Cationic Structure Affects the Dissolution of Cellulose in Ionic Liquids.” *Green Chemistry: an International Journal and Green Chemistry Resource: GC*, vol. 16, no. 3, 2014, pp. 1326–35, https://doi.org/10.1039/C3GC41733F.

7. Dufresne, Alain. “Cellulose Nanomaterial Reinforced Polymer Nanocomposites.” *Current Opinion in Colloid & Interface Science*, vol. 29, Elsevier Ltd, 2017, pp. 1–8, https://doi.org/10.1016/j.cocis.2017.01.004.

8. Festucci-Buselli, Reginaldo A., et al. “Structure, organization, and functions of cellulose synthase complexes in higher plants.” *Brazilian Journal of Plant Physiology*, vol. 19, no. 1, Brazilian Journal of Plant Physiology, 2007, pp. 1–13, https://doi.org/10.1590/S1677-04202007000100001.

9. Langan, Paul, et al. “X-Ray Structure of Mercerized Cellulose II at 1 Å Resolution.” *Biomacromolecules*, vol. 2, no. 2, American Chemical Society, 2001, pp. 410–16, https://doi.org/10.1021/bm005612q.

10. Isogai, Akira, et al. “TEMPO-Oxidized Cellulose Nanofibers.” *Nanoscale*, vol. 3, no. 1, 2011, pp. 71–85, https://doi.org/10.1039/c0nr00583e.

11. Kolpak, Francis J. et al. “Mercerization of cellulose: 1. Determination of the structure of Mercerized cotton.” *Polymer* 19 (1978): 123-131.

12. Gardiner, E S, and Sarko, A. *Celluloses IV/sub I/ and IV/sub II/: are they the same structure*. United States: N. p., 1983. Web.

13. Siqueira, Gilberto, et al. "Cellulosic Bionanocomposites: A Review of Preparation, Properties and Applications." *Polymers*, vol. 2, no. 4, MDPI AG, 2010, pp. 728–65, https://doi.org/10.3390/polym2040728.

14. HERBERT YEUNG, K. K., and K. P. RAO. "Mechanical Properties of Kevlar-49 Fibre Reinforced Thermoplastic Composites." *Polymers & Polymer Composites*, vol. 20, no. 5, Rapra, 2012, pp. 411–23, https://doi.org/10.1177/096739111202000501.

15. Herrick, F W, Casebier, R L, Hamilton, J K, and Sandberg, K R. *Microfibrillated cellulose: morphology and accessibility*. United States: N. p., 1983. Web.

16. Turbak, A F, Snyder, F W, and Sandberg, K R. *Microfibrillated cellulose, a new cellulose product: properties, uses, and commercial potential*. United States: N. p., 1983. Web.

17. Iwamoto, Shinichiro, et al. "Elastic Modulus of Single Cellulose Microfibrils from Tunicate Measured by Atomic Force Microscopy." *Biomacromolecules*, vol. 10, no. 9, American Chemical Society, 2009, pp. 2571–76, https://doi.org/10.1021/bm900520n.

18. Malainine, Mohamed E., et al. "Structure and Morphology of Cladodes and Spines of Opuntia Ficus-Indica. Cellulose Extraction and Characterisation." *Carbohydrate Polymers*, vol. 51, no. 1, Elsevier Ltd, 2003, pp. 77–83, https://doi.org/10.1016/S0144-8617(02)00157-1.

19. Y. Habibi, et al., "Bionanocomposites Based on Poly(ε-caprolactone)-Grafted Cellulose Nanocrystals by Ring-Opening Polymerization," *Journal of Materials Chemistry*, Vol. 18, No. 41, 2008, pp. 5002-5010. doi:10.1039/b809212e

20. Zimmermann, T., et al. "Cellulose Fibrils for Polymer Reinforcement." *Advanced Engineering Materials*, vol. 6, no. 9, WILEY-VCH Verlag, 2004, pp. 754–61, https://doi.org/10.1002/adem.200400097.

21. Pääkkö, M., et al. "Enzymatic Hydrolysis Combined with Mechanical Shearing and High-Pressure Homogenization for Nanoscale Cellulose Fibrils and Strong Gels." *Biomacromolecules*, vol. 8, no. 6, American Chemical Society, 2007, pp. 1934–41, https://doi.org/10.1021/bm061215p.

22. Henriksson, M., et al. "An Environmentally Friendly Method for Enzyme-Assisted Preparation of Microfibrillated Cellulose (MFC) Nanofibers." *European Polymer Journal*, vol. 43, no. 8, Elsevier Ltd, 2007, pp. 3434–41, https://doi.org/10.1016/j.eurpolymj.2007.05.038.

23. Saito, Tsuguyuki, et al. "Cellulose Nanofibers Prepared by TEMPO-Mediated Oxidation of Native Cellulose." *Biomacromolecules*, vol. 8, no. 8, American Chemical Society, 2007, pp. 2485–91, https://doi.org/10.1021/bm0703970.

24. Saito, Tsuguyuki, et al. “Homogeneous Suspensions of Individualized Microfibrils from TEMPO-Catalyzed Oxidation of Native Cellulose.” *Biomacromolecules*, vol. 7, no. 6, American Chemical Society, 2006, pp. 1687–91, https://doi.org/10.1021/bm060154s.

25. Miao, Chuanwei, and Wadood Y. Hamad. “Cellulose Reinforced Polymer Composites and Nanocomposites: a Critical Review.” *Cellulose (London)*, vol. 20, no. 5, Springer Netherlands, 2013, pp. 2221–62, https://doi.org/10.1007/s10570-013-0007-3.

26. Anglès, M. Neus, and Alain Dufresne. “Plasticized Starch/Tunicin Whiskers Nanocomposite Materials. 2. Mechanical Behavior.” *Macromolecules*, vol. 34, no. 9, American Chemical Society, 2001, pp. 2921–31, https://doi.org/10.1021/ma001555h.

27. Matos Ruiz, M., et al. “Processing and Characterization of New Thermoset Nanocomposites Based on Cellulose Whiskers.” *Composite Interfaces*, vol. 7, no. 2, Taylor & Francis Group, 2000, pp. 117–31, https://doi.org/10.1163/156855400300184271.

28. Araki, Jun, et al. “Flow Properties of Microcrystalline Cellulose Suspension Prepared by Acid Treatment of Native Cellulose.” *Colloids and Surfaces. A, Physicochemical and Engineering Aspects*, vol. 142, no. 1, Elsevier B.V, 1998, pp. 75–82, https://doi.org/10.1016/S0927-7757(98)00404-X.

29. Camarero Espinosa, Sandra et al. “Isolation of thermally stable cellulose nanocrystals by phosphoric acid hydrolysis.” *Biomacromolecules* vol. 14,4 (2013): 1223-30. doi:10.1021/bm400219u

30. Filpponen, Ilari, and Dimitris S. Argyropoulos. “Regular Linking of Cellulose Nanocrystals via Click Chemistry: Synthesis and Formation of Cellulose Nanoplatelet Gels.” *Biomacromolecules*, vol. 11, no. 4, American Chemical Society, 2010, pp. 1060–66, https://doi.org/10.1021/bm1000247.

31. Wang, Neng, et al. “Thermal Degradation Behaviors of Spherical Cellulose Nanocrystals with Sulfate Groups.” *Polymer (Guilford)*, vol. 48, no. 12, Elsevier Ltd, 2007, pp. 3486–93, https://doi.org/10.1016/j.polymer.2007.03.062.

32. Hirota, Masayuki, et al. “Water Dispersion of Cellulose II Nanocrystals Prepared by TEMPO-Mediated Oxidation of Mercerized Cellulose at pH 4.8.” *Cellulose (London)*, vol. 17, no. 2, Springer Netherlands, 2009, pp. 279–88, https://doi.org/10.1007/s10570-009-9381-2.

33. Tan, Xiao Yun, et al. “Preparation of High Crystallinity Cellulose Nanocrystals (CNCs) by Ionic Liquid Solvolysis.” *Biomass & Bioenergy*, vol. 81, Elsevier Ltd, 2015, pp. 584–91, https://doi.org/10.1016/j.biombioe.2015.08.016

34. Castro-Guerrero, Carlos F., and Derek G. Gray. “Chiral Nematic Phase Formation by Aqueous Suspensions of Cellulose Nanocrystals Prepared by Oxidation with Ammonium Persulfate.” *Cellulose (London)*, vol. 21, no. 4, Springer Netherlands, 2014, pp. 2567–77, https://doi.org/10.1007/s10570-014-0308-1.

35. Rovera, Cesare, et al. “Enzymatic Hydrolysis in the Green Production of Bacterial Cellulose Nanocrystals.” *ACS Sustainable Chemistry & Engineering*, vol. 6, no. 6, American Chemical Society, 2018, pp. 7725–34, https://doi.org/10.1021/acssuschemeng.8b00600.

36. Reid, Michael S., et al. “Benchmarking Cellulose Nanocrystals: From the Laboratory to Industrial Production.” *Langmuir*, vol. 33, no. 7, American Chemical Society, 2017, pp. 1583–98, https://doi.org/10.1021/acs.langmuir.6b03765.

37. Siqueira, Gilberto, et al. “New Process of Chemical Grafting of Cellulose Nanoparticles with a Long Chain Isocyanate.” *Langmuir*, vol. 26, no. 1, American Chemical Society, 2010, pp. 402–11, https://doi.org/10.1021/la9028595.

38. Dufresne, Alain. “Nanocellulose Processing Properties and Potential Applications.” *Current Forestry Reports*, vol. 5, no. 2, Springer International Publishing, 2019, pp. 76–89, https://doi.org/10.1007/s40725-019-00088-1.

39. Dufresne, Alain. *Nanocellulose: From Nature to High Performance Tailored Materials*. 1. Aufl., Walter de Gruyter GmbH Co.KG, 2012.

40. Flauzino Neto, Wilson Pires, et al. “Mechanical Properties of Natural Rubber Nanocomposites Reinforced with High Aspect Ratio Cellulose Nanocrystals Isolated from Soy Hulls.” *Carbohydrate Polymers*, vol. 153, Elsevier Ltd, 2016, pp. 143–52, https://doi.org/10.1016/j.carbpol.2016.07.073.

41. Liu, Chao, et al. “Properties of Nanocellulose Isolated from Corncob Residue Using Sulfuric Acid, Formic Acid, Oxidative and Mechanical Methods.” *Carbohydrate Polymers*, vol. 151, Elsevier Ltd, 2016, pp. 716–24, https://doi.org/10.1016/j.carbpol.2016.06.025.

42. Kallel, Fatma, et al. “Isolation and Structural Characterization of Cellulose Nanocrystals Extracted from Garlic Straw Residues.” *Industrial Crops and Products*, vol. 87, Elsevier B.V, 2016, pp. 287–96, https://doi.org/10.1016/j.indcrop.2016.04.060.

43. Zhang, Chunmei et al. “Incorporation of poly(ethylene glycol) grafted cellulose nanocrystals in poly(lactic acid) electrospun nanocomposite fibers as potential scaffolds for bone tissue engineering.” *Materials science & engineering. C, Materials for biological applications* vol. 49 (2015): 463-471. doi:10.1016/j.msec.2015.01.024

44. Bras, Julien, et al. “Mechanical, Barrier, and Biodegradability Properties of Bagasse Cellulose Whiskers Reinforced Natural Rubber Nanocomposites.” *Industrial Crops and Products*, vol. 32, no. 3, Elsevier B.V, 2010, pp. 627–33, https://doi.org/10.1016/j.indcrop.2010.07.018.

45. Biyani, Mahesh V., et al. “Light-Healable Supramolecular Nanocomposites Based on Modified Cellulose Nanocrystals.” *ACS Macro Letters*, vol. 2, no. 3, American Chemical Society, 2013, pp. 236–40, https://doi.org/10.1021/mz400059w.

46. Ruiz-Palomero, Celia, et al. “Gels Based on Nanocellulose with Photosensitive Ruthenium Bipyridine Moieties as Sensors for Silver Nanoparticles in Real Samples.” *Sensors and Actuators. B, Chemical*, vol. 229, Elsevier B.V, 2016, pp. 31–37, https://doi.org/10.1016/j.snb.2016.01.098.

47. Mariano, Marcos, et al. “Cellulose nanomaterials: size and surface influence on the thermal and rheological behavior.” *Polímeros*, vol. 28, no. 2, Associação Brasileira de Polímeros, 2018, pp. 93–102, https://doi.org/10.1590/0104-1428.2413.

48. Nakagaito, Antonio Norio, and Hiroyuki Yano. “The Effect of Fiber Content on the Mechanical and Thermal Expansion Properties of Biocomposites Based on Microfibrillated Cellulose.” *Cellulose (London)*, vol. 15, no. 4, Springer Netherlands, 2008, pp. 555–59, https://doi.org/10.1007/s10570-008-9212-x.

49. Kim, Dae-Young, et al. “Thermal Decomposition of Cellulose Crystallites in Wood.” *Holzforschung*, vol. 55, no. 5, Walter de Gruyter, 2001, pp. 521–24, https://doi.org/10.1515/HF.2001.084.

50. Petersson, L., et al. “Structure and Thermal Properties of Poly(lactic Acid)/cellulose Whiskers Nanocomposite Materials.” *Composites Science and Technology*, vol. 67, no. 11, Elsevier Ltd, 2007, pp. 2535–44, https://doi.org/10.1016/j.compscitech.2006.12.012.

51. van den Berg, Otto, et al. “Preparation of Homogeneous Dispersions of Tunicate Cellulose Whiskers in Organic Solvents.” *Biomacromolecules*, vol. 8, no. 4, American Chemical Society, 2007, pp. 1353–57, https://doi.org/10.1021/bm061104q.

52. Salajková, Michaela, et al. “Hydrophobic Cellulose Nanocrystals Modified with Quaternary Ammonium Salts.” *Journal of Materials Chemistry*, vol. 22, no. 37, 2012, pp. 19798–1985, https://doi.org/10.1039/c2jm34355j.

53. Heux, L., et al. “Nonflocculating and Chiral-Nematic Self-Ordering of Cellulose Microcrystals Suspensions in Nonpolar Solvents.” *Langmuir*, vol. 16, no. 21, American Chemical Society, 2000, pp. 8210–12, https://doi.org/10.1021/la9913957.

54. Torres-Rocha, Olga Lidia, et al. “Non-Covalent Polymer Surface Modification of Cellulose Nanocrystals Using Block Copolymers.” *Macromolecular Reaction Engineering*, Wiley-VCH Verlag, 2021, p. 2100046–, https://doi.org/10.1002/mren.202100046.

55. Dufresne, Alain. “Cellulose Nanomaterial Reinforced Polymer Nanocomposites.” *Current Opinion in Colloid & Interface Science*, vol. 29, Elsevier Ltd, 2017, pp. 1–8, https://doi.org/10.1016/j.cocis.2017.01.004.

56. Akindoyo, John O., et al. “Polyurethane Types, Synthesis and Applications - a Review.” *RSC Advances*, vol. 6, no. 115, 2016, pp. 114453–82, https://doi.org/10.1039/c6ra14525f.

57. Si, Pengxiang, and Boxin Zhao. “Water-based Polyurethanes for Sustainable Advanced Manufacture.” Canadian Journal of Chemical Engineering, vol. 99, no. 9, John Wiley & Sons, Inc, 2021, pp. 1851–69, https://doi.org/10.1002/cjce.24049.

58. Szycher, M. (1999) Szycher’s Handbook of Polyurethanes. CRC Press, Boca Raton, Florida.

59. Akindoyo, John O., et al. “Polyurethane Types, Synthesis and Applications - a Review.” *RSC Advances*, vol. 6, no. 115, ROYAL SOC CHEMISTRY, 2016, pp. 114453–82, https://doi.org/10.1039/c6ra14525f.

60. Gum, Wilson F., et al. *Reaction Polymers: Polyurethanes, Epoxies, Unsaturated Polyesters, Phenolics, Special Monomers, and Additives: Chemistry, Technology, Applications, Markets*. Hanser Publishers, 1992.

61. Gama, Nuno V., et al. “Polyurethane Foams: Past, Present, and Future.” *Materials*, vol. 11, no. 10, MDPI AG, 2018, p. 1841–, https://doi.org/10.3390/ma11101841.

62. Polyurethane and Related Foams; Chemistry and Technology.” *SciTech Book News*, vol. 30, no. 4, Ringgold, Inc, 2006.

63. Tersac, Gilles. “Chemistry and Technology of Polyols for Polyurethanes. Milhail Ionescu. Rapra Technology, Shrewsbury, UK.” *Polymer International*, vol. 56, no. 6, John Wiley & Sons, Ltd, 2007, pp. 820–820, https://doi.org/10.1002/pi.2159.

64. Cinelli, Patrizia, et al. “Green Synthesis of Flexible Polyurethane Foams from Liquefied Lignin.” *European Polymer Journal*, vol. 49, no. 6, Elsevier Ltd, 2013, pp. 1174–84, https://doi.org/10.1016/j.eurpolymj.2013.04.005.

65. Singhal, Pooja, et al. “Low Density Biodegradable Shape Memory Polyurethane Foams for Embolic Biomedical Applications.” *Acta Biomaterialia*, vol. 10, no. 1, Elsevier Ltd, 2014, pp. 67-76, https://doi.org/10.1016/j.actbio.2013.09.027.

66. Hodlur, R. .., and M. .. Rabinal. “Self Assembled Graphene Layers on Polyurethane Foam as a Highly Pressure Sensitive Conducting Composite.” *Composites Science and Technology*, vol. 90, Elsevier Ltd, 2014, pp. 160–65, https://doi.org/10.1016/j.compscitech.2013.11.005.

67. Claeys, Bart, et al. “Thermoplastic Polyurethanes for the Manufacturing of Highly Dosed Oral Sustained Release Matrices via Hot Melt Extrusion and Injection Molding.” *European Journal of Pharmaceutics and Biopharmaceutics*, vol. 90, Elsevier B.V, 2015, pp. 44–52, https://doi.org/10.1016/j.ejpb.2014.11.003.

68. J.O. Hollinger An Introduction to Biomaterials CRC Press (2011)

69. KROL, Piotr. “Synthesis Methods, Chemical Structures and Phase Structures of Linear Polyurethanes. Properties and Applications of Linear Polyurethanes in Polyurethane Elastomers,

Copolymers and Ionomers." *Progress in Materials Science*, vol. 52, no. 6, Elsevier Ltd, 2007, pp. 915–1015, https://doi.org/10.1016/j.pmatsci.2006.11.001.

70. Charlon, M., et al. "Synthesis, Structure and Properties of Fully Biobased Thermoplastic Polyurethanes, Obtained from a Diisocyanate Based on Modified Dimer Fatty Acids, and Different Renewable Diols." *European Polymer Journal*, vol. 61, Elsevier Ltd, 2014, pp. 197–205, https://doi.org/10.1016/j.eurpolymj.2014.10.012.

71. Honarkar, Hengameh. "Waterborne Polyurethanes: A Review." *Journal of Dispersion Science and Technology*, vol. 39, no. 4, Taylor & Francis, 2018, pp. 507–16, https://doi.org/10.1080/01932691.2017.1327818.

72. Cakic, Suzana M., et al. "Synthesis and Degradation Profile of Cast Films of PPG-DMPA-IPDI Aqueous Polyurethane Dispersions Based on Selective Catalysts." *Polymer Degradation and Stability*, vol. 94, no. 11, Elsevier Ltd, 2009, pp. 2015–22, https://doi.org/10.1016/j.polymdegradstab.2009.07.015.

73. Arnoldus, R. (1990) Waterborne Coating, Surface Coating. In: Wilson, A.D., Nicholson, J.W. and Prosser, H.J., Eds., Surface Coating, Vol. 3, Elsevier Applied Science, New York, 93-127.

74. Rosthauser, J.W. and Nachtkamp, K. (1987) Advances in Urethane Science and Technology, edited by K.C. Frisch and D. Klempner; Lancaster: Technomic; pp. 121–162.

75. Dieterich, D. "Aqueous Emulsions, Dispersions and Solutions of Polyurethanes; Synthesis and Properties." *Progress in Organic Coatings*, vol. 9, no. 3, Elsevier B.V, 1981, pp. 281–340, https://doi.org/10.1016/0033-0655(81)80002-7.

76. Figovsky, O. L. (2000). U.S. Patent No. 6,120,905. Washington, DC: U.S. Patent and Trademark Office.

77. Guan, Jing, et al. "Progress in Study of Non-Isocyanate Polyurethane." *Industrial & Engineering Chemistry Research*, vol. 50, no. 11, American Chemical Society, 2011, pp. 6517–27, https://doi.org/10.1021/ie101995j.

78. Kong, Xiaohua, et al. "Novel Polyurethane Produced from Canola Oil Based Poly(ether Ester) Polyols: Synthesis, Characterization and Properties." *European Polymer Journal*, vol. 48, no. 12, Elsevier Ltd, 2012, pp. 2097–106, https://doi.org/10.1016/j.eurpolymj.2012.08.012.

79. Fang, Changqing, et al. "Synthesis and Characterization of Low Crystalline Waterborne Polyurethane for Potential Application in Water-Based Ink Binder." *Progress in Organic Coatings*, vol. 77, no. 1, Elsevier B.V, 2014, pp. 61–71, https://doi.org/10.1016/j.porgcoat.2013.08.004.

80. Cardoso, Grace Tibério et al. "Rigid foam polyurethane (PU) derived from castor oil (Ricinus communis) for thermal insulation in roof systems." *Collection of Frontiers of Architectural Research* 1 (2012): 348-356.

81. Chattopadhyay, D. .., and K. V. S. .. Raju. “Structural Engineering of Polyurethane Coatings for High Performance Applications.” *Progress in Polymer Science*, vol. 32, no. 3, Elsevier Ltd, 2007, pp. 352–418, https://doi.org/10.1016/j.progpolymsci.2006.05.003.

82. Blackwell, J., et al. “Structure of Polyurethane Elastomers: Effect of Chain Extender Length on the Structure of MDI/diol Hard Segments.” *Polymer (Guilford)*, vol. 23, no. 7, Elsevier Ltd, 1982, pp. 950–56, https://doi.org/10.1016/0032-3861(82)90392-5.

83. Sheikhy, H., et al. “Studying the Effects of Chain Extenders Chemical Structures on the Adhesion and Mechanical Properties of a Polyurethane Adhesive.” *Journal of Industrial and Engineering Chemistry (Seoul, Korea)*, vol. 19, no. 6, Elsevier B.V, 2013, pp. 1949–55, https://doi.org/10.1016/j.jiec.2013.03.008.

84. MONTARNAL, Damien, et al. “Silica-Like Malleable Materials from Permanent Organic Networks.” *Science (American Association for the Advancement of Science)*, vol. 334, no. 6058, American Association for the Advancement of Science, 2011, pp. 965–68, https://doi.org/10.1126/science.1212648.

85. White, S. R., et al. “Autonomic Healing of Polymer Composites.” *Nature (London)*, vol. 409, no. 6822, Nature Publishing Group, 2001, pp. 794–97, https://doi.org/10.1038/35057232.

86. Hayes, S. .., et al. “A Self-Healing Thermosetting Composite Material.” *Composites. Part A, Applied Science and Manufacturing*, vol. 38, no. 4, Elsevier Ltd, 2007, pp. 1116–20, https://doi.org/10.1016/j.compositesa.2006.06.008.

87. Hayes S A, Zhang W, Branthwaite M, et al. Self-healing of Damage in Fibre-reinforced Polymer-matrix Composites[J]. Journal of the Royal Society Interface, 2007, 4(13): 381.

88. Bowman, Christopher N., and Christopher J. Kloxin. “Covalent Adaptable Networks: Reversible Bond Structures Incorporated in Polymer Networks.” *Angewandte Chemie (International Ed.)*, vol. 51, no. 18, WILEY-VCH Verlag, 2012, pp. 4272–74, https://doi.org/10.1002/anie.201200708.

89. Maeda, Takeshi, et al. “Dynamic Covalent Polymers: Reorganizable Polymers with Dynamic Covalent Bonds.” *Progress in Polymer Science*, vol. 34, no. 7, Elsevier Ltd, 2009, pp. 581–604, https://doi.org/10.1016/j.progpolymsci.2009.03.001.

90. Rowan, Stuart J., et al. “Using the Dynamic Bond to Access Macroscopically Responsive Structurally Dynamic Polymers.” *Nature Materials*, vol. 10, no. 1, 2011, pp. 14–27, https://doi.org/10.1038/nmat2891.

91. Rowan, Stuart J., et al. “Dynamic Covalent Chemistry.” *Angewandte Chemie (International Ed.)*, vol. 41, no. 6, WILEY-VCH Verlag GmbH, 2002, pp. 898–952, https://doi.org/10.1002/1521-3773(20020315)41:6<898::AID-ANIE898>3.0.CO;2-E.

92. Skene, Williams G., and Jean-Marie P. Lehn. “Dynamers: Polyacylhydrazone Reversible Covalent Polymers, Component Exchange, and Constitutional Diversity.” *Proceedings of the National Academy of Sciences - PNAS*, vol. 101, no. 22, National Academy of Sciences, 2004, pp. 8270–75, https://doi.org/10.1073/pnas.0401885101.

93. Lehn, Jean-Marie. “Dynamers: Dynamic Molecular and Supramolecular Polymers.” *Progress in Polymer Science*, vol. 30, no. 8, Elsevier Ltd, 2005, pp. 814–31, https://doi.org/10.1016/j.progpolymsci.2005.06.002.

94. Deng, Guohua, et al. “Covalent Cross-Linked Polymer Gels with Reversible Sol−Gel Transition and Self-Healing Properties.” *Macromolecules*, vol. 43, no. 3, American Chemical Society, 2010, pp. 1191–94, https://doi.org/10.1021/ma9022197.

95. Zheng, Peiwen, and Thomas J. McCarthy. “A Surprise from 1954: Siloxane Equilibration Is a Simple, Robust, and Obvious Polymer Self-Healing Mechanism.” *Journal of the American Chemical Society*, vol. 134, no. 4, American Chemical Society, 2012, pp. 2024–27, https://doi.org/10.1021/ja2113257.

96. XIANGXU CHEN, et al. “A Thermally Re-Mendable Cross-Linked Polymeric Material.” *Science (American Association for the Advancement of Science)*, vol. 295, no. 5560, American Society for the Advancement of Science, 2002, pp. 1698–702, https://doi.org/10.1126/science.1065879.

97. Zhang, Youchun, et al. “Thermally Self-Healing Polymeric Materials: The Next Step to Recycling Thermoset Polymers?” *Macromolecules*, vol. 42, no. 6, American Chemical Society, 2009, pp. 1906–12, https://doi.org/10.1021/ma8027672.

98. Adzima, Brian J., et al. “Rheological and Chemical Analysis of Reverse Gelation in a Covalently Cross-Linked Diels−Alder Polymer Network.” *Macromolecules*, vol. 41, no. 23, American Chemical Society, 2008, pp. 9112–17, https://doi.org/10.1021/ma801863d.

99. Reutenauer, P., et al. “Room Temperature Dynamic Polymers Based on Diels–Alder Chemistry.” *Chemistry: a European Journal*, vol. 15, no. 8, WILEY-VCH Verlag, 2009, pp. 1893–900, https://doi.org/10.1002/chem.200802145.

100. Lu, Yi-Xuan, et al. “Making Insoluble Polymer Networks Malleable via Olefin Metathesis.” *Journal of the American Chemical Society*, vol. 134, no. 20, American Chemical Society, 2012, pp. 8424–27, https://doi.org/10.1021/ja303356z.

101. GHOSH, Biswajit, and Marek W. URBAN. “Self-Repairing Oxetane-Substituted Chitosan Polyurethane Networks.” *Science (American Association for the Advancement of Science)*, vol. 323, no. 5920, American Association for the Advancement of Science, 2009, pp. 1458–60, https://doi.org/10.1126/science.1167391.

102. Zhang, Mingming, et al. “Self-Healing Supramolecular Gels Formed by Crown Ether Based Host-Guest Interactions.” *Angewandte Chemie*, vol. 124, no. 28, WILEY-VCH Verlag, 2012, pp. 7117–21, https://doi.org/10.1002/ange.201203063.

103. SCOTT, Timothy F., et al. “Photoinduced Plasticity in Cross-Linked Polymers.” *Science (American Association for the Advancement of Science)*, vol. 308, no. 5728, American Association for the Advancement of Science, 2005, pp. 1615–17, https://doi.org/10.1126/science.1110505.

104. Spitalsky, Zdenko, et al. “Carbon Nanotube–polymer Composites: Chemistry, Processing, Mechanical and Electrical Properties.” *Progress in Polymer Science*, vol. 35, no. 3, Elsevier Ltd, 2010, pp. 357–401, https://doi.org/10.1016/j.progpolymsci.2009.09.003.

105. Kloxin, Christopher J., et al. “Covalent Adaptable Networks (CANs): A Unique Paradigm in Crosslinked Polymers.” *Macromolecules*, vol. 43, no. 6, 2010, pp. 2643–53, https://doi.org/10.1021/ma902596s.

106. Kloxin, Christopher J., and Christopher N. Bowman. “Covalent Adaptable Networks: Smart, Reconfigurable and Responsive Network Systems.” *Chemical Society Reviews*, vol. 42, no. 17, 2013, pp. 7161–73, https://doi.org/10.1039/c3cs60046g.

107. ANGELL, C. A. “Formation of Glasses from Liquids and Biopolymers.” *Science (American Association for the Advancement of Science)*, vol. 267, no. 5206, American Society for the Advancement of Science, 1995, pp. 1924–35, https://doi.org/10.1126/science.267.5206.1924.

108. Denissen, Wim, et al. “Vitrimers: Permanent Organic Networks with Glass-Like Fluidity.” *Chemical Science (Cambridge)*, vol. 7, no. 1, Royal Society of Chemistry, 2015, pp. 3–38, https://doi.org/10.1039/c5sc02223a.

109. Dyre, Jeppe C. “Colloquium: The Glass Transition and Elastic Models of Glass-Forming Liquids.” *Reviews of Modern Physics*, vol. 78, no. 3, American Physical Society, 2006, pp. 953–72, https://doi.org/10.1103/RevModPhys.78.953.

110. Yu, Kai, et al. “Influence of Stoichiometry on the Glass Transition and Bond Exchange Reactions in Epoxy Thermoset Polymers.” *RSC Advances*, vol. 4, no. 89, 2014, pp. 48682–90, https://doi.org/10.1039/C4RA06543C.

111. Capelot, Mathieu, et al. “Metal-Catalyzed Transesterification for Healing and Assembling of Thermosets.” *Journal of the American Chemical Society*, vol. 134, no. 18, American Chemical Society, 2012, pp. 7664–67, https://doi.org/10.1021/ja302894k.

112. Brutman, Jacob P., et al. “Polylactide Vitrimers.” *ACS Macro Letters*, vol. 3, no. 7, American Chemical Society, 2014, pp. 607–10, https://doi.org/10.1021/mz500269w.

113. Denissen, Wim, et al. “Vinylogous Urethane Vitrimers.” *Advanced Functional Materials*, vol. 25, no. 16, Blackwell Publishing Ltd, 2015, pp. 2451–57, https://doi.org/10.1002/adfm.201404553.

114. Stefani, Hélio A., et al. “An Easy Synthesis of Enaminones in Water as Solvent.” *Synthesis (Stuttgart)*, vol. 2000, no. 11, 2000, pp. 1526–28, https://doi.org/10.1055/s-2000-7608.

115. Obadia, Mona M., et al. “Reprocessing and Recycling of Highly Cross-Linked Ion-Conducting Networks through Transalkylation Exchanges of C–N Bonds.” *Journal of the American Chemical Society*, vol. 137, no. 18, American Chemical Society, 2015, pp. 6078–83, https://doi.org/10.1021/jacs.5b02653.

116. Zhang, Xuzhen, et al. “Structure and Properties of Surface-Acetylated Cellulose Nanocrystal/poly(butylene Adipate-Co-Terephthalate) Composites.” *Polymer Bulletin (Berlin, Germany)*, vol. 73, no. 7, Springer Berlin Heidelberg, 2016, pp. 2073–85, https://doi.org/10.1007/s00289-015-1594-y.

117. Robles, Eduardo, et al. “Surface-Modified Nano-Cellulose as Reinforcement in Poly(lactic Acid) to Conform New Composites.” *Industrial Crops and Products*, vol. 71, Elsevier B.V, 2015, pp. 44–53, https://doi.org/10.1016/j.indcrop.2015.03.075.

118. Pöllänen, Maija, et al. “Influence of Carbon Nanotube–polymeric Compatibilizer Masterbatches on Morphological, Thermal, Mechanical, and Tribological Properties of Polyethylene.” *Composites Science and Technology*, vol. 71, no. 10, Elsevier Ltd, 2011, pp. 1353–60, https://doi.org/10.1016/j.compscitech.2011.05.009.

119. Dufresne, Alain. “Processing of Polymer Nanocomposites Reinforced with Polysaccharide Nanocrystals.” *Molecules (Basel, Switzerland)*, vol. 15, no. 6, MDPI AG, 2010, pp. 4111–28, https://doi.org/10.3390/molecules15064111.

120. Auad, María L., et al. “Polyaniline-Modified Cellulose Nanofibrils as Reinforcement of a Smart Polyurethane.” *Polymer International*, vol. 60, no. 5, John Wiley & Sons, Ltd, 2011, pp. 743–50, https://doi.org/10.1002/pi.3004.

121. Zhang, Xuzhen, and Yong Zhang. “Reinforcement Effect of Poly(butylene Succinate) (PBS)-Grafted Cellulose Nanocrystal on Toughened PBS/polylactic Acid Blends.” *Carbohydrate Polymers*, vol. 140, Elsevier Ltd, 2016, pp. 374–82, https://doi.org/10.1016/j.carbpol.2015.12.073.

122. Tang, Wenzhong, et al. “Melt Processing and Mechanical Property Characterization of Multi-Walled Carbon Nanotube/high Density Polyethylene (MWNT/HDPE) Composite Films.” *Carbon (New York)*, vol. 41, no. 14, Elsevier Ltd, 2003, pp. 2779–85, https://doi.org/10.1016/S0008-6223(03)00387-7.

123. Ray, Dipa, and Sunanda Sain. “In Situ Processing of Cellulose Nanocomposites.” *Composites. Part A, Applied Science and Manufacturing*, vol. 83, Elsevier Ltd, 2016, pp. 19–37, https://doi.org/10.1016/j.compositesa.2015.09.007.

124. Liao, Lei et al. “Chemistry makes graphene beyond graphene.” *Journal of the American Chemical Society* vol. 136,35 (2014): 12194-200. doi:10.1021/ja5048297

125. Frankland, S. J. V., et al. “Molecular Simulation of the Influence of Chemical Cross-Links on the Shear Strength of Carbon Nanotube−Polymer Interfaces.” *The Journal of Physical Chemistry. B*, vol. 106, no. 12, American Chemical Society, 2002, pp. 3046–48, https://doi.org/10.1021/jp015591+.

126. Zhou, Chengjun, et al. “Application of Rod-Shaped Cellulose Nanocrystals in Polyacrylamide Hydrogels.” *Journal of Colloid and Interface Science*, vol. 353, no. 1, Elsevier Inc, 2011, pp. 116–23, https://doi.org/10.1016/j.jcis.2010.09.035.

127. Zhou, Chengjun, et al. “Dynamic Rheology Studies of in Situ Polymerization Process of Polyacrylamide–cellulose Nanocrystal Composite Hydrogels.” *Colloid and Polymer Science*, vol. 289, no. 3, Springer-Verlag, 2010, pp. 247–55, https://doi.org/10.1007/s00396-010-2342-3.

128. Goussé, Cécile, et al. “Stable Suspensions of Partially Silylated Cellulose Whiskers Dispersed in Organic Solvents.” *Polymer (Guilford)*, vol. 43, no. 9, Elsevier Ltd, 2002, pp. 2645–51, https://doi.org/10.1016/S0032-3861(02)00051-4.

129. Trifol, Jon, et al. “A Comparison of Partially Acetylated Nanocellulose, Nanocrystalline Cellulose, and Nanoclay as Fillers for High-Performance Polylactide Nanocomposites.” *Journal of Applied Polymer Science*, vol. 133, no. 14, Blackwell Publishing Ltd, 2016, https://doi.org/10.1002/app.43257.

130. Mariano, Marcos, et al. “Melt Processing of Cellulose Nanocrystal Reinforced Polycarbonate from a Masterbatch Process.” *European Polymer Journal*, vol. 69, no. 70, Elsevier Ltd, 2015, pp. 208–23, https://doi.org/10.1016/j.eurpolymj.2015.06.007.

131. Zhang, Wei, et al. “A Facile In Situ Approach to Polypyrrole Functionalization Through Bioinspired Catechols.” *Advanced Functional Materials*, vol. 25, no. 10, Blackwell Publishing Ltd, 2015, pp. 1588–97, https://doi.org/10.1002/adfm.201403115.

132. Cao, Xiaodong, et al. “New Nanocomposite Materials Reinforced with Flax Cellulose Nanocrystals in Waterborne Polyurethane.” *Biomacromolecules*, vol. 8, no. 3, American Chemical Society, 2007, pp. 899–904, https://doi.org/10.1021/bm0610368.

133. Marchant, R. .., et al. “Degradation of a Poly(ether Urethane Urea) Elastomer: Infra-Red and XPS Studies.” *Polymer (Guilford)*, vol. 28, no. 12, Elsevier Ltd, 1987, pp. 2032–39, https://doi.org/10.1016/0032-3861(87)90037-1.

134. Socrates, G. Infrared and Raman Characteristic Group Frequencies: Tables and Charts, 3rd ed. John Wiley & Sons, Chichester, UK (2004).

135. Kim, Min Su, et al. “Influences of Cellulose Nanofibril on Microstructures and Physical Properties of Waterborne Polyurethane-Based Nanocomposite Films.” *Carbohydrate Polymers*, vol. 225, Elsevier Ltd, 2019, p. 115233–, https://doi.org/10.1016/j.carbpol.2019.115233.

136. Arunbabu, Dhamodaran, et al. “Poly(AAc-Co-MBA) Hydrogel Films: Adhesive and Mechanical Properties in Aqueous Medium.” *The Journal of Physical Chemistry. B*, vol. 117, no. 1, American Chemical Society, 2013, pp. 441–49, https://doi.org/10.1021/jp3101688.

137. Chen, Mao, et al. “The Crucial Role in Controlling the Dynamic Properties of Polyester-Based Epoxy Vitrimers: The Density of Exchangeable Ester Bonds (υ).” *Macromolecules*, vol. 54, no. 21, American Chemical Society, 2021, pp. 10110–17, https://doi.org/10.1021/acs.macromol.1c01289.

138. Yang, Yang, et al. “A Repairable Anhydride-Epoxy System with High Mechanical Properties Inspired by Vitrimers.” *Polymer (Guilford)*, vol. 159, Elsevier Ltd, 2018, pp. 162–68, https://doi.org/10.1016/j.polymer.2018.11.031.